UC-94cc
LBL-20737 c.1

Lawrence Berkeley Laboratory

UNIVERSITY OF CALIFORNIA

RECEIVED
LAWRENCE
BERKELEY LABORATORY
APR 7 1986
LIBRARY AND
DOCUMENTS SECTION

APPLIED SCIENCE DIVISION

INVESTIGATION OF A VITREOUS ELECTROLYTE
FOR USE IN LITHIUM/SULFUR CELLS

M.L. Smith*, F.R. McLarnon, and E.J. Cairns
(*M.S. Thesis)

December 1985

For Reference
Not to be taken from this room

APPLIED SCIENCE
DIVISION

LBL-20737 c.1

Prepared for the U.S. Department of Energy under Contract DE-AC03-76SF00098

DISCLAIMER

This document was prepared as an account of work sponsored by the United States Government. While this document is believed to contain correct information, neither the United States Government nor any agency thereof, nor the Regents of the University of California, nor any of their employees, makes any warranty, express or implied, or assumes any legal responsibility for the accuracy, completeness, or usefulness of any information, apparatus, product, or process disclosed, or represents that its use would not infringe privately owned rights. Reference herein to any specific commercial product, process, or service by its trade name, trademark, manufacturer, or otherwise, does not necessarily constitute or imply its endorsement, recommendation, or favoring by the United States Government or any agency thereof, or the Regents of the University of California. The views and opinions of authors expressed herein do not necessarily state or reflect those of the United States Government or any agency thereof or the Regents of the University of California.

LBL-20737

INVESTIGATION OF A VITREOUS ELECTROLYTE FOR USE IN LITHIUM/SULFUR CELLS

by

Michael L. Smith, Frank R. McLarnon and Elton J. Cairns

December 1985

Applied Science Division
Lawrence Berkeley Laboratory
University of California
Berkeley, California 94720

This work was supported by the Assistant Secretary for Conservation and Renewable Energy, Office of Energy Storage and Distribution of the U.S. Department of Energy under Contract No. DE-AC03-76SF00098.

INVESTIGATION OF A VITREOUS ELECTROLYTE FOR USE IN LITHIUM/SULFUR CELLS

Michael L. Smith

ABSTRACT

Novel Li/S cells, which employed a fast-lithium-ion conducting lithium chloroborate glass as the solid electrolyte, have been built and operated at 400 °C. The composition of glass used for this study, 7.3 mol% $(LiCl)_2$, 25.7 mol% Li_2O, and 67.0 mol% B_2O_3, had an ionic conductivity of 2.9×10^{-3} $(\Omega^{-1} \cdot cm^{-1})$ at 400 °C, which was somewhat lower than those of other lithium chloroborate glasses, which have shown ionic conductivities as high as 2×10^{-2} $(\Omega^{-1} \cdot cm^{-1})$.[1]

The current-voltage characteristics of these cells were examined; they were found to be capable of supporting pseudo-steady-state current densities up to 15 mA/cm^2 for 15-20 hours. A limiting current was found to exist at approximately 23 mA/cm^2. These cells could be charged and discharged with approximately equal polarization in either direction. However, the accumulation of a crystalline reaction layer on the surface of the electrolyte during discharge caused the cells to fail before the completion of a full charge-discharge cycle.

These cells were also used to measure the the solubility of lithium (as a polysulfide) in sulfur. The solubility limit was found to occur at $0.04 \,^{+0.03}_{-0.01}$ mol% Li at 400 °C. This is in qualitative agreement with the value reported by Sharma.[2]

CHAPTER 1

INTRODUCTION

1.1. The Need for High-Performance Secondary Batteries

The uncertainities in the supply and the instabilities of the price of fossil fuels over the past twenty years have resulted in increasing research and development efforts in the field of electrochemical energy conversion. The impetus for this increasing emphasis has been the need to decrease the national dependency on such potentially unstable resources as oil and gasoline. It is generally agreed that if an efficient electrochemical energy storage system could be built, one which could be used as a secondary energy source for load-leveling in an electric power plant or as a battery in an electric vehicle, it could satisfy some of the energy demands now filled by petroleum and, therefore, relieve some of this dependency.[3,4] For example, if automobiles could be built which were powered by electrochemically stored energy rather than by the combustion of gasoline, the demand for gasoline would be decreased and, therefore, the dependency would be lessened. However, the technical feasibility of a commercially acceptable electric vehicle depends on the production of a reliable, low-cost battery with high specific energy and specific power.

The theoretical specific energy is defined as the change of Gibbs free energy for the overall reaction divided by the total weight of reactants:

$$\text{theoretical specific energy} = -\Delta G \,/\, \sum \nu_i M_i \tag{1-1}$$

where ν_i is the number of moles of reactants i and M_i is the molecular weight of reactant i. Therefore, a high-specific-energy battery would be one which exhibited a combination of a large change in free energy and a low total weight of reactants. A typical set of performance goals for an electric-vehicle-type battery includes a specific energy of 100 Whr/kg, a specific power of 100 W/kg, and a cycle life of at least 500 cycles (at 100% depth of discharge).[5] Among the leading choices for meeting these goals, based partly on its high theoretical specific energy, is the high-

temperature lithium/sulfur battery.

1.2. Lithium/Sulfur Battery

The theoretical specific energy of the Li/S battery, based on the overall cell reaction of lithium and sulfur to form lithium sulfide:

$$2Li + S \rightleftarrows Li_2S, \tag{1-2}$$

is approximately 2700 Wh/kg. The open-circuit cell potential of a Li/S battery, based on this reaction with all species at unit activity would be 2.18 volts at 400 °C.

The achievable specific energy of any battery is never as high as its theoretical value. This is because the theoretical specific energy of a battery does not take into account the weight of additional parts such as the electrolyte, current collectors, separators, cell casings, insulation, or any control and safety features included in the battery. After considering the weight of these additional battery parts, the calculated practical specific energy is usually reduced to a fraction (approximately 0.25-0.20) of the theoretical. Even after these reductions, the specific energy of the Li/S battery would be approximately 600 Wh/kg, which is comfortably above the goal of 100 Wh/kg.

The possibility of developing an efficient high-temperature Li/S battery, one which could successfully be built and achieve the performance goals established for a high-specific-energy battery, provided the incentive for work which began at Argonne National Laboratory in the early 1960s.[6] These research efforts made use of molten-salt electrolytes with molten electrodes, but the results were largely unsatisfactory because the liquid lithium could not be retained by the current collectors and because the lithium polysulfides were highly soluble in the molten-salt electrolytes. The search for a solution to this problem led to the idea of alloying the lithium with other metals and combining the sulfur with some non-participating materials. This design reduced the mobility and the solubility of the electrode materials, but it also introduced some problems and disadvantages. Among the disadvantages was the increase in the weight of the electrode reactants and, therefore, a decrease in the theoretical specific energy and power. Further, the open-circuit cell

potentials for these batteries were lowered because the alloying materials reduced the activities of the lithium and the sulfur. For example, the LiAl/FeS battery, which utilizes a LiCl-KCl molten-salt electrolyte in conjunction with solid electrodes, has a theoretical specific energy of 458 Wh/kg with a cell potential of 1.33 volts.[7] These values are considerably reduced from those listed above for the Li/S cell.

There is another potential solution to the problem of high lithium mobility and high polysulfide solubility; that is to use a solid electrolyte in conjunction with the molten electrodes. The solid electrolyte would necessarily exhibit high ionic conductivity, low electronic conductivity, and stability to the materials used as the electrodes. This solution would eliminate the need to alloy the electrode materials because the solid electrolyte would act as a rigid barrier to contain both the metallic lithium and the lithium polysulfides in their respective compartments. Thus, it would effectively solve the problem of high mobility and solubility previously encountered in the Li/S cell, without the disadvantages created in the LiAl/FeS battery. Therefore, this solution would preserve the high theoretical specific energy and open-circuit potential of the Li/S cell.

1.3. Solid Electrolytes

The choice of which material to use as a solid electrolyte in a Li/S cell would be between two types of materials: crystalline and vitreous. Both of these types of materials have been used in the analogous Na/S systems,[8,9] and they both have shown great promise. However, the idea of using a fast-ionically-conductive vitreous material as an electrolyte in a Li/S cell is particularly appealing because there are some advantages that vitreous materials have over crystalline or ceramic materials. Among these advantages are: ease of fabricability into complex shapes, lack of grain boundaries, and isotropic transport and other properties.

The ability to form such glasses into complex shapes has been demonstrated by Dow Chemical Co.; they have formed a sodium borate glass into thin-walled fibers.[10,11] These fibers exhibit a very low wall-thickness to surface-area ratio which allows for a low overall cell resistance. The lack of grain boundaries in vitreous materials would be especially beneficial when the glasses came

into contact with the electrode materials at elevated temperatures. Studies of alkali attack on crystals has shown that, in many instances, the grain boundaries are the areas most heavily attacked by the alkali metals. Therefore, vitreous materials should be more resistant to attack by alkali metals such as lithium. Finally, the advantage of a vitreous material exhibiting isotropic transport would be most evident when the glasses were formed into complex shapes. The glasses could be molded into any configuration because their conductivity would be equal in all directions.

The above mentioned advantages of vitreous materials over crystalline bodies or ceramics are significant and very influential in choosing which material to use in a Li/S cell. However, perhaps more important would be how the conductivities of the materials compare. The conductivities of certain fast-ion-conducting glasses have been reported to be higher than those of crystalline materials of similar compositions.[12] The higher intrinsic conductivities combined with the ability of forming the fast-ion-conducting glassy materials into thinner and more complex shapes means that the overall ohmic resistance of the glasses could be much lower than the overall resistance of crystalline materials of similar composition.

1.4. Lithium Borate Glasses

A promising group of fast-lithium-ion conducting glasses is the family of lithium borate glasses. These glasses have been reported to have lithium-ion conductivities as high as $5 \times 10^{-3}\ \Omega^{-1}\mathrm{cm}^{-1}$ at 300 °C, or with the addition of LiCl, as high as $2 \times 10^{-2}\ \Omega^{-1}\mathrm{cm}^{-1}$ at 300 °C with a corresponding activation energy of 0.46 eV.[1] These glasses have also been found to retain their structure in molten lithium alloys of various lithium activities despite the formation of a black reaction layer. These characteristics make these glasses attractive candidates for use as solid electrolytes in Li/S cells. However, there have been no reports on the compatibility of these glasses with sulfur or lithium polysulfides. An assessment of the feasibility of using a lithium borate glass as an electrolyte in a Li/S cell requires an evaluation of the stability of these glasses to attack by sulfur and lithium polysulfides.

CHAPTER 2

BACKGROUND and THEORY

2.1. Introduction

Certain glasses are known to exhibit ionic conductivities many times greater than their electronic conductivities. This characteristic has been understood for many years and has provided the means for these glasses to be used as solid electrolytes. For example, as early as 1905, glasses were being used as solid electrolytes in thermochemical probes;[13] however, only recently has research been directed towards understanding and optimizing the conductivities of glasses. As a result of this research, more than 100 materials have been identified that exhibit unusually high ionic conductivities.[14,15] Of special interest here is the discovery of certain oxide glasses with very high lithium-ion conductivities. One of these discoveries is the whole family of lithium borate glasses.[16] This material has been shown to have lithium-ion conductivities as high as $10^{-2}\ \Omega^{-1}\ \mathrm{cm}^{-1}$ at 300 °C with an activation energy of 0.46 eV. Tuller has shown that the addition of various lithium salts, such as LiCl, has a profound effect on the lithium-ion conductivity of the lithium borate glasses. The stability of the lithium borate glasses in the presence of water and molten lithium of various activities has also been studied.[17]

2.2. General Theory of Transport in Glass

The following review of ionic transport in solids is essentially that presented by Tuller *et al.*[18] It is presented to demonstrate the differences between fast ion conductors, (FICs), and normal ionic conductors.

The conductivity in solids may be expressed by

$$\sigma = n\,(Ze\,)u\,, \tag{2-1}$$

where n is the concentration of charge carriers with charge Ze and mobility u. This equation

assumes that conduction occurs predominantly by the transport of a single ionic species.

The mobility u may be related to a diffusion coefficient D by the Nernst-Einstein equation,

$$ukT = ZeD. \tag{2-2}$$

A diffusion coefficient for the mobile species may be obtained by assuming Boltzmann statistics for a model based on isolated jumps and random walks. In this model ions are visualized as vibrating within a potential well of energy E_m, at a characteristic vibrational frequency ν_o. The diffusion coefficient would depend on the jump distance, d, and on a geometrical factor, α,

$$D = \alpha d^2 \nu_o \exp(-E_m/kT). \tag{2-3}$$

The concentration of charge carriers depends on the formation of point defects either by a Schottky (cation and anion vacancy pairs) or a Frenkel (cation vacancy and interstitial pairs) process. In either case the defect concentration is given by

$$n = n_o \exp(-E_d/kT) \tag{2-4}$$

where E_d is 1/2 the defect-pair formation energy. The fraction of ions which are mobile, n/n_o, is often designated by the symbol, β. Since E_d is generally large ($E_d \sim 1$ eV: NaCl), the fraction of defect sites n/n_o is usually quite small. The overall equation of conductivity is given by substituting into Equation (2-1),

$$\sigma = \frac{n_o (Ze)^2 \alpha \beta d^2 \nu_o}{kT} \exp(-E_m/kT). \tag{2-5}$$

Modifications of this relation must be made for heavily doped solids in which n is fixed by the concentration of aliovalent additives, and care must be taken to include the degree of defect-impurity association. Due to the characteristic disorder of the mobile ion sublattice in FIC's, high defect concentrations are expected without need for thermal generation; thus, for FIC's β may be considered to be nearly independent of temperature, and the activation energy should represent that of migration alone.

The product of the factors contributing to the pre-exponential term in Equation (2-5) for FICs is generally many orders of magnitude lower than for conventional ionic conductors. However, the only parameters in Equation (2-5) which can be expected to vary greatly from one solid to the next are β and ν_o. The value of β in FICs is expected to be larger than in normal ionic conductors. Therefore, the value for the attempt frequency ν_o must be very low. This is consistent with a model where the mobile ions are assumed to reside in broad but very shallow potential wells. Even though this model ignores the cooperative motion between carriers, which can lead to higher conductivities than if isolated jumps alone are considered, it is generally accepted as the explanation for the Arrenius-like temperature dependence of ionic conductivity in glasses.

The disordered structure of glasses makes many of the parameters in Equation (2-5) difficult to specify and then to verify experimentally. For example, it is not likely that a particular type of glass would contain a single characteristic migration energy or attempt energy; it is more likely that the glass would be characterized by a distribution of these properties. Therefore, the values specified for each parameter in Equation (2-5) for FICs would represent an average for the ions in the lattice. These averaged parameters can rarely be known *a priori* and many times can only be estimated. Therefore, Equation (2-5) may not be very helpful in trying to understand general transport nor in comparing different ionic conductors with one another.

A more general and perhaps more useful form of Equation (2-5) may be written:

$$\sigma = (\sigma_o / T)\ exp\,(-E_a / kT)\ . \tag{2-6}$$

This general equation for ionic conductivity holds true for nearly all crystalline and vitreous conductors. The value of the energy of activation E_a and the pre-exponential term σ_o for a given conductor can be derived from a plot of $\ln \sigma T$ versus $1/T$ for that system. The value of E_a is found from the slope and the value of σ_o from the intercept. The values of σ_o and E_a for different materials could then be compared and correlated with their intrinsic properties in an attempt to understand what and how different properties influence the conductivity of a particular material.

2.3. Lithium Borate Glasses

2.3.1. Transport Properties

In their studies of structure-transport relationships of the lithium borate glasses, Tuller *et al.*, have found that the addition of Li_2O to B_2O_3 increases the lithium-ion conductivity by reducing the energy of activation.[19] Up to ~25 mol% Li_2O, the energy of activation decreases nearly linearly and is accompanied by sharp increases in the conductivity. Above 25 mol% Li_2O, the energy of activation and the conductivity exhibit less dependency on Li_2O content, and the pre-exponential term σ_o becomes nearly constant at ~5.4 $\Omega^{-1}cm^{-1}K$. The decrease of the energy of activation has been correlated with the oxygen to boron ratio; that is, as the O/B ratio increases the conductivity increases. The initial sharp increase in the conductivity has been attributed to Li_2O causing the trigonal BO_3 units, present in B_2O_3, to be converted into tetrahedral BO_4 units, thereby, increasing the network linkage of the glass.[20] This conclusion is supported by increases in the density and glass transformation temperatures.[21,22] The subsequent leveling off of the conductivity at ~ 25 mol% Li_2O was ascribed to the formation of non-bridging oxygens.

It was shown by Tuller *et al.* that the conductivity of lithium borate glasses could also be increased by adding LiCl. During their research, they examined the effects that Cl had on the conductivity by adding LiCl to glasses of fixed O/B ratios and to glasses of fixed Li_2Z compositions where Z represents Cl_2 or O. In this way, they were able to separate the effects of O/B ratios, borate structures, and Cl/O ratios. They found, in both cases, that the addition of LiCl increased the glass conductivity. This increase in conductivity was attributed mostly to decrease in the energy of activation rather than an increase in the pre-exponential term.[19] In contrast to earlier studies which implied no changes in B-O network upon addition of Cl, Tuller found substantial changes in the glass B-O network, as suggested by variations in the density and glass transformation temperatures. These changes were not believed to be caused by Cl^- ions directly entering the borate framework but rather by being inserted into the interstices. This conclusion was in agreement with Raman, Infrared IR, and Electron Spin Resonance ESR results which show that Cl does not directly enter into the B-O network. Figure 2-1 is a plot according to Tuller *et*

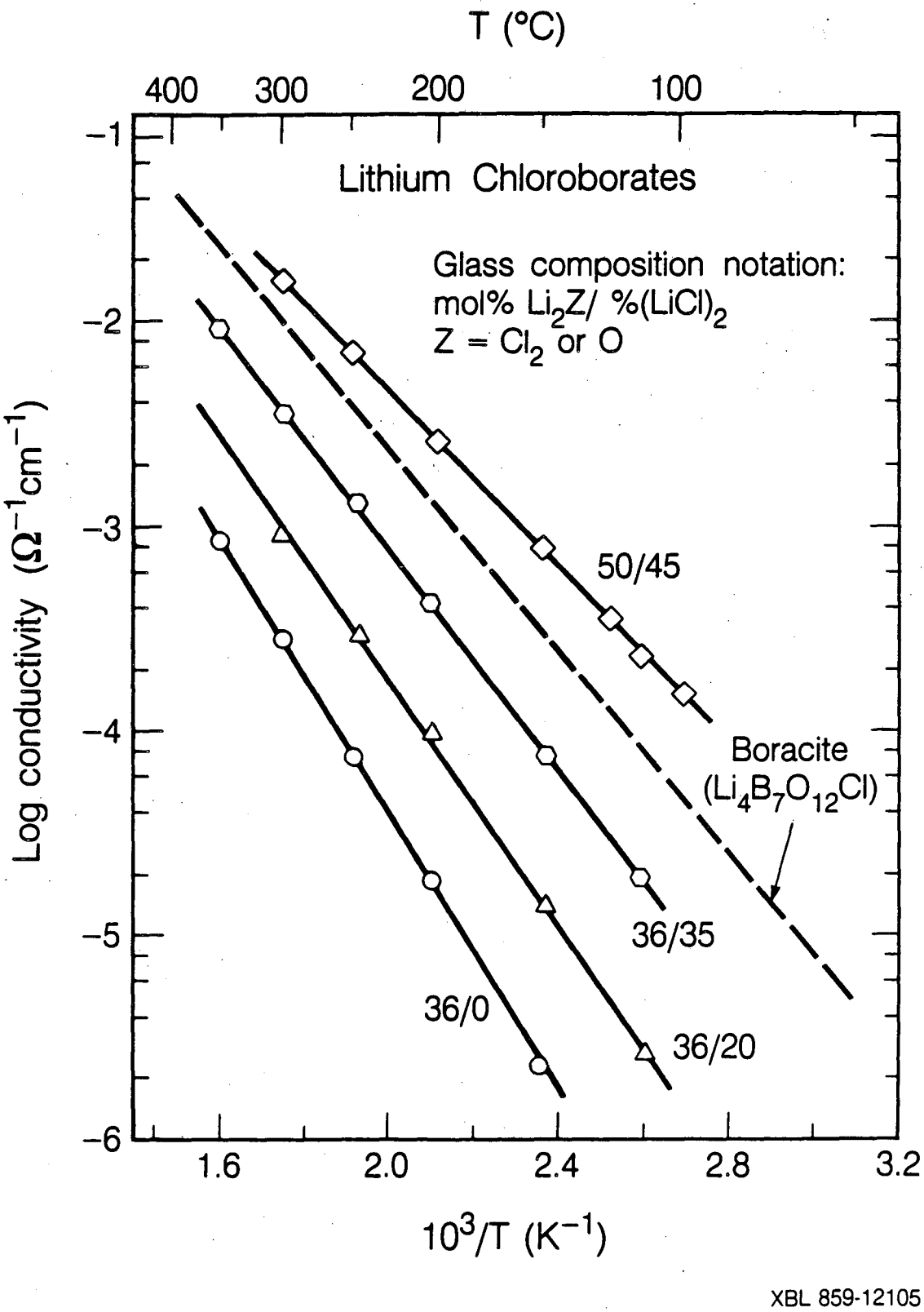

Figure 2-1. Logarithm of ionic conductivity versus inverse temperature for a series of lithium chloroborate glasses (1).

al. of the ionic conductivity versus $1/T$ for different ratios of $\left(\frac{Li_2Z}{Li_2Cl_2}\right)$ where Z is Cl_2 or O. A comparison of the ionic conductivities for the different glass compositions shown in Figure 2-1 demonstrates the trend that the addition of LiCl and Li_2O each increases the lithium-ion conductivity of the glass.

The range over which the conductivities of lithium borate glasses continue to increase with the addition of Li_2O and LiCl is limited by how much Li_2O and LiCl can be added before the glass devitrifies. That is, there is a limit to how much Li_2O and LiCl can be added, after which the melt has a strong tendency to crystallize and/or form two immiscible liquids. The addition of the Li_2O has been traced to increasing the tendency of the glass to crystallize while the amount of LiCl that can be added was found to be limited by the onset of two immiscible liquids. There are two factors affecting how much Li_2O can be added before causing the glass to crystallize. The first factor is the cooling rate of the glass; the more quickly molten glass is quenched the less likely it is to crystallize. The second factor which affects the formation of crystals in the glass is the addition of compounds which inhibit the propagation of crystal growth. Two compounds which are commonly used to suppress the formation of crystals in borate glasses are SiO_2 and Al_2O_3. Typically less than 2 mol% of either compound is added to suppress the formation of crystals. The highest composition of Li_2O reported for vitreous lithium borate was approximately 65 mol% Li_2O.

The factor which affects the amount of LiCl which can be added to lithium borate glass is the solubility of Cl as related to the O/B ratio and the ability of the network to accommodate Cl^- ions into its interstices.[19] As the composition of Li_2O is increased, the amount of LiCl which can be added is also increased. The value reported by Tuller *et al.* for the maximum ratio of LiCl to Li_2Z was $\sim$ 35 mol% $(LiCl)_2/Li_2Z$. This corresponds to approximately 12.7 mol% $(LiCl)_2$ coupled with 23.4 mol% Li_2O and 63.6 mol% B_2O_3. These values are in general agreement with the values reported by Takahashi[23] but significantly lower than the value reported by Levasseur *et al.*[24] However, Levasseur reported the vitreous domain to be limited by the formation of cubic LiCl micro-crystals rather than liquid-liquid immiscibility.

2.3.2. Corrosion Characteristics

The rates of dissolution and attack of lithium borate glasses by water and by molten lithium, respectively, have been studied by Tuller *et al.*[17] A summary of their findings in buffered solution with pH 7 at 30 °C is shown in Figure 2-2. The rate of dissolution of lithium borate glass in water varies as the mole percents of Li_2O and LiCl are changed. The rates shown for the compositions studied by Tuller *et al.* range from 10^{-4} to 10^{-6} g/cm^2·sec. These rates are high enough to suspect that moisture might cause damage to the glasses. Therefore, the glasses should be handled and stored in a dry atmosphere.

The studies done by Tuller *et al.* on the resistance of lithium borate glasses to attack by molten lithium were performed in molten lithium alloys of various lithium activities. They reported that the glasses were attacked by lithium, as demonstrated by the growth of a black reaction layer. The formation of this reaction layer was observed to occur in the presence of Li-Al with a lithium activity of $\sim 10^{-2.82}$ and in the presence of Li-Sn with a lithium activity as low as $\sim 10^{-9}$. However, the rates of attack were significantly lower for the lower activities than they were in pure lithium. The composition of the black corrosion layer has been identified as crystalline $3Li_2O \cdot B_2O_3$.

It was found that the formation of the layer did not interfere with the passage of current nor did it affect the measured cell potentials. These two facts led to the conclusion that the reaction layer was ionic in nature and, therefore, did not interfere with the conductivity. Unfortunately, the thickness of the layer was found to grow parabolically with time, and the volume mismatch between it and the glass substate would eventually cause the glass to crack. Figure 2-3 is a plot of measured and extrapolated values of the rate of attack k (mm^2/h) versus composition at 200 and 230 °C for the ternary system of lithium chloroborate glasses. Addition of Cl at 230 °C is seen to increase the reaction rate with high B_2O_3 content but to decrease the rate with low B_2O_3 rate.

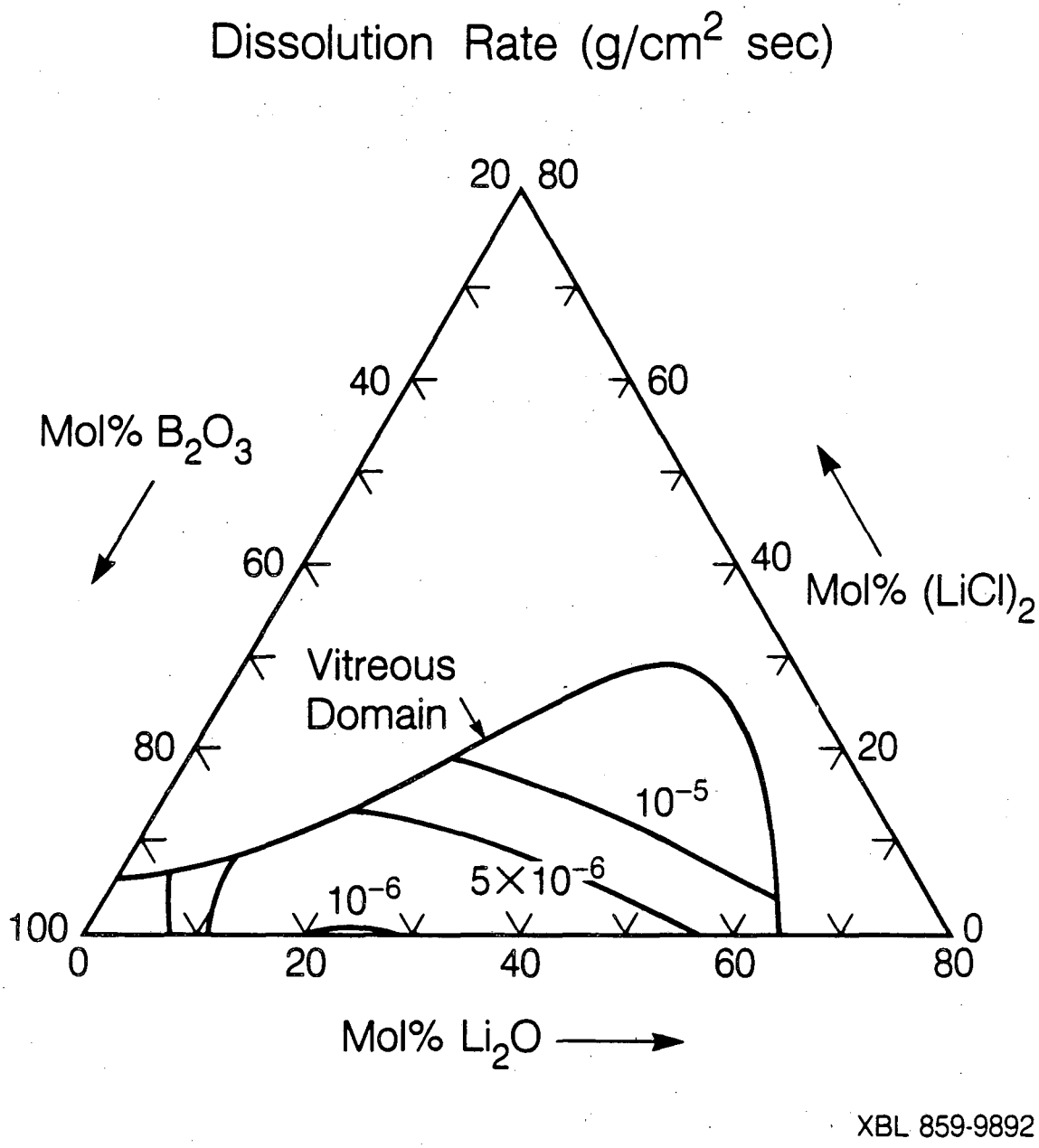

Figure 2-2. Dissolution rate of lithium chloroborate glasses in buffered solutions of pH 7 at 30 °C (17).

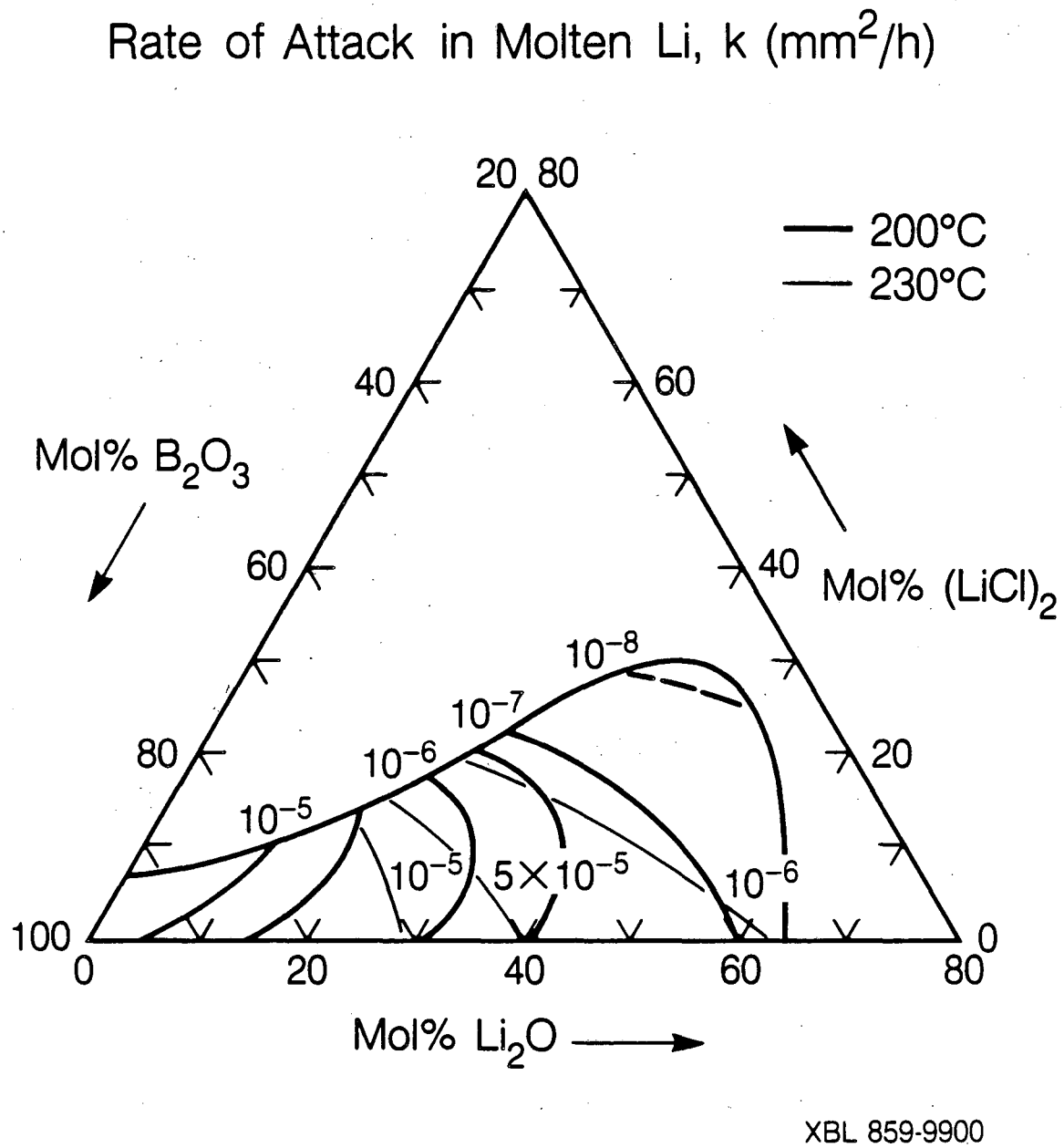

Figure 2-3. Rate of attack of lithium chloroborate glasses in molten lithium (17).

2.3.3. Other Properties

Along with their studies of conductivity and stability of various lithium borate glasses, Tuller *et al.* have examined the effects of varying the glass composition on the glass transition temperature and density. The results of Tuller's work are shown in Figures 2-4 and 2-5 as plots of glass transition temperature and density, respectively, versus the O/B ratios. The effects that composition has on these two properties show similar trends with a slight shift of the O/B ratio. The transition temperature and density reach a maximum at ~30 and 40 mol% Li_2O, respectively. This corresponds to approximately the saturation point of the trigonal BO_3 units transforming into tetrahedral BO_4 units. As explained in section 2.3.1, the addition of Li_2O beyond the saturation point results in the formation of non-bridging oxygens and a resultant decrease in the transition temperature and density.

Figures 2-4 and 2-5 also show that the addition of LiCl to the glass has the effect of lowering the transition temperature and density. This is true for the addition of LiCl to glasses where the O/B ratios are held constant and for glasses were the composition Li_2Z is held constant. An explanation for the decrease in the transition temperature and the density with the addition of LiCl can be given in terms of the weak electrolyte theory by stating that there would be a "decrease in the dissociation energy based on a decreased binding energy between Li^+ and Cl^- as opposed to Li^+ and BO^- complexes in the simple binary glass."[19] Therefore, the Cl^- ions would cause the borate network to be more spread out, which in turn would cause the density and glass transition temperatures to be decreased.

From the discussion on the properties of lithium borate glass and how they are affected by compositional variations, it appears that there is a range of glass compositions for which the restrictions on conductivity, resistivity to lithium attack, transition temperature, and vitreous domain can be satisfied. Thus, the glass appears to be an attractive candidate for use as an electrolyte in a high-temperature Li/S cell; however, nothing has previously been reported on the stability of the glasses in the presence of sulfur or lithium polysulfides.

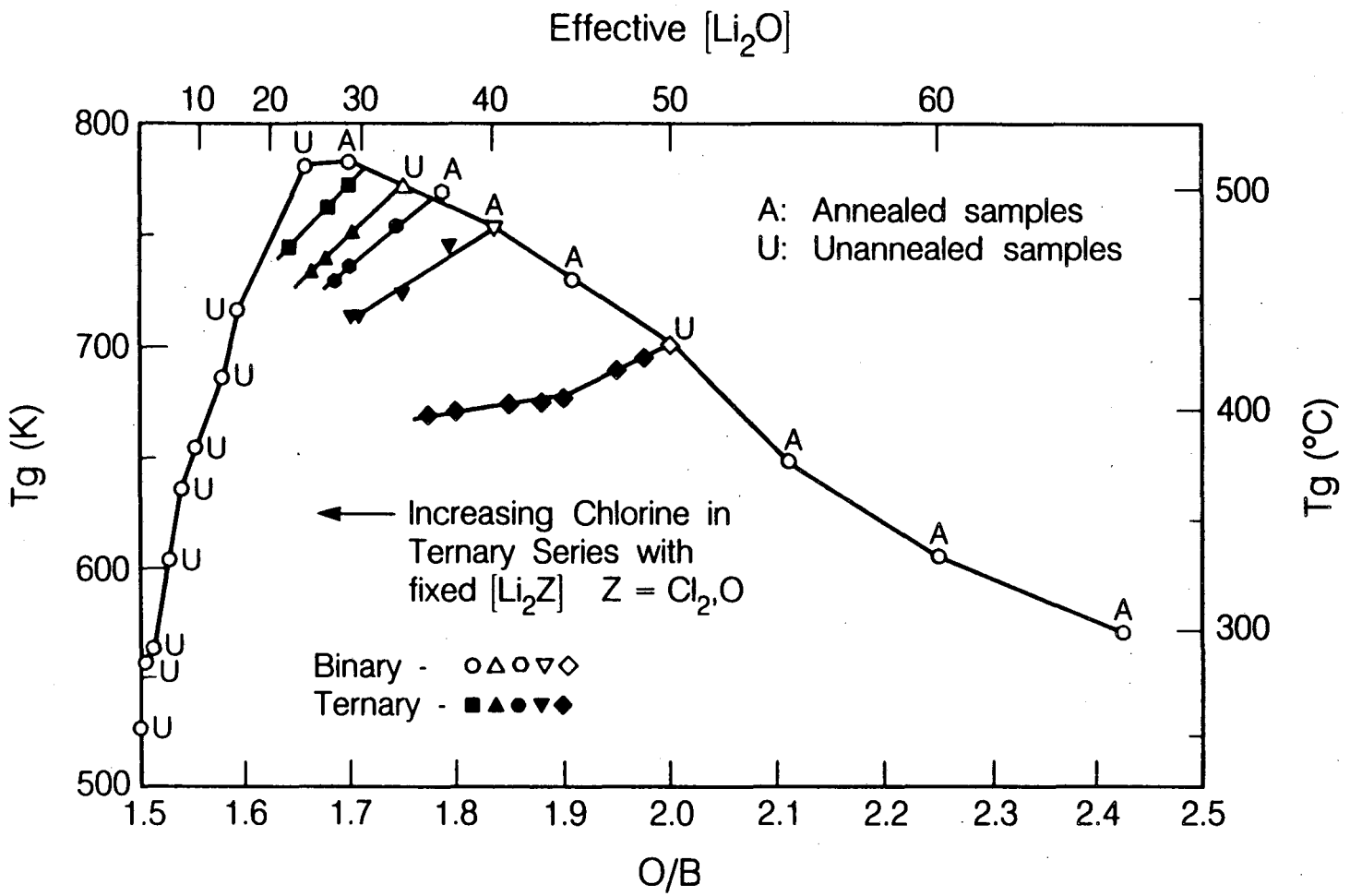

XBL 859-12102

Figure 2-4. Transition temperature versus O/B ratios in lithium chloroborate glasses (1).

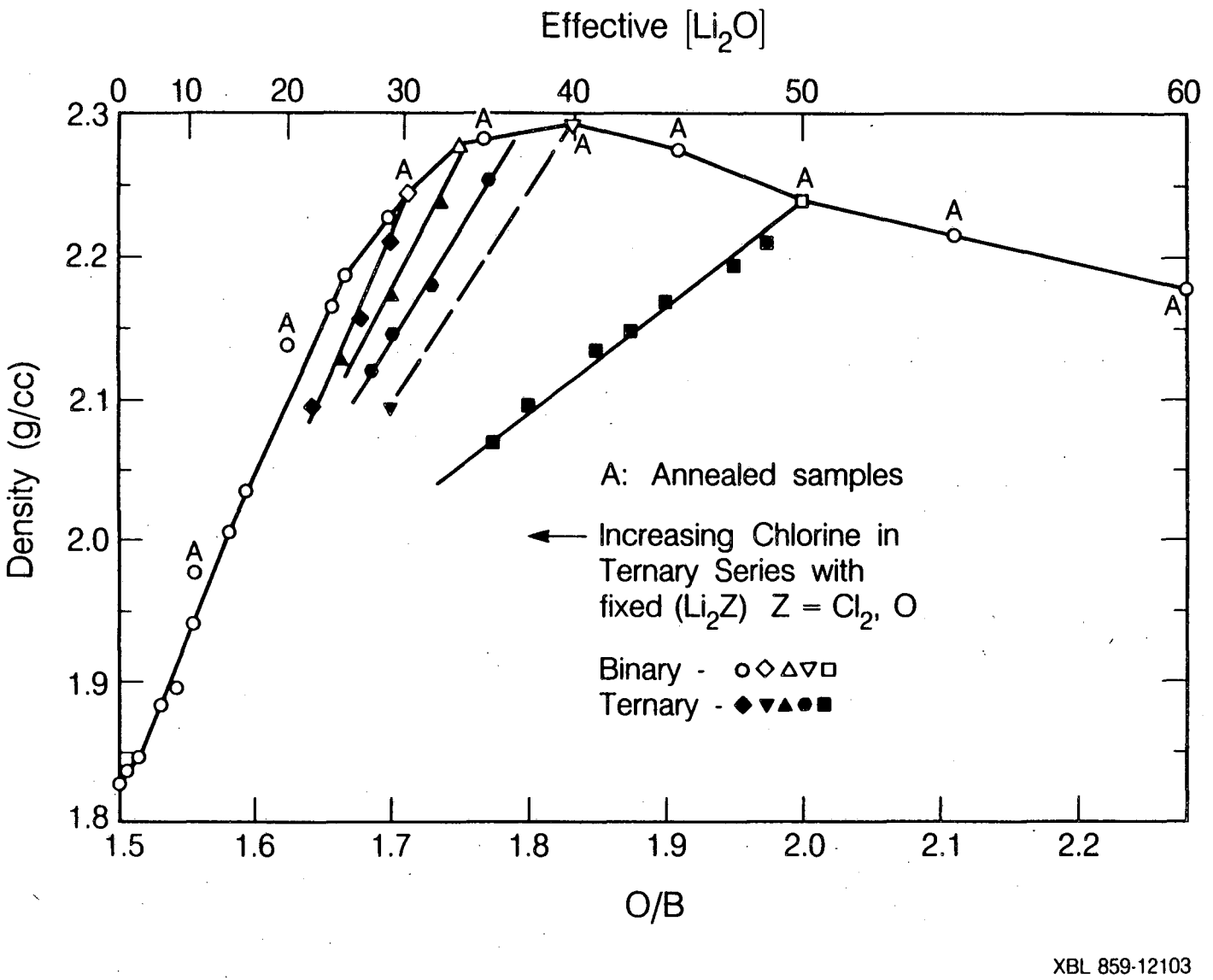

Figure 2-5. Density versus O/B ratios in lithium borate and lithium chloroborate glasses (1).

CHAPTER 3

STATIC TESTS

3.1. Introduction

The high lithium-ion conductivity of lithium borate glasses makes them natural choices for use as electrolytes in high-temperature lithium batteries. The research being done by Tuller *et al.*[1,17-20] on the lithium borate glasses has been focused mainly on maximizing their conductivity and examining their stability to molten lithium alloys of different lithium activities. Before a particular glass can be considered seriously as an electrolyte for a lithium battery, it also needs to be tested for its stability to the material used as the positive electrode. The static tests performed in this work were designed to test the resistance of lithium borate glass to attack by sulfur and polysulfides. These tests were divided into two groups. The first group was a screening of the various kinds of lithium borate glasses to determine which ones were resistive to attack by sulfur. Based on the results of this group of experiments, one composition of lithium borate glass was selected for further testing. The second group of experiments was designed to be a more thorough examination of the reaction between the glass which was chosen, lithium chloroborate glass, and sulfur-polysulfide mixtures.

3.2. Screening Experiments

3.2.1. Experimental Procedure

The preliminary screening experiments involved testing several types of lithium borate glasses for their resistance to attack by sulfur. The pieces of glass tested had been prepared at MIT and sent to LBL as samples. They were hygroscopic and, therefore, had to be stored in a dry-atmosphere container. The pieces of glass were of random size and shape and represented three types of lithium borate glasses: lithium borate, lithium chloroborate, and lithium sulfoborate. The pieces of glass were loaded into evacuated pyrex ampoules, which were partially

filled with sulfur, and placed in a 400 °C temperature-controlled furnace. After approximately two weeks in the furnace, the ampoules were removed and allowed to cool. After cooling, the pieces of glass were removed from the ampoules, cleaned, weighed, and then examined for shape and color changes. A more thorough description of this procedure is given in section 3.3.2.3.

3.2.2. Results of Screening Experiments

The three glasses tested for stability in the presence of molten sulfur were lithium borate, lithium chloroborate, and lithium sulfoborate. The lithium borate glass was 20 mol% Li_2O and 80 mol% B_2O_3; the lithium chloroborate glass was 11.6 mol% $(LiCl)_2$, 21.4 mol% Li_2O, and 67.0 mol% B_2O_3; and the lithium sulfoborate glass was 15 mol% Li_2SO_4, 35 mol% Li_2O, and 50 mol% B_2O_3. The glass samples were placed in molten sulfur and left for 288 hours (12 days). After this period of time the discs were cleaned, and the following observations were made: first, the lithium sulfoborate sample was covered with a white film which would not dissolve in CS_2 or methanol. The weight gain of this sample was very slight; only 8 mg or 1.4% of the weight of the sample. The other two glass samples showed no visible changes or weight gain. It appeared that the lithium borate and lithium chloroborate glasses were equally resistive to attack by pure sulfur. Table 3-1 is a summary of the results.

Table 3-1 Summary of Preliminary Static Corrosion Tests: 288 hr in Sulfur at 400°C

	Composition	Weight Change	Film Formation
Lithium Borate	20.0 mol% Li_2O 80.0 mol% B_2O_3	no change	none
Lithium Chloroborate	11.6 mol% Li_2Cl_2 21.4 mol% Li_2O 67.0 mol% B_2O_3	no change	none
Lithium Sulfoborate	15.0 mol% Li_2SO_4 35.0 mol% Li_2O 50.0 mol% B_2O_3	gained 8 mg	white film

3.2.3. Discussion of Selection

The lithium borate and lithium chloroborate glasses examined in this screening experiment appeared to be equally resistive to attack by pure sulfur. To make a selection, it was necessary to consider and compare other important characteristics of the two glasses. The properties considered to be important in making the selection were conductivity, resistance to lithium attack, transition temperature, and vitreous domain. A presentation of how these properties are affected by variations in composition is given in section 2.3.

For application as an electrolyte in a Li/S cell the following restrictions for choosing a composition can be imposed: the conductivity should be as high as possible with $\sim 10^{-3}$ ($\Omega^{-1}cm^{-1}$) being determined to be the lowest acceptable value, the resistance to attack by lithium should be as high as possible, the transition temperature of the glass must be at least 50 °C above the operating temperature of the cell (400 °C), and finally the composition must be in the vitreous domain. Figure 3-1 shows the results of imposing the above restrictions on the glass properties shown in Figures 2-1, 2-3, and 2-4 and then overlaying the windows of feasibility to identify one final range of workable compositions. The glass chosen for testing in the second part of the static corrosion tests was a lithium chloroborate glass with a composition of 11.6 mol% Li_2Cl_2, 21.4 mol% Li_2O, and 67.0 mol% B_2O_3. This falls slightly above the center of the window shown in Figure 3-1.

3.3. Sulfur/Polysulfide Corrosion Tests

3.3.1. Introduction

The sulfur-polysulfide corrosion tests employed two fabrication procedures. The first procedure was to prepare and form the lithium chloroborate glass into discs. These discs were suspended in either molten sulfur or some fixed composition of lithium polysulfides and sealed in quartz ampoules. After the desired length of time, the ampoules were removed from the furnace, allowed to cool, and cracked open. The discs were then soaked in carbon disulfide (CS_2) and finally in methanol to remove the excess sulfur and polysulfides. These cleaned discs were

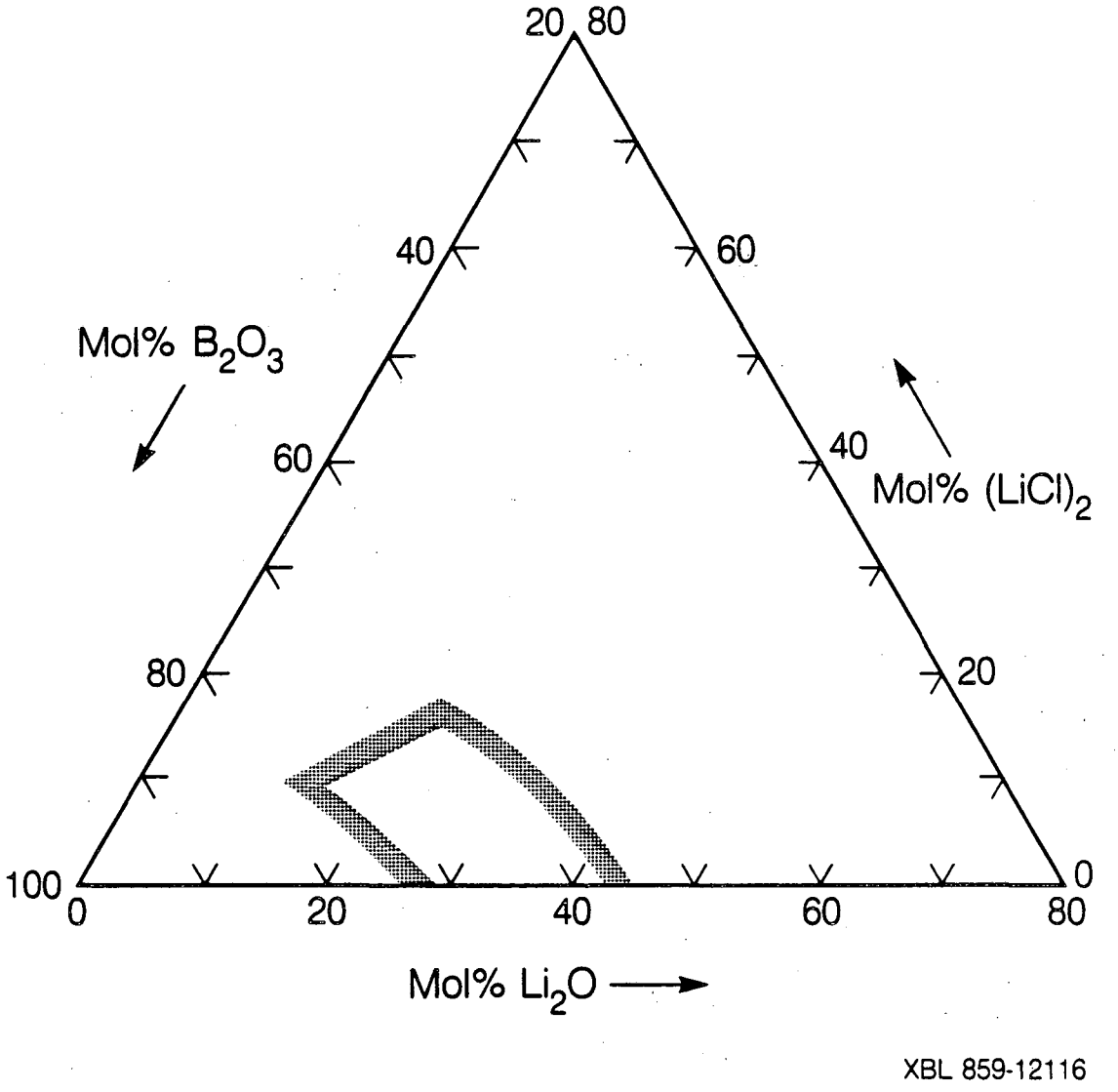

Figure 3-1. Lithium chloroborate ternary phase diagram with window of compositional feasibility for use in Li/S cells.

weighed and examined for shape and color changes. Any reaction layer formed was examined with an X-ray diffractometer to identify crystalline materials.

The second fabrication procedure involved forming the glass into thin-walled tubes. The tubes were filled with sulfur or some premixed sulfur-polysulfide composition, sealed to prevent sulfur vapor from escaping, and then heated for some known length of time. The reaction layer on the walls of these tubes was scraped off and analyzed under an X-ray diffractometer.

3.3.2. Experimental Procedure

3.3.2.1. Inert Atmosphere Specification

The storage and handling of lithium, lithium polysulfides, and the glass-forming chemicals was carried out in a Dri-Lab model DL 002-D-P four-station helium-filled glove box, with a vacuum ante-chamber. This glove box and its ancillary equipment were manufactured by Vacuum Atmospheres Corporation (VAC). Pedatrol and Safe-Trol pressure control systems, from VAC, were included for convenience and safety. The helium atmosphere of the glove box was continuously purified of water, oxygen, and nitrogen with a VAC model MO40-2 Dri-Train and a VAC model NI-2 Ni-Train. A VAC model AO 316-H Oxygen Analyzer, with a model A A-1 Audio Alarm, was added as a safety precaution to protect the Ni-Train. Also in-line with the glove box was a 5880A Hewlett Packard gas chromatograph equipped with a thermal conductivity detector and a 305 cm x 0.3 cm molecular-sieve column. This column was chosen because of its ability to separate oxygen from nitrogen. The concentrations of oxygen and nitrogen were measured hourly and found to be on the order of 1 ppm. Also, periodically a 183 cm x 0.3 cm poropak Q column was placed in the gas chromatograph. This column, though not able to separate oxygen from nitrogen, is useful for detecting water in low concentrations. No more than 1 ppm of water was ever detected.

Two 15-cm diameter by 41-cm deep furnace wells were mounted on the floor of the glove box. The temperatures in these furnace wells were independently controlled by model 61010 Panel Packers from Research, Inc. To offset any temperature increases in the box, a VAC model

DK-3E Dri-kool refrigeration unit was installed. Figure 3-2 is a photograph of the glove box.

3.3.2.2. Glass Formation

3.3.2.2.1. Glass Preparation

The chemicals used to prepare the glass were: 99.9% lithium chloride, LiCl, from Mallinckrodt, 99.9% lithium oxide, Li_2O, from Cerac, and 99% pure anhydrous boron oxide, B_2O_3, from Spectrum Chemicals Mfg. Corp. These chemicals are all hygroscopic and, therefore, were stored in the helium-atmosphere glove box. However, the high temperature required and large vapor losses observed during heating made it necessary to prepare the glass outside of the glove box. It was found that, even though the handling of boron oxide outside of the glove box was minimized, it hydrated appreciably. This problem made it necessary to deviate slightly from the glass-forming procedure outlined by Button *et al.*[19] The following is the modified procedure used to prepare glasses of the desired compositions.

First, approximately 40 grams of boron oxide were poured into a 100-ml platinum crucible and heated above 500 °C until all signs of bubbling had ceased. It was assumed that what remained after bubbling was anhydrous boron oxide. An accurate weight of boron oxide was determined by weighing the full crucible and subtracting from this the known weight of the empty crucible. Next, the appropriate amounts of lithium oxide and lithium chloride were added to the crucible. The nominal composition of the glass used for this study was, 11.6 mol% $(LiCl)_2$, 21.4 mol% Li_2O, and 67.0 mol% B_2O_3. The crucible was then put into the furnace for 15-20 minutes at approximately 950 °C. After this first heating, the crucible was removed from the furnace, and the molten glass was stirred with a platinum rod. The glass was reheated for a second 15-20 minute period, stirred, and then returned to the furnace for a final 20-30 minute period. After this final heating, the glass could be either poured into a mold and made into discs or it could be placed in the glove box where it was stored until ready to be blown into tubes.

The addition of lithium chloride to the molten lithium borate glass at 800-1000 °C caused a heavy vapor to be released from the melt. Therefore, the heating was performed in a well-vented fume hood and a platinum lid was placed over the crucible to minimize the loss. Even with this

CBB 858-6511

Figure 3-2. Photograph of helium atmosphere glove box with purification system.

precaution, the weight of the glass remaining in the crucible after heating was found to be roughly 1-2% less than the weight of the starting materials. For this reason, the glass was dissolved in a nitric acid solution and then analyzed for Li, B, and Cl content by atomic absorption spectroscopy. It was found to be lower in LiCl than expected. Therefore, the reported glass composition was the concentration determined by atomic absorption spectroscopy rather than the nominal concentration. The composition of the lithium chloroborate glass as analyzed by atomic absorption spectroscopy was 7.3 mol% $(LiCl)_2$, 25.7 mol% Li_2O, and 67.0 mol% B_2O_3.

3.3.2.2.2. Discs

Immediately following the final heating described in the previous section, the molten glass (to be made into discs) was poured into a stainless-steel mold which had been pre-heated to 100-200 °C. The mold consisted of two 0.64 cm x 10 cm x 10 cm pieces of stainless steel stacked on top of one another. The bottom plate served as the base while the top plate, which had four 2.5 cm diameter holes drilled through it, served as the mold and provided spaces for four discs to be made at once. The glass discs were allowed to cool and solidify before being removed from the mold and placed in the helium-atmosphere glove box. The result of this disc preparation procedure was the formation of lithium chloroborate glass discs approximately 0.5 cm thick by 2.5 cm diameter. Because of the hygroscopic nature of the glass, great care was taken not to handle the glass discs directly nor leave them in a moist environment any longer than necessary.

3.3.2.2.3. Tubes

The formation of thin-walled tubes required that a glass-blowing technique for lithium chloroborate glass be developed. It was found that once the molten glass cooled, it could not be re-heated to its softening temperature and blown into shapes without causing the glass to crystallize. Therefore, the tubes had to be formed from the molten glass before it was allowed to cool. The procedure for making these tubes was as follows: first, the platinum crucible full of molten glass at approximately 1000 °C was placed in a pre-heated 700 °C stainless-steel block. The high temperatures and heavy vapor losses made it necessary to make the glass tubes outside of the

glove box. After the molten glass was put into the stainless steel block, it was allowed to cool to about 700 °C, where its viscosity was approximately that of a heavy syrup. At this point, a flame-heated pyrex tube (~10 mm O.D.) was dipped into the molten glass and gently stirred to ensure wetting of the pyrex tube by the molten glass. Once the pyrex tube was completely wetted by the molten glass, it was pulled from the crucible while blowing a steady pressure of air into the other end of the pyrex tube. This resulted in pulling, with the pyrex, a constant-diameter tube of the molten glass. As it was pulled up, the molten glass would quickly cool and solidify into a rigid tube. Figure 3-3 is a photograph of a glass tube being pulled from the platinum crucible. As an attempt to eliminate some of the contact between the lithium chloroborate glass and air (or water), a steady pressure of argon gas was used to blow into the pyrex tube. However, there was no evidence that this procedure improved any of the properties of the glass, so it was discontinued. These tubes were drawn in lengths of 10-60 cm before the ends were allowed to close and be pulled away from the molten glass. After the tubes were allowed to cool, they were cut into lengths of roughly 10 cm, and then one end was sealed over the flame of a Bunsen burner. The wall thickness of these tubes varied from tube to tube, and to a lesser degree, along the length of each tube. The thickness was directly related to how hot and, thereby, how viscous the melt had been. The hotter the melt, the lower the viscosity and, therefore, the thinner the walls. The thinnest-walled tubes were approximately 0.02 cm thick while the thickest-walled tubes used were approximately 0.05 cm thick. Because these tubes were hygroscopic, they were stored in either a vacuum desiccator or in the helium glove box.

3.3.2.3. Ampoule Testing

Figure 3-4 shows a schematic drawing of a quartz ampoule used to test the stability of the lithium chloroborate glass discs in the presence of sulfur or lithium polysulfides. The first step in preparing the quartz ampoules was to load and seal the glass discs inside the ampoules. The sealing together of the ampoules and their necks was done with an acetylene torch and, therefore, had to be done outside of the helium glove box. After sealing, the ampoules were loaded into the helium-atmosphere glove box where they were partially filled with sulfur or lithium polysulfides.

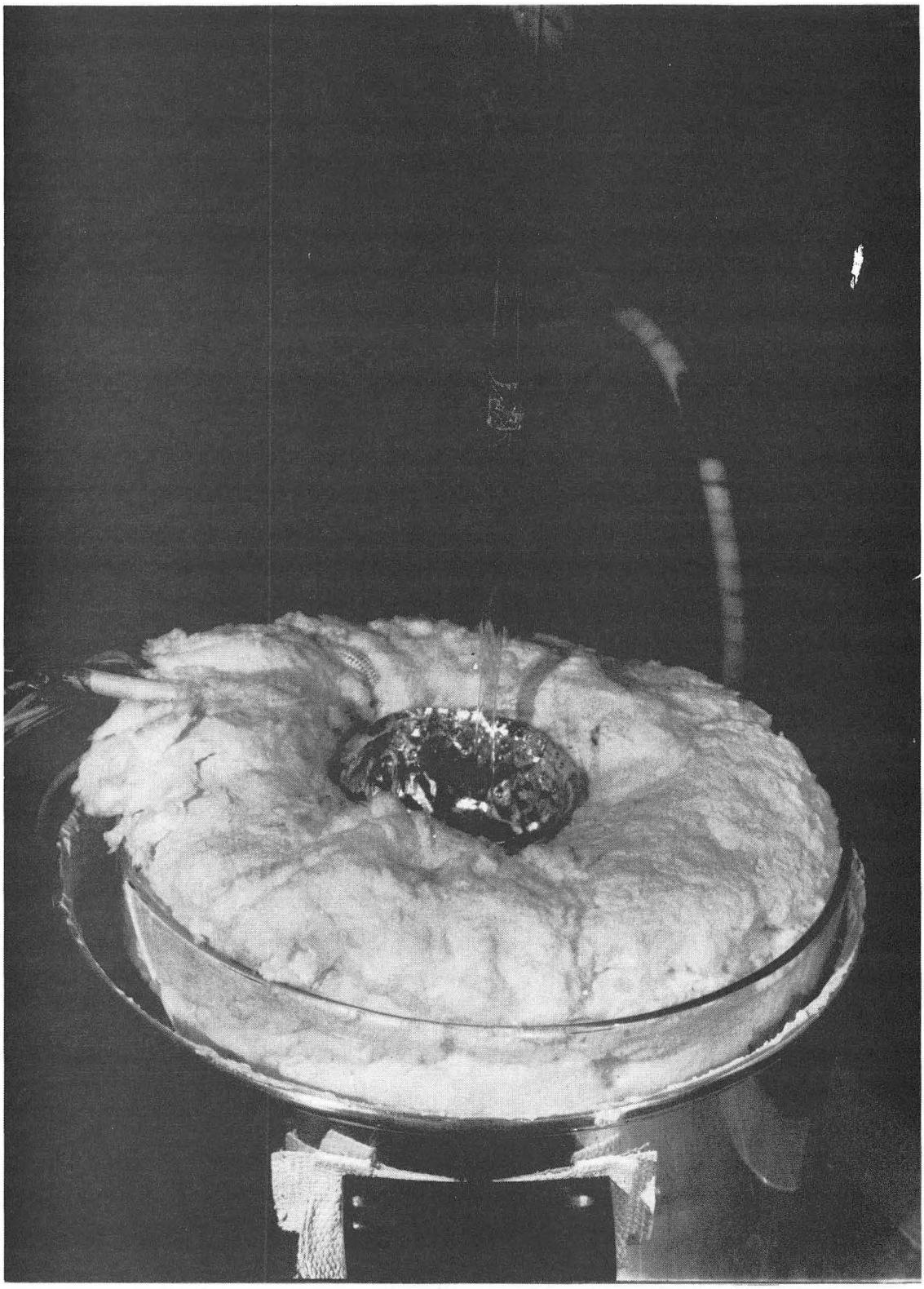

CBB 858-6505

Figure 3-3. Photograph of lithium chloroborate glass tube being drawn from a crucible containing molten glass.

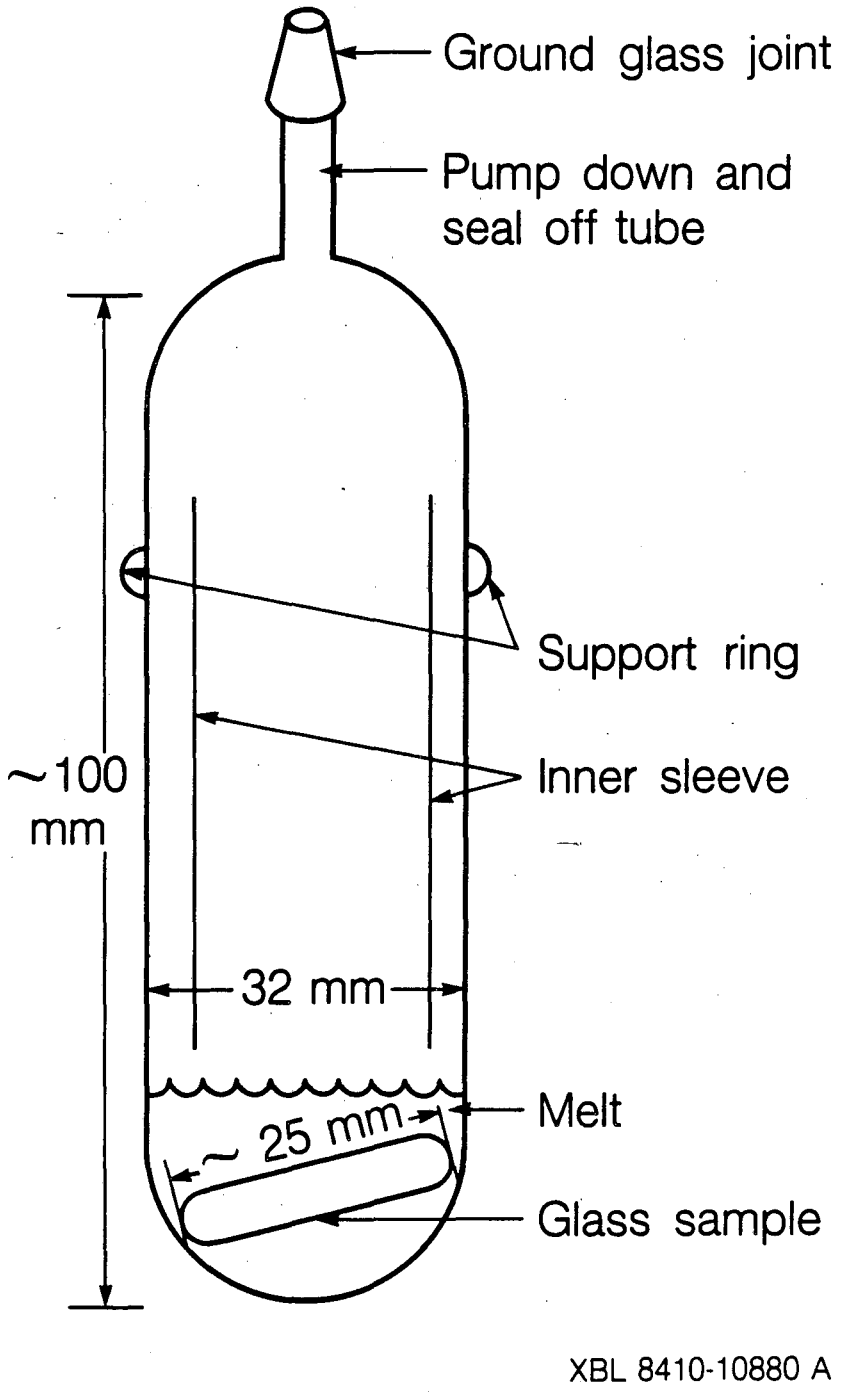

Figure 3-4. Schematic diagram of static corrosion ampoule.

The sulfur was reported by NOAH Chemical Co. to be 99.999% pure, and the lithium sulfide, Li_2S, was reported by Cerac to be 99.9% pure. The necks of the ampoules were cleaned with a cotton swab to remove any adhering sulfur or polysulfides. This was necessary to prevent the sulfur/polysulfides from interfering with the seal. A polytetrafluoroethylene stopcock was attached to the ampoules via a ground-glass joint at the end of ampoules' neck. A vacuum line was attached to the stopcock, and the ampoules were evacuated to approximately 0.1 atmosphere of helium. The stopcock was then closed to maintain the vacuum, and the ampoules were removed from the glove box. With an acetylene torch, the ampoules were then sealed off at the pump-down tube. The vacuum in the ampoules was verified by watching the behavior of the glass walls during melting. If the softened glass was drawn inwards, then the vacuum was assumed to be intact.

After loading, evacuating, and sealing, the ampoules were put into a 400 °C temperature-controlled furnace. In order to ensure a more uniform and constant temperature profile than that which the furnace could provide, a large aluminum block in which holes were drilled was placed into the furnace. The ampoules were placed in these holes and, thereby, any minor temperature fluctuations caused by the furnace temperature controller were not propagated to the ampoules. The temperature of the aluminum block was measured with a chromel-alumel thermocouple and found to be constant to ±1 degree Celsius.

The rings on the outside of the ampoules and the sleeves on the inside were added to simplify the cleaning of the discs. The rings supported the ampoules in an inverted position while the sleeves held the discs out of the pool of sulfur/polysulfides and allowed the excess fluid to drain from the discs.

3.3.2.4. Post-Test Examination

3.3.2.4.1. Discs

After the molten sulfur-polysulfides were allowed to drain from the discs and cool to room temperature, the ampoules were cracked open. The discs were immediately soaked in carbon disulfide and then methanol to remove any excess sulfur or polysulfides. Various discs were left in

the two solvents for differing lengths of time to determine how quickly the sulfur and polysulfides would dissolve from the discs. It was found by weight-change measurements that most of the sulfur and polysulfides dissolved very quickly. The extra amount of material that was removed by leaving the discs in CS_2 for hours, as compared with a few minutes, was negligible. However, when left in methanol for long periods of time, the discs would continue to lose weight at a slow but significant rate. Therefore, a standardized cleaning procedure that included a 20-minute soak in methanol was established. After the discs were cleaned, they were carefully weighed and examined for shape and color changes. The compositions of the reaction layers from these discs were analyzed using an X-ray diffractometer.

3.3.2.4.2. Tubes

The corrosion experiments on lithium chloroborate glass were extended to tubes to see whether the attack by lithium polysulfides would cause failure of the thin-walled tubes. The walls of the tubes were so thin that any destructive corrosion would have caused the tubes to fail, so such tests represent rapid screening experiments. In a qualitative fashion, the presence of a non-destructive reaction layer could be observed by tilting the hot tube to one side and allowing the bulk of the melt to drain to the other end. This exposed any reaction layer which had formed on the walls of the tubes. By cooling the tubes in this position, the exposed films could be scraped off and analyzed with an X-ray diffractometer. Because the pieces of film scraped from these tubes were so small, they could not be soaked in either CS_2 or methanol without being lost. Consequently, they were doubtless covered with excess sulfur; this was expected to be manifested in the X-ray diffraction patterns.

3.3.2.4.3. X-ray Diffraction

The crystalline compounds present in the reaction layers were identified by powder X-ray diffraction. The X-ray diffraction samples were prepared by carefully scraping the reaction layers off the glass samples and grinding them into powders in an agate mortar and pestle. Some of the lithium, borate, and sulfide compounds present in the reaction layers were hygroscopic; therefore,

the preparation of the samples for X-ray analysis was done in the glove box. The X-ray diffractometer used to analyze the powdered reaction layers was a Siemens model D-500, which was set up to run samples at ambient conditions. Unfortunately, this provided the means for some of the unstable compounds to hydrolyze or decompose before being identified. The tendency for this to occur could be observed by analyzing a sample of powder in the X-ray diffractometer and then, after 10-15 minutes, repeating the analysis with the same sample. The peaks on the X-ray pattern associated with anhydrous compounds were observed to shrink with time while the peaks associated with hydrates would grow; an example was Li_2O converting to LiOH. Although this phenomenon made it possible to identify some compounds positively, it also could prevent the identification of some others. Therefore, to minimize this problem, the samples were run through the diffractometer very quickly and very soon after being exposed to air.

There was another complicating factor in attempting to interpret the X-ray patterns obtained from the powdered reaction layers. There is a large number of lithium, borate, and sulfide compounds which could have been present in the reaction film. Although no two chemical compounds have exactly the same X-ray pattern with exactly the same relative intensities, there are similarities. For example, compounds with similar crystal structures can have similar X-ray patterns with many areas of overlap. Among the many potential lithium, borate, and sulfide compounds, there were many overlapping peaks and areas of uncertainity. When peaks from different compounds overlapped, the intensities of the resulting peaks did not match the reported relative intensities for either compound. This made it difficult to identify which of the potential compounds were represented in a given X-ray pattern. There were usually several compounds which could have been partially responsible for a given X-ray pattern. Furthermore, the X-ray patterns obtained from the reaction layers contained relatively noisy base lines. This made it possible to confuse some of the smaller peaks of candidate compounds with noise in the base line.

The convention that was followed in identifying which compounds were present in the reaction layers was to make a list of the potential compounds and indicate to what level of confidence their presence was confirmed. For example, if the three major peaks reported for the X-ray pattern of a given compound matched with major peaks on the X-ray pattern of the sample, then

that compound was reported to be one of the reaction products, with a high degree of confidence. If the peaks appeared slightly shifted, then the confidence level was lower.

One compound that was not expected to be formed, based on the thermodynamics of a reaction between the glass and lithium polysulfides, was lithium sulfate, Li_2SO_4. However, the formation of Li_2SO_4 would be likely if any absorbed oxygen was present. Therefore, Li_2SO_4 was included as one of the potential compounds in the reaction layer but not necessarily one of the potential reaction products. Furthermore, only trace amounts of it were expected.

3.3.3. Results of Sulfur/Polysulfide Corrosion

3.3.3.1. Corrosion Data

The tests concerning the attack of lithium chloroborate glass by sulfur and lithium polysulfides were carried out in two parts. The first part involved suspending some glass discs in sulfur or a sulfur/polysulfide mixture and checking for corrosion. The second tests involved filling some thin-walled test tubes with sulfur/polysulfide and noting the reactions. The results of these tests, when done with pure sulfur, were similar to the results reported in the previous section (Section 3.2.2) for lithium chloroborate glass, i.e. there was no apparent reaction between pure sulfur and lithium chloroborate glass. However, the results with the lithium polysulfides were different. A reaction layer was observed to form on the glass when it was tested with lithium polysulfides. Table 3-2 is a summary of the results of tests between lithium chloroborate glass and sulfur/polysulfides.

Table 3-2 Summary of Static Corrosion Tests of Lithium Chloroborate Glass in Sulfur/Polysulfide Melts

Sample No.	Sample Type	mol% Sulfur	mol% Li_2S	Temperature (°C)	Time (hrs)	Film Observed	Changes#
1	Disc	99.8	0.2	400	18	off-white	+ 2 mg
2	Disc	99.9	0.1	400	89	off-white	+ 5 mg
3	Disc	99.3	0.7	400	118	off-white	-
4	Disc	99.8	0.2	400	136	white	-
5	Disc	100	0.0	400	136	none	none
6	Tube	99.6	0.4	375	453	white	sl. dec.
7	Tube	99.8	0.2	375	453	white	sl. dec.
8	Tube	100	0.0	375	453	trace	sl.
9	Tube	82.5	17.5	400	30	white/red	dec.
10	Tube	82.0	18.0	400	50	white/red	dec.

(sl. = slight, dec. = decomposition.)

The growth of the white film was observed in each of samples which contained Li_2S but did not cause cracking or failure of the glass in any of the static corrosion tests. The initial growth of the film was not significantly dependent on the quantity of Li_2S. It appeared to form on the glass as readily as when the lithium sulfide composition was a few tenths of a percent as it would when it was tens of percents. However, in the higher concentration range, the layer continued to build up and the glass was attacked faster than at the lower concentrations of Li_2S.

3.3.3.2. X-ray Diffraction Results

The films from both the discs and the tubes were scraped off and ground into powders. These powders were individually analyzed with a Siemens X-ray Diffractometer. Figure 3-5 is the X-ray diffraction pattern for the reaction product prepared from tube #9. There is strong evidence in the pattern of crystalline lithium chloroborate and lithium hydroxide. There was also strong evidence of sulfur; this was to be expected because the samples were not soaked in methanol or carbon disulfide. A significant finding was that there was a major peak, 35 degrees,

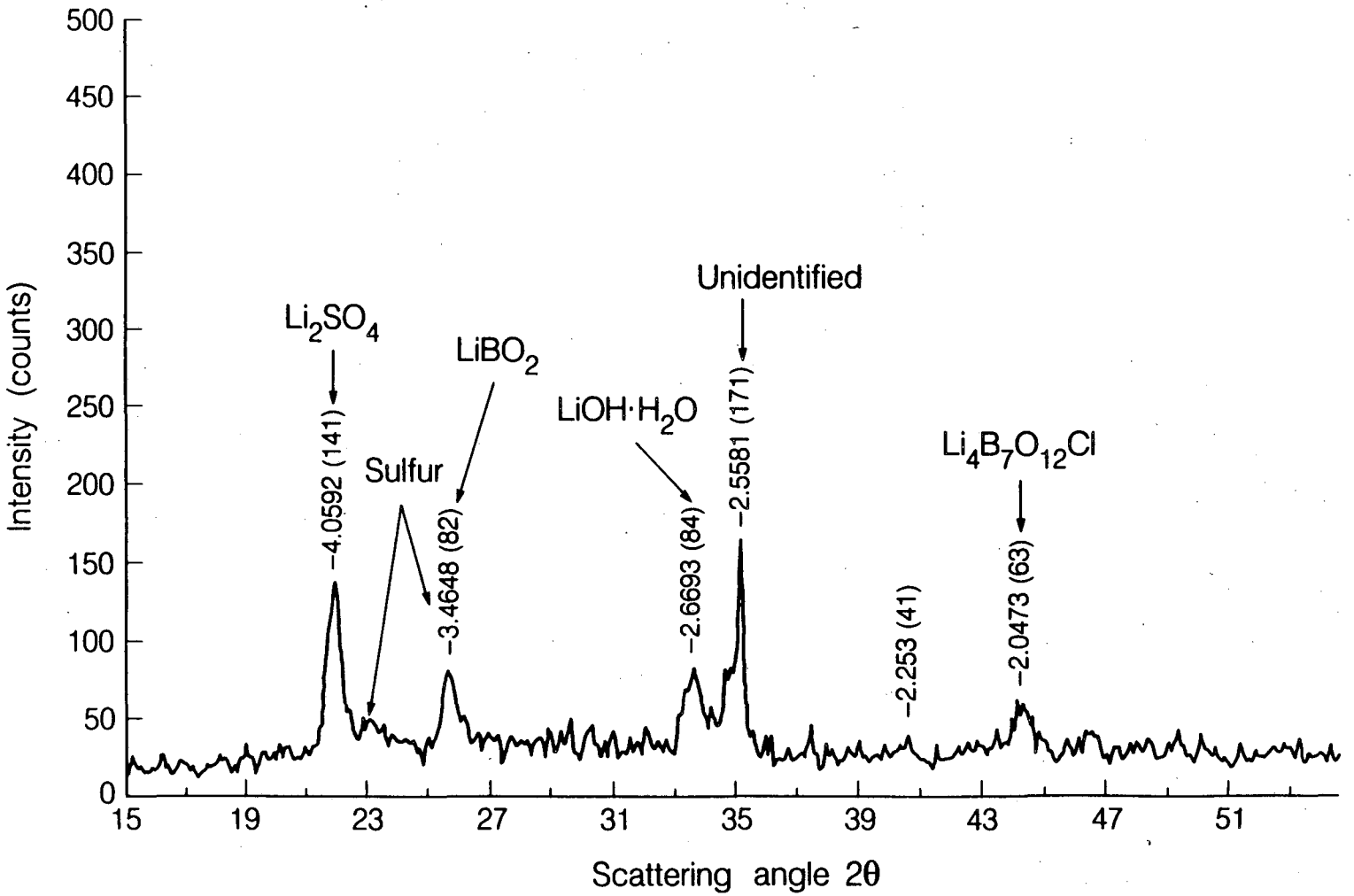

Figure 3-5. X-ray diffraction pattern for corrosion products of tube #9 in S-17.5 mol% Li_2S at 400 °C.

which could not be confidently assigned to any known compound. This raised the question of whether there could be a compound present which was not listed in the table of X-ray patterns. Two such compounds were found and will be addressed in the discussion section. Table 3-3 is a summary of the compounds which could be identified in the reaction layer of tube #9.

Table 3-3 Summary of Possible Compounds in Reaction Layer from Tube #9 (82.5 mol% S, 17.5 mol% Li_2S) based on X-ray Diffraction Patterns.

Compound	d values	2θ values	Confidence	Comments
$Li_4B_7O_{12}Cl$	2.05_x 2.70_3 3.48_2	44.1 33.2 25.6	High	9.1 mol% $(LiCl)_2$ 27.3 mol% Li_2O 63.6 mol% B_2O_3
$LiOH{\cdot}H_2O$	2.67_x 2.70_5 2.44_5	33.5 33.2 36.8	High	Hydrated Li_2O
Li_2S	3.30_x 2.02_4 1.72_3	27.0 44.8 53.2	Medium/Low	Hygroscopic
Li_2SO_4	4.04_x 4.00_x 3.92_5	22.0 22.2 23.7	High	Caused by Contamination
HBO_2	4.20_x 3.07_x 6.75_3	21.1 29.1 13.1	Medium	Hydrated B_2O_3
$LiBO_2$	3.53_x 2.19_x 1.80_8	25.2 41.2 50.7	Medium/High	50% Li_2O 50% B_2O_3
Li_3BO_3	3.02_x 2.63_6 2.67_5	29.5 34.1 33.5	Medium	75% Li_2O 25% B_2O_3
Sulfur -#	3.89_x 2.73_7 3.12_3	22.8 32.8 28.6	Medium/High	Hexagonal
Sulfur -#	3.29_x 6.65_3 3.74_2	27.1 13.3 23.8	Medium	Monoclinic
Sulfur -#	3.85_x 3.21_6 3.44_4	22.8 27.8 25.9	Medium	α-phase

References 25, 26, 27.

The level of confidence was reported as either high, medium, or low. A high level of confidence means that the three largest peaks reported for a particular compound occurred very near major peaks in the sample X-ray pattern and that the peaks on the sample pattern exhibited the proper relative intensity levels. A medium level of confidence means that one or possibly two

of the reported peaks occurred close to but not exactly on major peaks in the sample X-ray pattern. It could also mean that the peaks occurred where no major peak could be seen but in an area where a considerable amount of noise was present. A low level of confidence was declared when all three major peaks occurred in areas of noisy base lines.

Figure 3-6 is the X-ray diffraction pattern for the reaction product scraped from disc #4. This pattern shows more peaks and seems to be more scattered. Consequently, the confidence levels concerning which compounds were present were lower than in the pattern for the tube, with the exception of the sulfur peaks. The scatter can be attributed partially to the fact that the powder was not ground up as finely as those from the other samples and, therefore, interfered more with the scattering angle. Table 3-4 is a summary of the compounds which could be identified in the reaction film from disc #4.

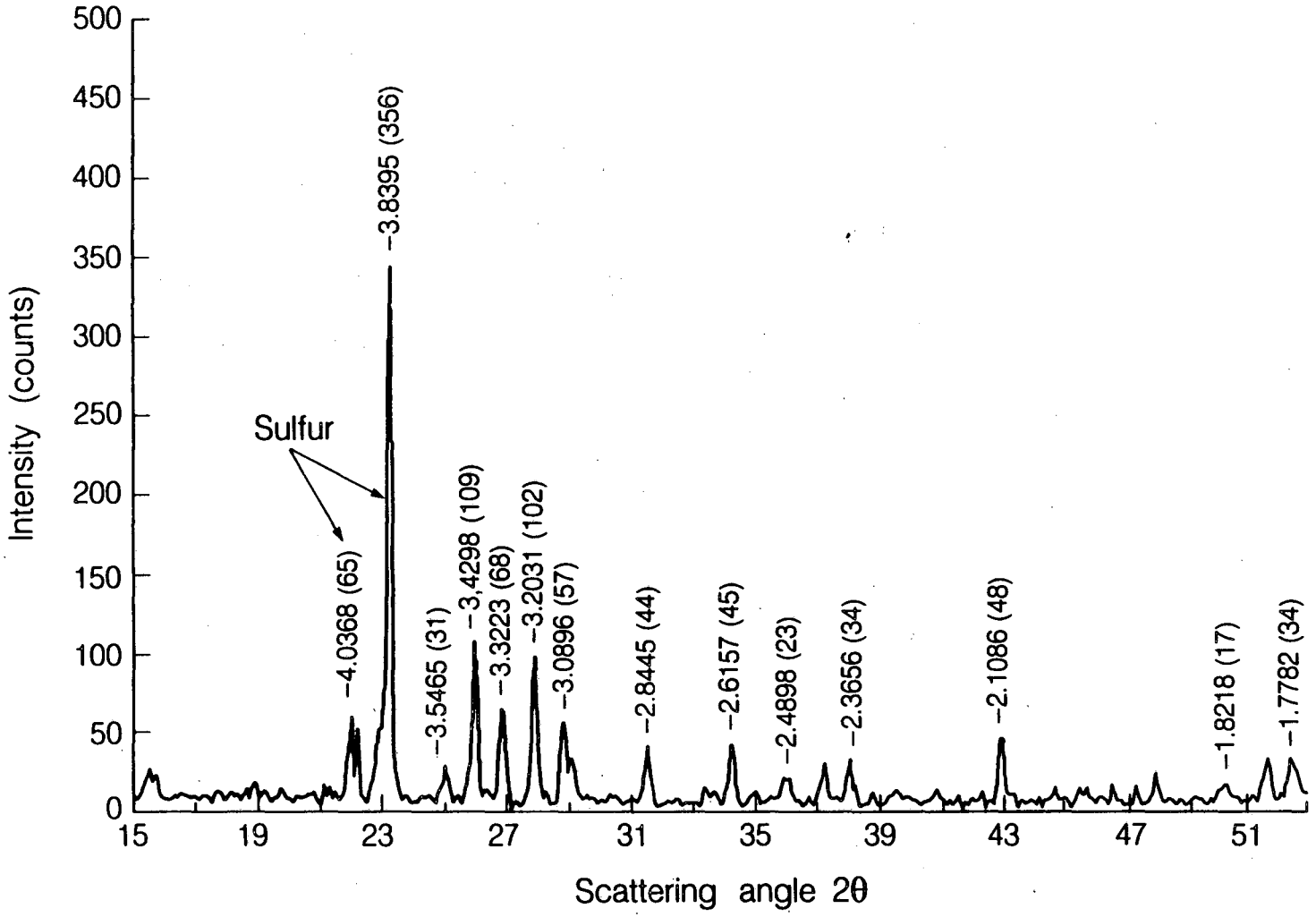

Figure 3-6. X-ray diffraction pattern for corrosion products of disc #4 in S-0.2 mol% Li_2S at 400 °C.

Table 3-4 Summary of Possible Compounds in Reaction Layer from Disk #4 (99.8 mol% S, 0.2 mol% Li_2S) based on X-ray Diffraction Patterns.

Compound	d values	2θ values	Confidence	Comments
$Li_4B_7O_{12}Cl$	2.05_x 2.70_3 3.48_2	44.1 33.2 25.6	Medium/Low	9.1 mol% $(LiCl)_2$ 27.3 mol% Li_2O 63.6 mol% B_2O_3
$LiOH{\cdot}H_2O$	2.67_x 2.70_5 2.44_5	33.5 33.2 36.8	Low	Hydrated Li_2O
Li_2S	3.30_x 2.02_4 1.72_3	27.0 44.8 53.2	Medium	Hygroscopic
Li_2SO_4	4.04_x 4.00_x 3.92_5	22.0 22.2 23.7	Medium	Caused by Contamination
HBO_2	4.20_x 3.07_x 6.75_3	21.1 29.1 13.1	Medium	Hydrated B_2O_3
$LiBO_2$	3.53_x 2.19_x 1.80_8	25.2 41.2 50.7	Medium	50% Li_2O 50% B_2O_3
Li_3BO_3	3.02_x 2.63_6 2.67_5	29.5 34.1 33.5	Medium	75% Li_2O 25% B_2O_3
Sulfur -#	3.89_x 2.73_7 3.12_3	22.8 32.8 28.6	High	Hexagonal
Sulfur -#	3.29_x 6.65_3 3.74_2	27.1 13.3 23.8	High	Monoclinic
Sulfur -#	3.85_x 3.21_6 3.44_4	22.8 27.8 25.9	High	α-phase

References 25, 26, 27.

When comparing the patterns from the different powders, it is important to keep in mind the compositions in which each was formed. For example, tube #9 was tested for 30 hours in a mixture of 82.5 mol% sulfur and 17.5 mol% Li_2S and showed high levels of confidence in the formation of crystalline $Li_4B_7O_{12}Cl$, while disc #4 which was tested for 136 hours in 99.8 mol% sulfur and 0.2 mol% Li_2S, showed a medium to low level of confidence. This comparison points to a conclusion that the sulfide species were the attacking species.

To establish a comparison reference frame and to help clarify some of the identities of the compounds in the reaction layers, two additional samples were analyzed by powder X-ray

diffraction. One was a powdered piece of lithium chloroborate glass, which gave no peaks at all. This verified that the glassy material did not contribute to the X-ray pattern. The second sample was a powdered piece of lithium chloroborate glass which had been intentionally allowed to crystallize. This sample gave the X-ray diffraction pattern shown in Figure 3-7. Table 3-5 is a summary of the compounds found in the crystallized lithium chloroborate.

Table 3-5 Summary of Possible Compounds found in Crystalline Lithium Chloroborate.

Compound	d values	2θ values	Confidence	Comments
$Li_4B_7O_{12}Cl$	2.05_x 2.70_3 3.48_2	44.1 33.2 25.6	High	9.1 mol% $(LiCl)_2$ 27.3 mol% Li_2O 63.6 mol% B_2O_3
$LiOH{\cdot}H_2O$	2.67_x 2.70_5 2.44_5	33.5 33.2 36.8	High	Hydrated Li_2O
HBO_2	4.20_x 3.07_x 6.75_3	21.1 29.1 13.1	Medium	Hydrated B_2O_3
$LiBO_2$	3.53_x 2.19_x 1.80_8	25.2 41.2 50.7	Medium	50% Li_2O 50% B_2O_3
Li_3BO_3	3.02_x 2.53_6 2.67_5	29.5 34.1 33.5	Medium	75% Li_2O 25% B_2O_3

3.3.4. Discussion

The lithium chloroborate glass was clearly chemically and mechanically stable in molten sulfur up to 400 °C and for up to 453 hours. However, when as little as a few tenths of a percent of lithium sulfide was added to the melt, the glass became coated with a white film. As the concentration of polysulfides was increased, the reaction between the glass and the melt became more pronounced. These facts indicate that the attacking species were the polysulfides.

The X-ray pattern showed strong evidence that the white film was composed of crystalline lithium chloroborate $Li_4B_7O_{12}Cl$. The sulfur and lithium polysulfide which were present in the X-ray diffraction patterns could possibly be simply entrapped in or around the glass crystals and not be a chemical constituent of the film. Another possible explanation is that the white film is a combination of crystalline lithium chloroborate and a lithium borosulfide reaction product caused

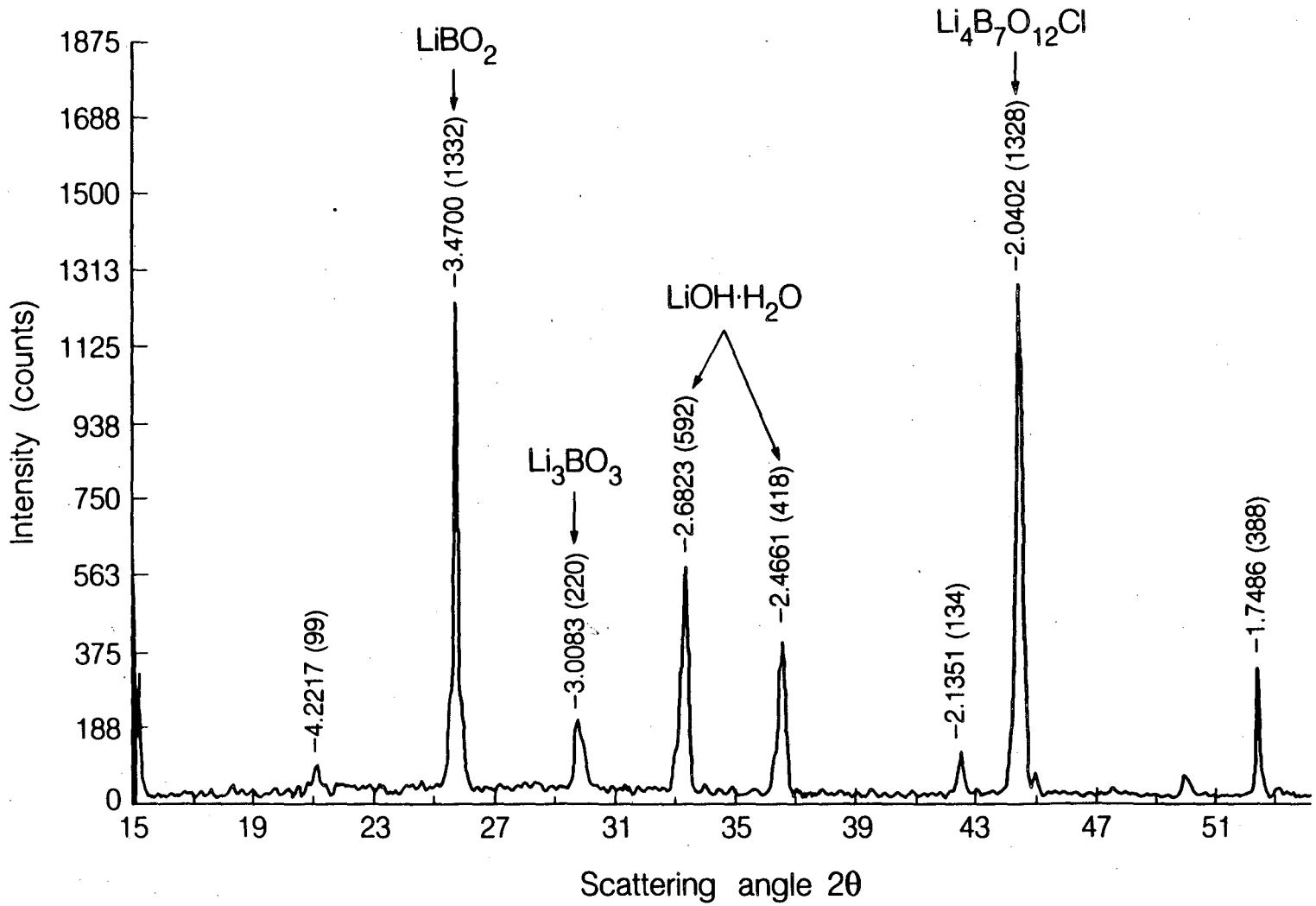

Figure 3-7. X-ray diffraction pattern for intentionally crystallized lithium chloroborate glass.

by lithium polysulfides attacking the lithium chloroborate glass. Even though a specific lithium borosulfide compound was not identified, it is possible that the unidentified peaks, such as the peak at 35 degrees, could be attributed to some lithium borosulfide reaction product. For example, possible candidates could be $Li_2B_2S_5$ or $LiBS_2$;[28] however, X-ray diffraction patterns for these compounds were not available.[29,30] Table 3-6 is a partial list of potential reactions which could be occurring between the lithium polysulfides and the lithium chloroborate glass.

Table 3-6 Partial List of Reactions Between Lithium Polysulfides and Lithium Chloroborate Glass.

$$2Li_2S + 2B_2O_3 \rightleftarrows LiBS_2 + 3LiBO_2$$

$$2Li_2S + Li_4B_7O_{12}Cl \rightleftarrows LiBS_2 + LiCl + 6LiBO_2$$

$$(4Li_2S)\cdot S + 2Li_4B_7O_{12}Cl \rightleftarrows Li_2B_2S_5 + 2LiCl + 12LiBO_2$$

It is sometimes possible to to estimate the X-ray pattern of a compound based on the X-ray pattern of another compound which has a similar crystalline structure. With this in mind, it was suggested that the X-ray patterns for the lithium borosulfide compounds could be estimated based on the analogous sodium compounds. However, sodium ions are sufficiently larger than lithium ions that the crystalline structures of the two compounds would be significantly different; therefore, a direct prediction of the X-ray patterns for the lithium borosulfide compounds, based on the sodium borosulfide compounds, was not possible.

It is interesting to note that the glass would crystallize when lithium polysulfides were present but not when only sulfur was present. The crystallization was not caused by the elevated temperature, otherwise it would have occurred with or without the lithium sulfide being present. The lithium polysulfides could have been participating as catalysts by causing a corrosion reaction to occur, as postulated above, or they could have been non-participating catalysts, which somehow either increased the driving force or lowered the activation energy for the vitreous material to crystallize.

Even though the composition of the white film could not be conclusively identified, it was encouraging that the film did not cause structural failures in the glass in any of the static

immersion tests. Therefore, it was decided to carry out further testing of the glass as the electrolyte in lithium/sulfur electrochemical cells.

CHAPTER 4

DYNAMIC TESTS

4.1. Introduction

The high lithium-ion conductivity of lithium chloroborate glass and the fact that it is reported to maintain its structure in the presence of molten lithium alloys makes it attractive for possible use as an electrolyte in Li/S cells.[31] The static immersion tests presented in the previous chapter showed that the glass was resistant to attack by molten sulfur and somewhat resistant to lithium polysulfides. Therefore, it was decided to test the conductivity and stability of the glass in a set of dynamic experiments. That is, a Li/S cell was built that employed lithium chloroborate glass as the electrolyte. In this way, the conductivity of the glass and its feasibility of use in a practical cell were evaluated while testing the corrosion resistance of the glass under dynamic conditions.

Three specific types of electrochemical experiments were performed using the lithium chloroborate glass as a solid lithium-ion conducting electrolyte. The first was a Li/S electrochemical cell in which small quantities of lithium were titrated into the sulfur compartment, permitting the measurement of lithium solubility (as lithium polysulfide) in sulfur. The second set of experiments was designed to test the performance of the Li/S cells by two different methods. The first method was to measure the change in voltage caused by a step change in current. The second method was to monitor the voltage versus time at various fixed currents, or in other words, cell charge-discharge data. The third set of experiments included the measurement of the glass conductivity by using a metal/metal cell with the glass acting as the electrolyte. The data from these three types of electrochemical experiments will be reported in the results and interpretation section, whereas the discussion section will address the stability of the glass to corrosion.

4.2. Theory

4.2.1. General Electrochemistry

All electrochemical systems must have four basic components: an anode, a cathode, an electrolyte, and an electronic conductor. During an electrochemical reaction, the anodic material is oxidized while the cathodic material is reduced,

$$\text{anode:} \qquad M \rightarrow M^{z+} + ze^- \tag{4-1}$$

$$\text{cathode:} \qquad O + xe^- \rightarrow O^{z-}. \tag{4-2}$$

The symbols M and O represent the active material of the anode and the cathode, respectively, and the symbol e^- represents the electrons involved in the particular half-cell reaction. The overall reaction is the sum of two half-cell reactions, each multiplied by an appropriate factor to balance the overall number of electrons transferred,

$$xM + zO = M_x O_z . \tag{4-3}$$

The ions and electrons produced by this reaction are carried from one electrode to the other via the electrolyte and the electronic conductor, respectively. The driving force for the reaction is the electrochemical potential difference between the two electrode materials. This potential difference can be mathematically expressed in the following equation, known as the Nernst equation,

$$E = E^o - \left(\frac{RT}{nF}\right) \ln \prod a_i^{\nu_i} . \tag{4-4}$$

The potential difference E is measured in volts, R is the universal gas constant 8.314 J/(mol K), T is the temperature in degrees K, n represents the stoichiometric number of electrons transferred, F is the Faraday constant 96487 coulombs/eq, and $\prod a_i^{\nu_i}$ is the product of the species activities raised to the ν_i power, where ν_i is the stoichiometric coefficient of species i. The value of ν_i is positive for the reaction products and negative for the reactants. The overall cell potential difference may be thought of as the standard potential difference E^o, modified by the deviations of the activities from their standard-state values.

The standard potential difference E^o is the potential difference that would be measured across a cell if all the reactants and products were at unit activity. The E^o of a particular reaction can be calculated by subtracting the reduction potential of the anodic half-cell reaction from the reduction potential for the cathodic half-cell reaction. The reduction potentials (measured versus the Standard Hydrogen Electrode (SHE)) for many half-cell reactions have been tabulated.[32] Because E^o is temperature-dependent, the E^o versus SHE, as calculated from the half-cell reactions in these tables, is only applicable to a system whose temperature is 25 °C. However, if the E^o of a reaction is needed at a different temperature, it may be calculated by the equation,

$$\Delta G_r^o = -nFE^o \tag{4-5}$$

where ΔG_r^o is the Gibbs free energy of reaction. The ΔG_r^o at a particular temperature can be calculated by subtracting the free energy of formation of the reactants from the free energy of formation of the products, at the desired temperature,

$$\Delta G_r^o = \sum | \nu_i | G_f^o(products) - \sum | \nu_i | G_f^o(reactants) . \tag{4-6}$$

Barin and Knacke[33,34] have published two volumes of tables containing free energies of formation for many substances versus temperature. These are not the only sources for free energies of formation; however, care is needed when using free energies of formation from more than one source, especially at different temperatures, because of the possibility that different tables are based on different reference states.

The second group of terms affecting the electrochemical potential of a cell is $\left(\frac{RT}{nF}\right) \ln \prod a_i^{\nu_i}$. This term is an activity-dependent measure of the potential difference caused by the deviations from unit activity of the reactants and products. For example, based on Equation (4-3), the natural log of the product of the activities would be,

$$\ln \frac{\left(a_{M_x O_y}\right)}{\left(a_M^z\right)\left(a_O^z\right)}. \tag{4-7}$$

If all species were held at unit activity, this term would be zero, and the measured cell potential would be equal to the standard cell potential, $E = E^o$. At the other extreme, if the cell reaction proceeded to equilibrium, the measured cell potential E would be zero, so $E^o = \left(\frac{RT}{nF}\right) \ln \prod a_i^{\nu_i}$ at equilibrium. This suggests another method of determining the E^o for a reaction at a given temperature.

The research described here is directed at the high-temperature, secondary (rechargeable) lithium/sulfur battery. Lithium, as the active material for the negative electrode, is oxidized during cell discharge by the following half reaction,

$$\mathrm{Li} \rightarrow \mathrm{Li}^+ + e^-. \tag{4-8}$$

Sulfur, as the active material in the positive electrode, is reduced during discharge by the following half reaction,

$$\mathrm{S} + 2e^- \rightarrow \mathrm{S}^{2-}. \tag{4-9}$$

Note that Equation (4-9) is a simplified representation of the sulfur-electrode chemistry; it is known that several polysulfide species (e.g., S_3^{2-},S_4^{2-},$\cdots$) exist in the melt.[35] The overall reversible electrochemical reaction for this system is

$$2\mathrm{Li} + \mathrm{S} \rightleftarrows \mathrm{Li_2S}. \tag{4-10}$$

At 400 °C the E^o for this electrochemical reaction is 2.178 volts. Thus, the Nernst equation for the Li/S system yields

$$E = 2.178 - (6.93\times10^{-3}) \ln \frac{\left(a_{Li_2S}\right)}{\left(a_{Li}^2\right)\left(a_S\right)}. \tag{4-11}$$

4.2.2. Electrolyte

In order for a material to be a suitable electrolyte, it must be an ionic conductor while at the same time being an electronic insulator. It must also be chemically stable in contact with

both electrodes and must have a decomposition potential higher than the cell operating voltage. The materials which satisfy these requirements can be classified into four large groups, aqueous solutions, non-aqueous solution, molten salts, and solids. The type of electrolyte used in a particular system depends on the electrode materials and on the operating conditions. For example, an aqueous or non-aqueous solution electrolyte can never be used with a high-temperature battery, such as the Li/S battery, because these electrolytes are only stable at, or near, room temperature. Molten-salt electrolytes, on the other hand, can be used in batteries whose operating temperatures reach several hundred degrees Celcius. An example of such a system is the LiAl/FeS molten-salt electrolyte cell, which has been studied at Argonne National Laboratory.[36]

The use of a high-temperature solid electrolyte has been restricted mainly to Na/S batteries. The material used as the electrolyte in these systems has been either a β-alumina ceramic or a fast-ion-conducting (FIC) glass.[8,9] The lack of a high-temperature material which exhibits both high lithium-ion conductivity and reasonable resistance to attack by lithium has made impractical the idea of using a solid ionic electrolyte in a Li/S cell. However, as discussed earlier, lithium borate glasses have recently shown promising characteristics for application as such solid electrolytes.

4.2.3. Sulfur Electrode

A systematic investigation of the use of sulfur in the positive electrode for a secondary lithium battery was carried out at Argonne National Laboratory in the early 1960s. This investigation has been reviewed by Cairns [6,37,38] and Kyle *et al.*[39] The loss of lithium and sulfur by solubilization in the molten-salt electrolytes caused research on the Li/S cell to be halted. The recent discovery of solid electrolytes with high ionic conductivity and stability to lithium has spurred renewed interest in the Li/S cell. Sulfur remains an attractive choice for the positive electrode; however, it is not an easy material with which to work.

The vapor pressure of sulfur at 400 °C is 53.3 kPa. This makes it necessary to contain the sulfur in a tightly sealed compartment; otherwise, at the cell operating temperature, the sulfur would evaporate very quickly. Another major problem with using sulfur as an electrode material

is its low conductivity. Pure sulfur at 350 °C has a electronic conductivity of $\sim 10^{-8}$ $(\Omega\text{-cm})^{-1}$. This makes current collection difficult in the fully-charged state. As a partial solution to this problem, some sort of high-porosity, electrically conductive matrix material can be packed into the sulfur compartment. This has the effect of increasing the surface area of the current collector and, thereby, increasing the number of sites where electrons can react with the sulfur. The most commonly used material is porous graphite or carbon felt; however, graphite and carbon in other forms have also been investigated. Sudworth [8] shows a table of the types of graphite and carbon materials used as current collectors in sulfur electrodes.

Another significant complication in the sulfur electrode is how and to what degree the properties of sulfur change as lithium enters and forms sulfides. Table 4-1 shows a compilation of several important properties of sulfur and some lithium polysulfides.

Table 4-1 Physical Properties of Sulfur and Lithium Polysulfide.

Properties	Sulfur	$Li_2S_{3.9}$ #	$Li_2S_{3.88}$ %
vapor pressure	53.3 kPa @ 400°C	-	-
electronic conductivity	2.3×10^{-7} $(\Omega^{-1}cm^{-1})$ @ 417°C	1.405 $(\Omega^{-1}cm^{-1})$ @ 432°C	1.188 $(\Omega^{-1}cm^{-1})$* @ 425°C
density	1.6172 (g cm^{-3}) @ 700K	1.721 (g cm^{-3}) @ 700K	1.722 (g cm^{-3}) @ 698K
melting point	118.8°C	365° ± 4°C	-

#- Reference 40.
% Reference 41.
* extrapolated from data.

In order to understand why there are such large changes in conductivity and melting point, one needs to consider the lithium-sulfur phase diagram. Figure 4-1 shows the lithium-sulfur phase diagram according to Cunningham *et al.*[42] The solubility of lithium polysulfide in sulfur is very low, and after the solubility limit of lithium polysulfide in sulfur is reached at a given temperature, the addition of more lithium causes the formation of two immiscible liquids. The compositions of the two phases are fixed by the composition at the phase boundaries. Even though the composition of the two phases does not change as more lithium is added, the relative quantity of

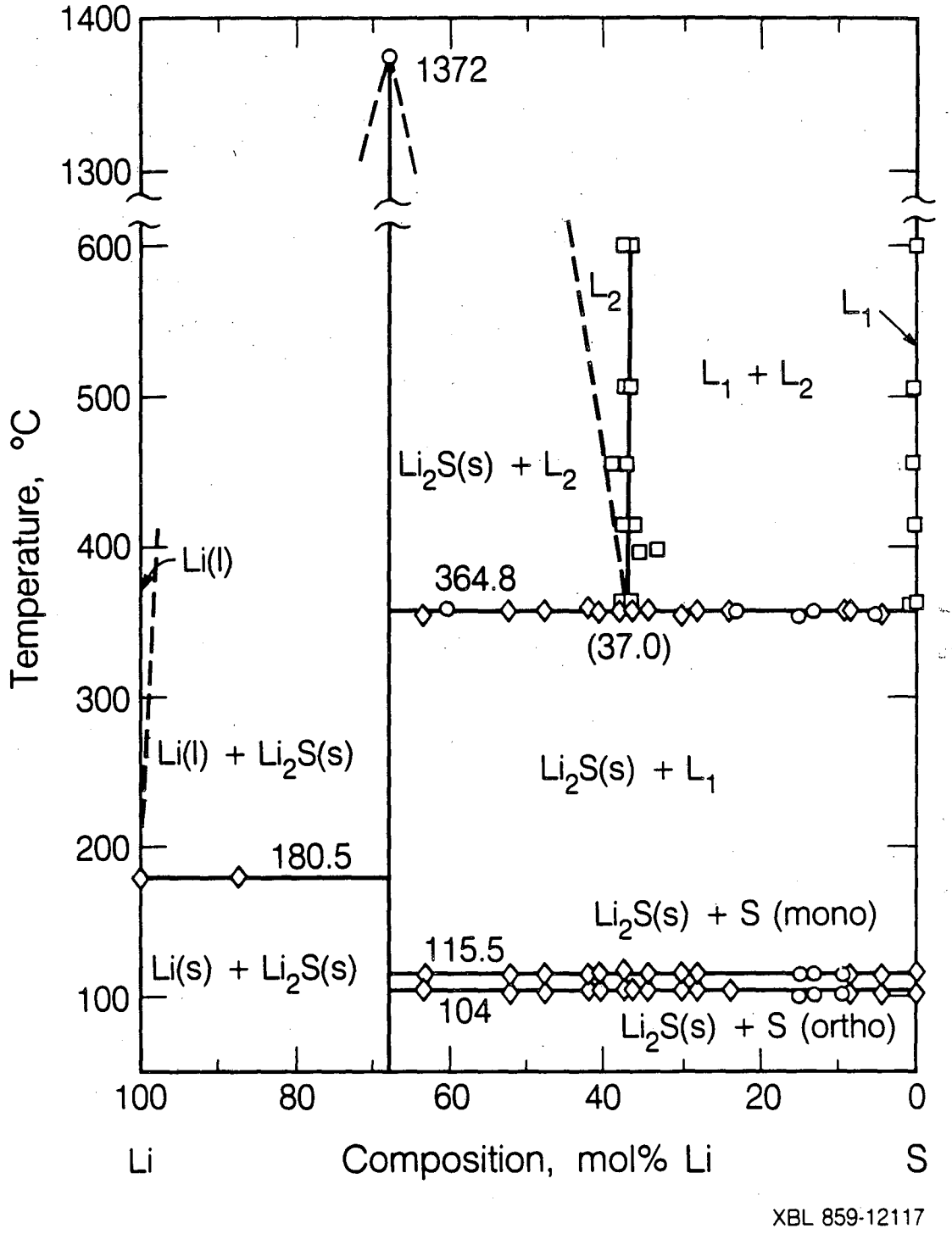

Figure 4-1. Lithium/sulfur phase diagram according to Cunningham *et al* (42).

each phase does. This change in relative quantity of the two phases causes the properties of the melt to change significantly. Unfortunately many of these changes are not well documented.

The region between $Li_2S_{3.7}$ and $Li_2S_{3.9}$ at 400 °C is a single-liquid phase. The composition in this region is not fixed; it varies as different quantities of lithium are added. Eventually, the addition of more lithium causes the melt to enter a a second two-phase region. Here the two phases are a solid and a liquid. The composition of the solid phase is Li_2S, and the composition of the liquid phase at 400 °C is $Li_2S_{3.7}$. The precipitation of a solid phase could cause problems in discharging a cell; the solid phase may act as a passivation layer by blocking the transport of lithium into the sulfur compartment. This problem, although not yet observed in the lithium-sulfur system, has been observed in the analogous sodium-sulfur system.[43]

4.2.4. Lithium Electrode

Lithium is an attractive candidate for the negative electrode material of a high-performance cell because it is such an active, light-weight metal. Its reduction potential is -3.045 volts vs SHE, and its equivalent weight is 6.94 grams/equivalent. Unfortunately, these same characteristics are also what make it a difficult material with which to work. It is such an active metal that, at high temperatures, it reacts with virtually everything with which it comes in contact. In spite of the lithium chloroborate glass being chosen for its apparent stability to lithium, it was not sufficiently stable to resist attack by unit-activity lithium for any reasonable amount of time. Therefore, the lithium should be alloyed with another metal to reduce the activity of lithium.

In choosing a lithium alloy for use in a practical Li/S cell, one would search for an alloy which could be characterized by low weight per electrochemical equivalent, low cost, ability to be recharged many times, high exchange-current density, and high lithium diffusion coefficient. However, for basic research and data generation, some of these requirements can be relaxed. For example, the cost of a research cell would not be a limiting factor, provided that it demonstrates principles that may lead to the development of practical cells. Also, for purposes of studying general cell reactions, it would not be critical that the equivalent weight of the electrode be very low.

Consideration of which lithium alloy to use in a research cell is influenced by the selection of a reference electrode. For example, for use of the negative electrode as the reference electrode, an alloy must be selected which would cause this electrode to have a constant potential. This could be done by selecting a lithium alloy which exhibits a two-phase region at the cell operating conditions, and using a sufficiently large excess of this alloy so that, regardless of the state-of-charge, it is always in the two-phase region. Under these conditions, the potential of the lithium alloy electrode would not vary with state-of-charge, but only with temperature. Any change in the cell open-circuit voltage would then be a result of a change in the sulfur electrode.

After consideration of these factors and examination of many alloying metals, tin was selected. Tin forms a low-lithium-activity two-phase alloy with lithium in the molar composition range of 33-50 mol% lithium at 400° C. Figure 4-2 shows a lithium-tin phase diagram according to Huggins *et al.*[44] The lithium activity of this alloy at this temperature is 4.5×10^{-5}, compared to unity for pure lithium.[44] This translates into a potential of +0.577 volts with respect to pure lithium. The temperature dependence of the emf for the Li-Sn alloy was reported to be $\frac{\partial E}{\partial T} =$ -0.74 mV/K.[44] The high rate of chemical diffusion exhibited in the Li-Sn alloy[45] is another important factor in favor of the Li-Sn alloy. Therefore, despite tin being a relatively heavy metal, it is a good choice to alloy with lithium, particularly for use as a research electrode.

4.2.5. Lithium Titration

The Nernst equation for the overall reaction of lithium and sulfur forming lithium sulfide, is

$$E = E^o - \frac{RT}{2F} \ln \frac{\left(a_{Li_2S}\right)}{\left(a_{Li}^2\right)\left(a_S\right)} . \tag{4-12}$$

At a fixed temperature, the standard cell potential, E^o, and the activity of lithium in the lithium-tin negative electrode, a_{Li}, would be constants. The activity of sulfur, a_S, in the limit of a nearly pure sulfur electrode, could be approximated by one. After making these substitu-

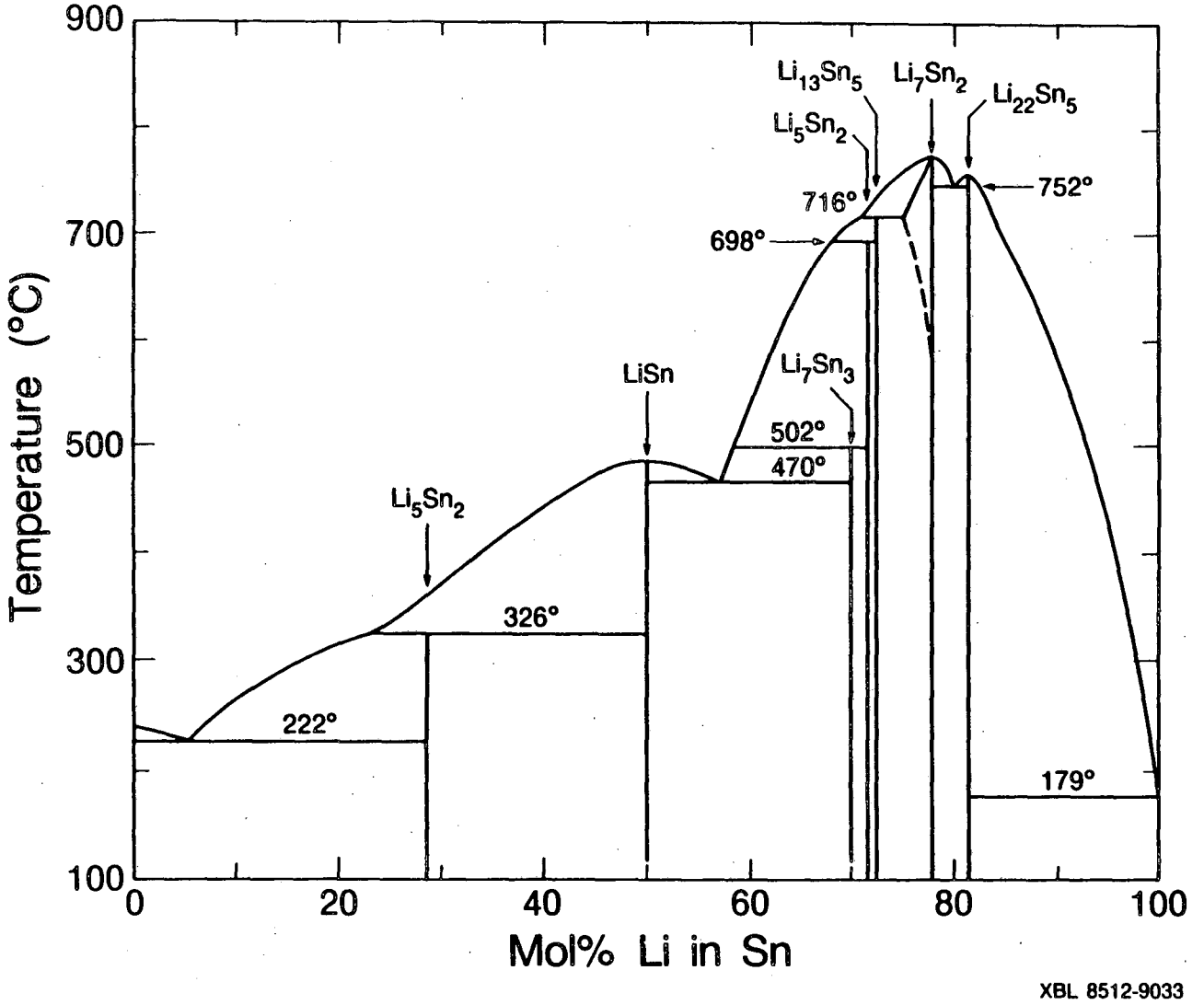

Figure 4-2. Lithium-tin phase diagram according to Huggins *et al* (44).

tions, the Nernst equation can be rewritten as

$$E = \mathrm{k} - \frac{RT}{2F} \ln a_{Li_2S}, \tag{4-13}$$

where k is a constant.

In a fully-charged cell, where no lithium sulfide is present in the sulfur electrode, the theoretical activity of Li_2S would be zero. This would cause the open-circuit cell potential, E, to be infinite. However, due to practical considerations, a real system is never able to achieve an a_{Li_2S} of zero. The addition of even one lithium ion causes the activity of Li_2S to become greater than zero which, in turn, causes the cell potential to become finite. As lithium is titrated into the sulfur electrode, the activity of Li_2S increases and this causes the cell potential to decrease. At first, the change-in-voltage for a given amount of lithium is very high. However, as more lithium is added, the voltage changes associated with a given quantity of lithium become less. This trend continues until the sulfur electrode reaches the two-phase immiscible-liquid region (see the lithium-sulfur phase diagram, Figure 4-2). By examining the degrees of freedom predicted by the phase rule, it can be shown that when two phases are present, the open-circuit cell potential would have to be constant.

$$F = m - \pi + 2 . \tag{4-14}$$

The degrees of freedom F are equal to the number of components m minus the number of phases π plus two.[46] In the two immiscible-liquid region, there would be two components and two phases and, therefore, there would be two degrees of freedom, temperature and pressure. Therefore, there would be no extra degrees of freedom, and the cell potential can not change. This implies that the solubility limit of lithium in sulfur may be identified as the point at which the cell potential stops decreasing with the addition of lithium and becomes constant.

If in the region of changing a_{Li_2S}, cell potential versus a_{Li_2S}, (Equation 4-13) were plotted on a semi-logarithmic graph, the result should be a straight line with a slope of $\frac{-RT}{2F}$. However, it is not convenient to plot the *activity* of Li_2S because it cannot be measured directly. It is

much simpler to measure and plot the *molefraction* of lithium. Therefore, a relationship between the activity of Li_2S and the mole fraction of lithium must be found. The activity of Li_2S is equal to its activity coefficient times its mole fraction,

$$a_{Li_2S} = \gamma_{Li_2S}\, x_{Li_2S}\,. \tag{4-15}$$

It can be assumed that the activity coefficient, γ_{Li_2S}, over very small changes in dilute concentrations of Li_2S in sulfur, is constant. Furthermore, the mole fraction of Li_2S is equal to one half the mole fraction of lithium,

$$x_{Li_2S} = 1/2\; x_{Li}\,. \tag{4-16}$$

After making these substitutions and rearranging, the Nernst equation can be rewritten as

$$E = \mathrm{k}' - \frac{RT}{2F} \ln x_{Li}\,, \tag{4-17}$$

Therefore, the cell potential may be plotted versus x_{Li} on semi-logarithmic graph paper and be expected to have a slope of $\frac{-RT}{2F}$. This slope would continue until the solubility limit was reached and the melt entered the two-immiscible-liquids region. At that point, as explained previously, the open-circuit cell potential should remain constant.

4.3. Experimental Methods

4.3.1. Introduction

The experimental electrochemical cell consisted of a thin-walled lithium chloroborate glass tube filled with molten sulfur and suspended in a molten lithium-tin alloy. Figure 4-3 is a schematic drawing of the cell assembly. The glass tube served as the electrolyte, the sulfur was the active material for the positive electrode, and the lithium was the active material for the negative electrode. The activity of lithium in the negative electrode was lowered by alloying the lithium with tin. The equipotential liquid-solid two-phase lithium-tin electrode was also used as a reference electrode. The hygroscopic nature of the electrode and electrolyte materials made it

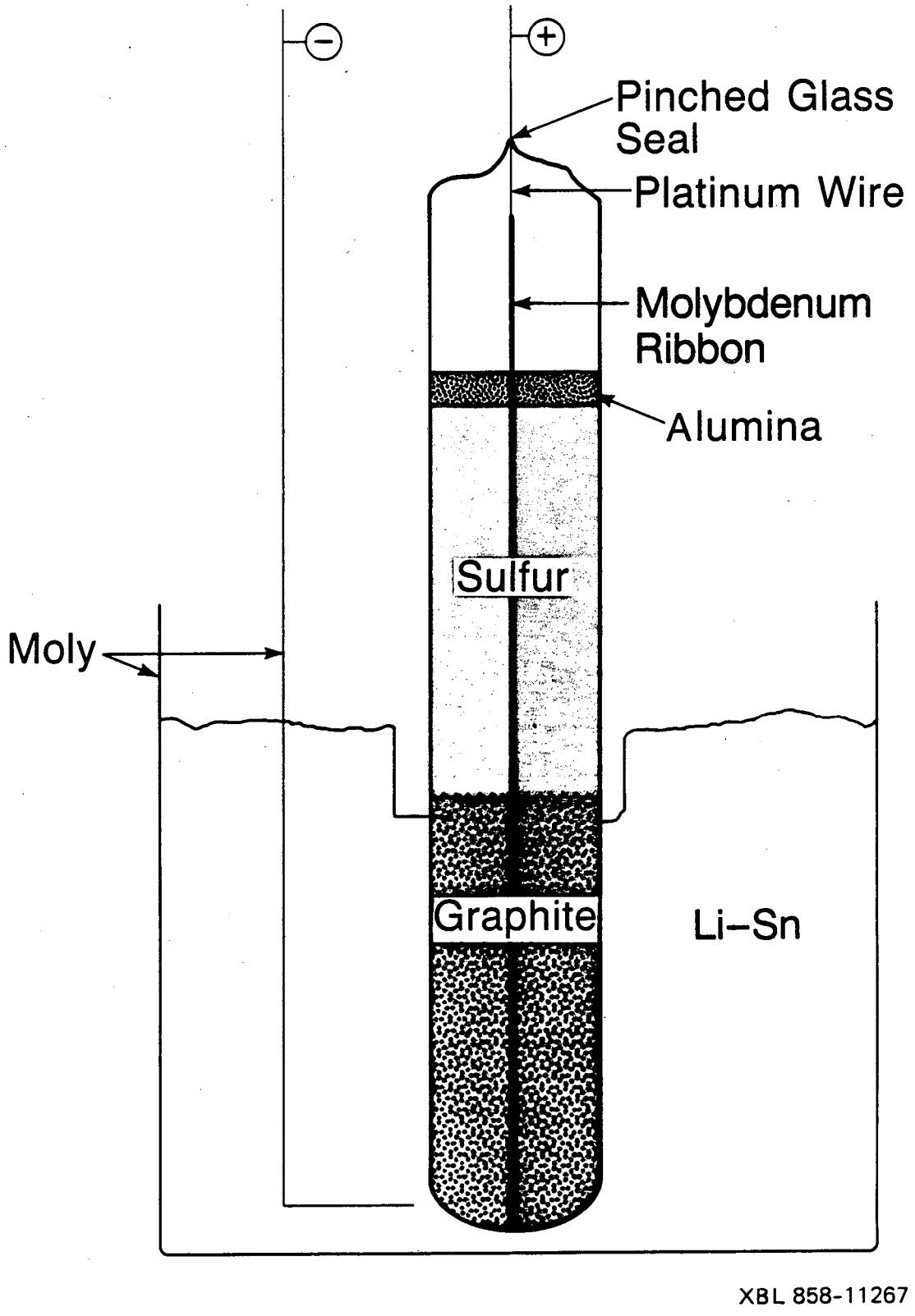

Figure 4-3. Schematic of cell assembly.

necessary to store and handle them in the helium-atmosphere glove box.

4.3.2. Electrolyte

In order to be of use as an electrolyte in an electrochemical cell, the lithium chloroborate glass had to first be fabricated into thin-walled tubes. The easiest method of doing this was blowing them from a pot of molten glass. The procedure to prepare the glass and blow it into tubes was described in sections 3.3.2.2.1 and 3.3.2.2.3, respectively. Before the thin-walled tubes were used as electrolytes, they were screened for structural weaknesses or flaws. For example, some of the tubes had angular variations in their wall thicknesses of up to 0.03 cm, or roughly 100% deviation. These tubes were not used as electrolyte tubes; they were found to be structurally weak and would frequently crack or break apart during assembly. The tubes whose wall thicknesses were angularly uniform were found to be more sound structurally. They could withstand more pressure and more mechanical stress than the non-uniform tubes.

Another reason for not using the non-uniform tubes is the uncertainty introduced when calculating the glass' resistivity. The resistance of the glass in the cell walls is given by the equation

$$R = \frac{\rho}{2\pi h} \ln \frac{r_o}{r_i},$$

where R is the cell resistance, ρ is the glass resistivity, h is the cell height, and r is the radius of the tube, where the subscripts refer to the inner and outer radii. The large ratio of cell-radius to wall-thickness made it possible to approximate $\ln \frac{r_o}{r_i}$ by $(\frac{r_o}{r_i} - 1)$. The error introduced by making this substitution was found to be less than 5%, which was less than the experimental error. With this substitution, the equation for cell resistance can be written as

$$R = \rho \frac{l}{A}, \tag{4-18}$$

where l, equal to $r_o - r_i$, is the wall thickness and A, equal to $2\pi r_i h$, is the cell surface area. If the thickness of a cell wall were to vary substantially from side to side, then an average value would have to be estimated and used to calculate the glass' resistivity. This could result in a

significant uncertainty. Thus, a relatively constant wall thickness is not only more structurally sound, it also facilitates calculation of a more accurate glass resistivity.

Another structural weakness observed with some tubes was the entrapment of air bubbles and crystals. Sometimes when the tubes were being pulled from the melt, small air bubbles would form or crystals would grow and become entrapped in the walls of the tubes. The result in either case was a point of stress in the glass and cracks were frequently observed to form at these sites. The tubes were thus carefully screened and were not used if either an air bubble or a crystal was found.

4.3.3. Sulfur Electrode

4.3.3.1. Design and Preparation

The sulfur was obtained from NOAH Chemical Co. and reported to be 99.999% pure. It was kept in the helium-atmosphere glove box to minimize contamination. The sulfur electrode was assembled by first inserting a 0.08 mm thick cleaned molybdenum ribbon into one of the glass tubes and then packing around it 95% porosity graphite felt to a depth of approximately 3 cm. The graphite felt was packed tightly to make good electrical contact with both the molybdenum and the glass. This combination served as the current collector for the sulfur electrode. Molybdenum and graphite were chosen to be the current collectors for the sulfur electrode because of their stability to sulfur and lithium polysulfides.[47] Once the current collector was in place, the tube was loaded with enough sulfur(0.5 to 2.0 grams) so that when melted, it would fill the voids in the porous graphite felt. Finally, a small piece of alumina insulation was packed in the tube to hold the sulfur chips in place during the sealing procedure. Figure 4-4 is a photograph of a loaded and sealed cell before heating.

4.3.3.2. Sealing

The vapor pressure of sulfur at 400 °C is 53.3 kPa. In order to prevent sulfur vapor from escaping from the tube and contaminating the glove box, the tube had to be sealed. Unfortunately, due to the mismatch of thermal coefficients of expansion between molybdenum and the

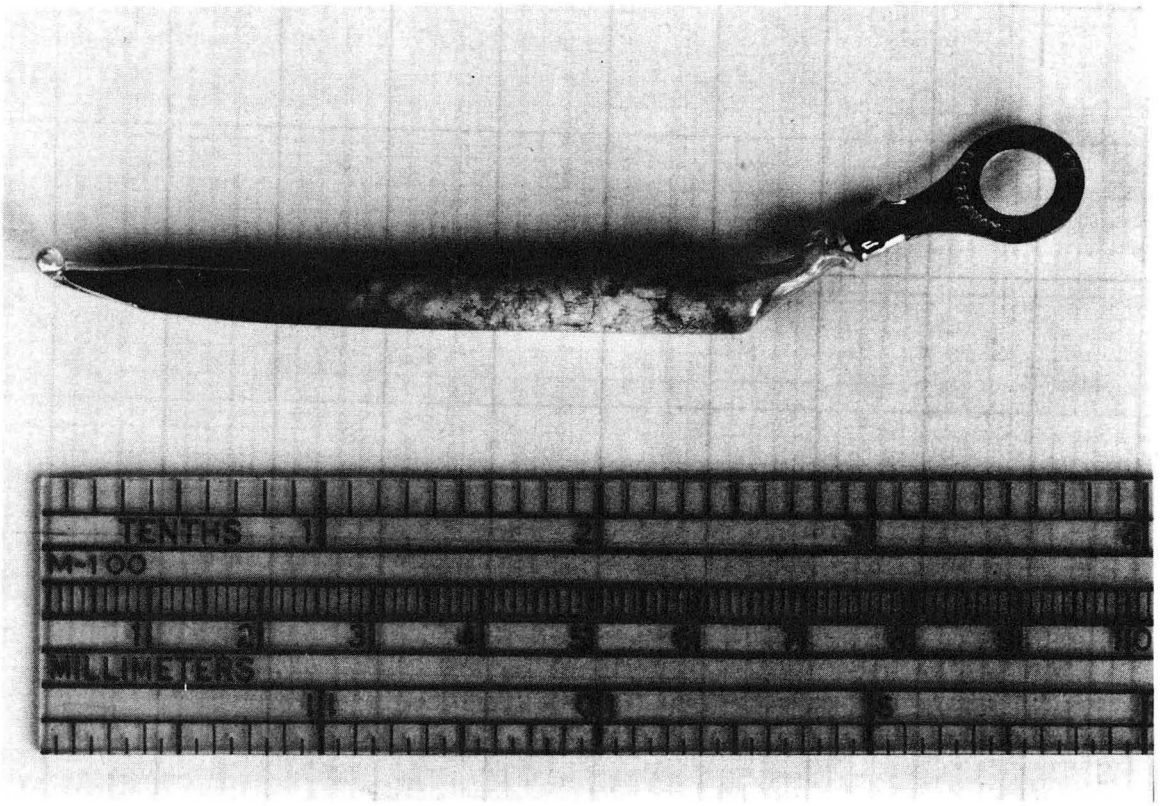

CBB 858-6513

Figure 4-4. Photograph of sealed tube, packed with carbon felt, loaded with sulfur, and showing platinum lead wire.

glass, it was not possible to seal the molybdenum to the glass. It was found that the glass could be sealed to a 0.25-mm diameter platinum wire, but the platinum wire could not be used as the current collector because it would corrode in contact with lithium polysulfide. A short piece of platinum wire was spot-welded to one end of the molybdenum ribbon, and the glass was sealed around the platinum wire, so that only the corrosion-resistant molybdenum contacted the sulfur/graphite mixture.

The tubes were sealed inside the glove box by rapidly heating the glass to its softening point in an electrically heated coil of molybdenum wire and then gently pinching it closed with a preheated pair of needle-nose pliers. The coil temperature was not measured, but it had to be sufficiently high to soften the glass very quickly. For example, when the current in the coil was decreased to the point where the glass would not soften in 5 seconds, the glass would crystallize. The molybdenum coil was typically yellow-white when at the necessary temperature. The current was then turned off, and the heating coil was allowed to cool, while the glass remained in the coil. The glass-to-metal seal was then examined for signs of cracking. Rather than attempt to accommodate the high vapor pressure of sulfur at the cell operating temperature by partially evacuating the tube during sealing, a simple test was performed. The tubes were partially filled with sulfur, heated, and stored at 400 °C for one month. The tubes were structurally able to withstand the excess internal pressure caused by heating, and over the one-month period they lost no appreciable sulfur.

4.3.4. Lithium Electrode

4.3.4.1. Alloying

The chemicals used were 99.9% Li ribbon and 99.9% Sn wire, both from AESAR Co. First, approximately 11 grams of lithium were melted in a 100-ml molybdenum crucible. At this point, if there was any evidence of a floating film on the molten lithium, it was removed with a molybdenum screen until all that remained in the crucible was a shiny metallic lithium melt. A more accurate mass of lithium was then determined by subtracting the mass of the empty crucible from its mass when full. Next, the appropriate amount of tin, enough to make approximately an

equal molar ratio of lithium to tin, was added to the crucible. The enthalpy of mixing for lithium and tin at 415 °C ranges from -40 kJ/mole for LiSn to -45 kJ/mole for $Li_{13}Sn_5$.[44] These values are highly exothermic, so as a precautionary measure, the tin was added slowly and very carefully. The alloy was then heated to 500 °C and allowed to equilibrate for several hours. At this time the alloy was considered to be homogeneous and ready to shape into the electrode configuration.

4.3.4.2. Shaping

Two structural modifications to the Li-Sn alloy were necessary to prepare it for use as the negative electrode in the Li-Sn/S cell. First, a molybdenum wire was used as the current collector, and it was inserted into the alloy while the alloy was still molten. The second modification was to make a hole in the middle of the Li-Sn alloy. This hole provided a place to position the glass tube in an upright and stable position, thereby minimizing subsequent movement of the tube and providing a means for the Li-Sn alloy to flow around it and make good contact. The hole was made by dipping a 1.9-cm diameter molybdenum rod into the molten Li-Sn and then carefully pulling it out just before the alloy solidified.

4.3.5. Cell Apparatus

4.3.5.1. Assembly

The sealed glass tube, loaded with sulfur, was placed in the hole in the Li-Sn alloy and approximately 25 grams of tin wire, cut into one-inch pieces, was placed around the tube. The function of the pieces of tin was to melt before the Li-Sn alloy and flow around the tube, thereby making a large and even contact area between the glass and the tin. Shortly thereafter, lithium from the melting Li-Sn alloy would diffuse into the liquid tin and form a liquid-solid two-phase Li-Sn alloy. This equipotential two-phase alloy was used as the reference electrode as well as the working electrode. The molybdenum crucible, filled with Li-Sn, was placed in an electrically insulating alumina crucible, which was then inserted into a 10-cm long by 10-cm diameter aluminum block. The large thermal mass of the aluminum block helped stabilize the temperature of the cell. The appropriate electrical connections were made, and then the aluminum block was

lowered into one of the 40-cm deep furnace wells. Five stainless-steel heat shields were fitted between the aluminum block and the top of the furnace well. Two chromel-alumel thermocouple probes were placed in the furnace wells very near to the block. One of the thermocouples was actually in the aluminum block, and the other was suspended about 5 cm above the Li-Sn melt. Figure 4-5 is a photograph of the aluminum-block heat-shield assembly. The temperature in the cell compartment was allowed to equilibrate until these two thermocouples were within 1 degree Celcius of one another before the cells were considered to be in thermal equilibrium.

4.3.5.2. Equipment

The cell potential was measured with a model 3468A Hewlett Packard multimeter, as well as with a model SR-204 Heath strip-chart recorder. The input impedance of the multimeter was $10^{10}\ \Omega$ in the range of 0-3 volts, and the floating-input impedance of the chart recorder was $>$ $10^{7}\ \Omega$ with $<$ 10 nA bias current on the 1-volt range. A Princeton Applied Research model 173 Potentiostat/Galvanostat was used to control the current and/or the potential of the cells. Resistance measurements were made by two methods. One was a current interrupt method using a model 2090-IIIA Digital Oscilloscope from Nicolet Instrument Corporation. The other was an AC impedance technique. A model B642 Autobalance Universal Bridge from Wayne Kerr was used for these measurements. Figure 4-6 is a schematic drawing of the experimental set up for testing the cells.

4.3.6. Experimental Procedures

4.3.6.1. Lithium Titration

This experiment required an accurate accounting of the number of coulombs that were transferred. Therefore, great care was taken to avoid passing any current that could not be measured and timed. With this in mind, the cell was first brought to temperature (400 °C) while monitoring only the cell potential with the high-impedance multimeter. After the cell reached complete thermal equilibrium, the open-circuit cell potential was recorded, and then a small discharge current, approximately 10μA, was passed through the cell for an accurately measured length of

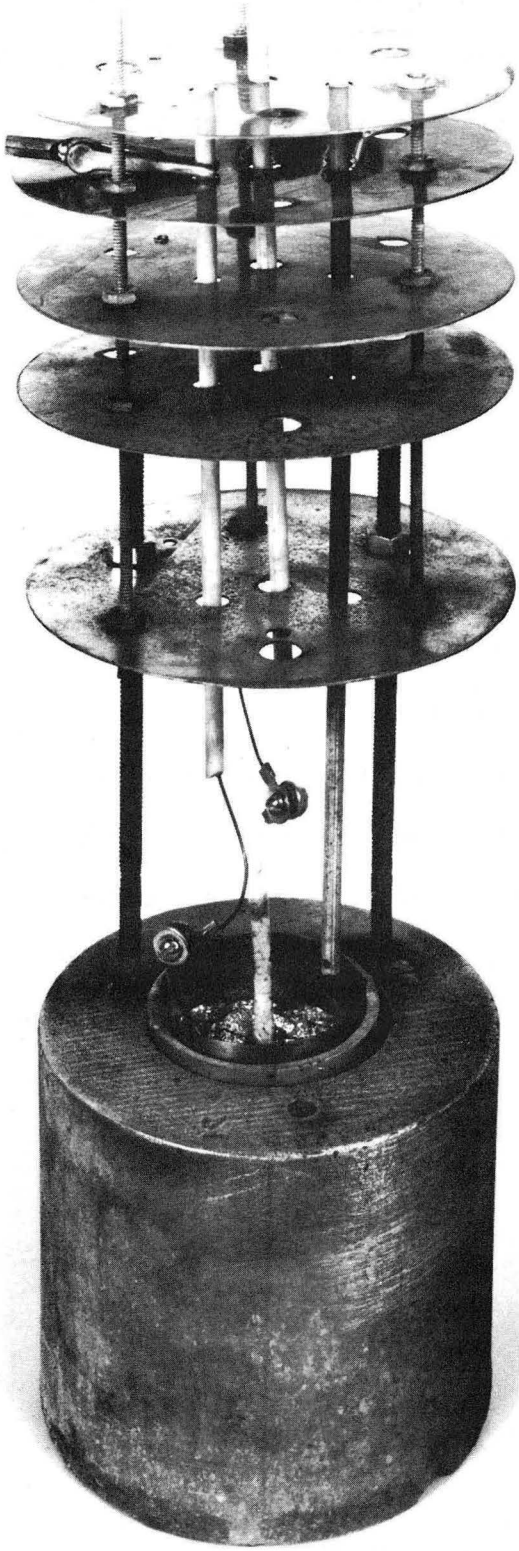

CBB 858-6507

Figure 4-5. Photograph of aluminum block and heat shield assembly.

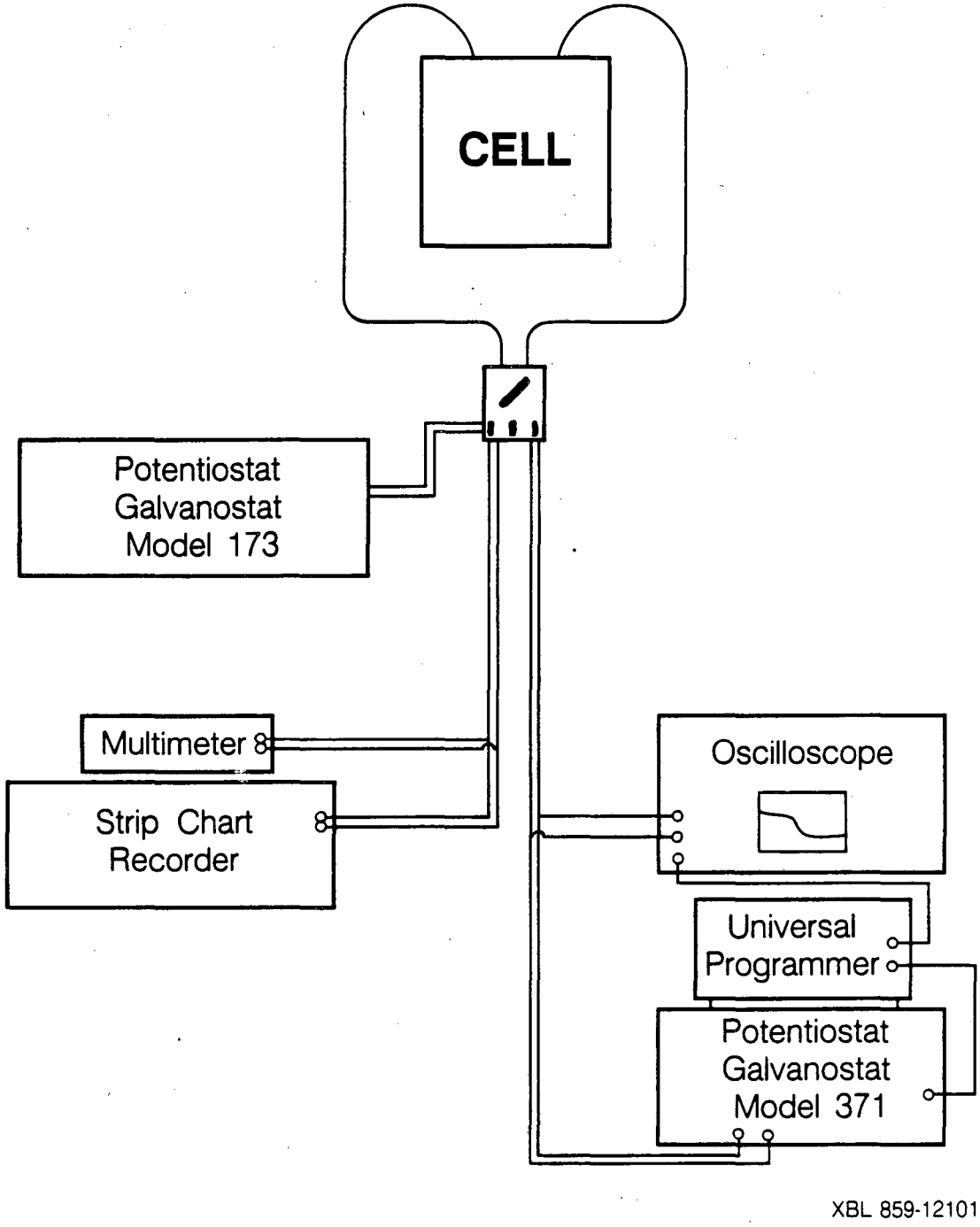

Figure 4-6. Schematic of cell equipment.

time. The length of time, which varied from cell to cell depending on its capacity, was chosen to produce approximately 0.0001 mol% Li in the sulfur electrode. The current was very small because the resistance of the fully-charged cell was very large (the overall effective resistance of the fully-charged cells ranged from approximately 50 to 150 kΩ.)

As the sulfur electrode became more rich in lithium polysulfides, its resistance would decrease, so the current could then be increased. After the prescribed number of coulombs had passed, the cell was switched to open-circuit and left idle until the voltage became constant. This procedure was repeated several times, each time allowing the cell a relaxation period for the voltage to stabilize. Depending upon how many coulombs had been passed and the level of current, the relaxation period varied from a few hours up to a few days. When the lithium content of the sulfur electrode was less than 0.03-0.05 mol% Li, it was observed that the cell voltage would continue to drop as more lithium was titrated. However, after reaching approximately 0.03 mol% Li, the open-circuit voltage of the cell would remain constant, even with the addition of more lithium. This point of transition should represent the boundary between the single-phase region and the two immiscible-liquid phase region.

At this state-of-charge, the lithium titration experiment was terminated, and the current-voltage experiments were started. The above set of experiments was repeated at several temperatures to provide a measure of the solubility of lithium polysulfides in sulfur as a function of temperature.

4.3.6.2. Current-Voltage Experiments

There were two types of experiments employed when recording current-voltage data. The first experiment recorded the change-in-voltage, ΔV, caused by a change in current, performed at various states-of-charge. The second type of data resulted from measuring the cell voltage, while passing a known current, and recording it versus time (or the percent lithium in the sulfur electrode). The resistance of the cell, once the immiscible-liquids region was entered, was much smaller than that when the sulfur electrode was nearly pure sulfur. Therefore, in these experiments, a much larger current could be passed through the cell than in the previous experiments.

A current of 10-36 mA (approximately 5-15 mA/cm^2) could be passed for as long as 6 hours without the potential continuing to decline.

The first set of cell performance experiments consisted of passing a current through the cell and then recording the steady-state cell voltage. Unfortunately, when the current densities were above a certain value, 15-25 mA/cm^2, the cell voltage would continue to decline indefinitely; this made a steady-state potential impossible to achieve. In these instances, a pseudo-steady-state potential was recorded. The convention adopted for determining the pseudo-steady-state potential was one of three, depending on the current density. First, when the current densities were 1-5 mA/cm^2, the pseudo-steady-state potentials were fairly stable and could be accurately recorded after one minute of passing the current. Second, when the current densities were in the range of 5-25 mA/cm^2 the pseudo-steady-state potentials would continue to decline with time. The values recorded to be the pseudo-steady-state potentials were the values at which the rate of decline became constant. The time to reach this constant rate varied from 2 to 5 minutes, depending on the current density. The declining potential was attributed to local Li_2S concentration gradients. That is, as Li_2S accumulated near the walls of the tubes, the a_{Li_2S} in that area would increase and cause the potential to decrease relative to what it would be if the a_{Li_2S} in the bulk solution were available. Therefore, the pseudo-steady-state potentials recorded in this range of current densities are equivalent to larger polarizations than if the pseudo-steady-state potential relative to the bulk concentrations could be measured. Third, when the current densities were higher than approximately 23 mA/cm^2, the cell potentials not only continued to decline but did so at increasing rates. This behavior was consistent with the idea that approximately 23 mA/cm^2 was the limiting current density of the cell. This was, therefore, outside of the range of a pseudo-steady-state potential.

In addition to current density, there were found to be two other independent factors affecting the pseudo-steady-state potential of a cell: state-of-charge and hysteresis. The effect of state-of-charge on the pseudo-steady-state cell potential was attributed to changes in the conductivity of the molten sulfur-polysulfide mixture. As the cell was discharged, the conductivity of

the melt was increased; therefore, for a given current the ΔV would get smaller. The hysteresis of a cell was related to the condition of the cell immediately prior to recording the pseudo-steady-state potential. That is, if the change-in-potential for a given current was measured immediately following a long discharge period, it would be greater than if the cell had been left on open-circuit for a long period of time. This was true regardless of the state-of-charge of the cell. In fact, it was found that the current-voltage data were just as dependent on the cell's immediate history as on its state-of-charge. Therefore, the condition of the cell, just before the ΔV was taken, was controlled and manipulated to be as consistent as possible. If there was a change in the condition, then the condition was noted and recorded as such.

The second set of experiments was simply to attempt to cycle the cells through repeated charges and discharges. Although most cycles were galvanostatic, some cells were cycled potentiostatically. The current density used during the cycles ranged from 5 to 15 mA/cm^2. However, the maximum current density was as high as $\sim$ 70 mA/cm^2. This high current density could only be maintained for a few minutes because the cell potential would continue to drop at an increasing rate. This was attributed to the local concentration gradients near the electrolyte, as for the current-step experiments described above.

There were several problems with the cells which greatly limited their ability to be cycled. One of these problems became evident whenever the sulfur electrode entered the solid Li_2S-liquid Li_2S_x two-phase region. Here the cells always shorted out internally. The cell discharge was, therefore, usually terminated before the sulfur electrode was discharged beyond the immiscible-liquid two phase region. Another problem with the cells was observed whenever current was passed for more than 15-20 hrs. This also seemed to cause the cells to short.

In an attempt to lengthen the cycle life, the cells were allowed some relaxation time during discharge. Instead of discharging from a fully charged cell directly to the cut off point ($\sim$ 33 mol% Li), the current was stopped near 15-20 mol% Li and the cell was left idle for approximately 24 hours. After this relaxation period, the discharge was then continued until it reached the cut-off point. At this time, the charging process would be started. The possibility of the pure

sulfur passivating the positive electrode and, thereby, driving up the resistance, made it necessary to charge the cells potentiostatically. However, for short periods of time and under careful observation, the cells could be charged galvanostatically.

4.3.6.3. Glass Conductivity

The conductivity of the glass at elevated temperatures was measured using a current-interrupt method. An oscilloscope was used to measure the change in potential of the cell at interruption of a steady current. The ohmic portion of the potential change is expected to be that portion of the change which occurs in the first 2-3 μs after the current is interrupted. The ohmic resistance was measured at four different temperatures, converted to resistivity by Equation (4-18), and plotted versus $1/T$. From this plot, the energy of activation was calculated. In order to eliminate the resistance due to the sulfur electrode, the Li-Sn/S cells were replaced with Li-Sn/Sn cells. Although these experiments replicate experiments done by Tuller *et al.* and Wen, they were not performed simply to accumulate glass conductivity data. Instead, the aim was to measure the glass conductivity to determine the degree to which the sulfur electrode was adding to the effective Li-Sn/S cell resistance.

The Li-Sn alloy used as the negative electrode in these cells was of the same composition as the negative electrode used in the Li-Sn/S cell experiments. Sufficient excess of the Li-Sn alloy was used so that its composition remained in the two-phase region. The positive electrode was simply molten tin with a molybdenum current collector in a lithium chloroborate tube. The vapor pressure of tin at 400 °C is only 10^{-13} Pa; thus the tubes did not have to be sealed. The same two types of current-voltage data recorded for the Li-Sn/S cells were obtained for these cells. However, there was no need for the long relaxation periods as in the Li-Sn/S cells, because these cells equilibrated in only a few seconds. In addition to the glass conductivity data, these experiments yielded some data on the activity of lithium in a Sn-rich Li-Sn liquid.

4.4. Results and Interpretations

4.4.1. Lithium Titration

The data for measuring the solubility of Li_2S in sulfur were taken with two different cells at two different temperatures, 390 °C and 400 °C. The mass of sulfur in the two cells was different (0.798 g and 1.607 g) to assure that the solubility reported was not a function of the cell capacity. The transition from nearly pure sulfur to the two-immiscible-liquid region was found to occur at $0.03\ ^{+0.03}_{-0.01}$ mol% lithium in sulfur at 390 °C and $0.04\ ^{+0.03}_{-0.01}$ mol% for 400 °C (range of uncertainty based on scatter in break-point in curve in Figure 4-7). The increase in solubility at the higher temperature is inside the range of experimental uncertainty; however, based on the Li-S phase diagram, shown in Figure 4-1, the solubility limit should indeed increase with increasing temperature. These solubilities are in semi-quantitative agreement with the value reported by Sharma,[2] 0.03 mol% lithium in sulfur at 365 °C. Others, however, have found the solubility to be five and even ten times higher.[41,42,48] Table 4-1 is a summary of the cells' characteristics and solubilities, and Figure 4-7 is a plot of data from these two cells.

Table 4-1 Summary of Cell Characteristics for Li_2S Solubility in Sulfur Experiments.

	Sulfur (g)	Electrode Area (cm^2)	Temperature (°C)	Lithium Solubility (mol%)
Cell # 18	1.607	5	390	$0.03\ ^{+0.03}_{-0.01}$
Cell # 26	0.798	4	400	$0.04\ ^{+0.03}_{-0.01}$

The inclined lines have a slope of $\frac{-RT}{2F}$, or 0.067 volts per decade at 673 K. The constant potential line at 1.65 volts versus LiSn represents the equilibrium open-circuit cell potential for the two-immiscible-liquids region. A value of 1.65 volts versus LiSn translates to 2.24 volts versus pure Li, which is the same value reported by Cairns *et al.*[6] at 400 °C. The data points which fell below the line were points which were recorded before the cell was allowed the necessary relaxation time.

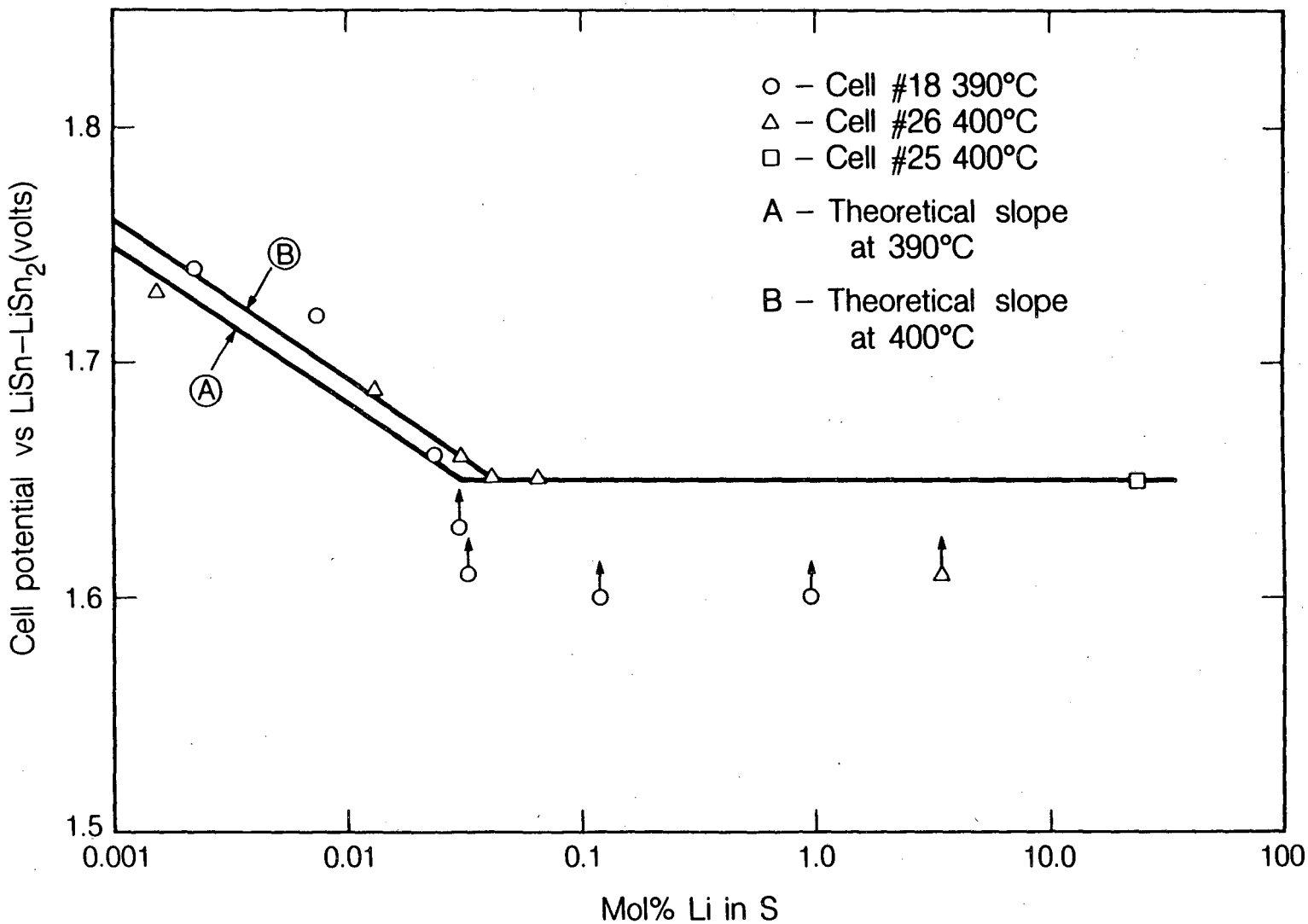

Figure 4-7. Open-circuit cell potential versus mol% lithium to show solubility of lithium (as a sulfide) in sulfur. Arrows point to equilibrium.

The length of time necessary for the cell potential to come completely to its open-circuit value was found to depend on the amount of lithium discharged. When the change in lithium mole fraction was less than 0.1 mol% Li, the cell potential would stabilize in less than one day. However, when the amount of lithium discharged was in the range of 1 mol% Li or higher, the time necessary for the cell potential to stabilize became very long. Several cells were left on open-circuit for as long as four days after being discharged to approximately 10 mol% Li, and they never recovered to higher than 1.60 volts versus LiSn. However, cell #25 was loaded in a partially discharged state (23.8 mol% Li), and its open-circuit potential at 400 °C was 1.65 volts versus LiSn. This cell was charged to ~6 mol% Li and then discharged to 14 mol% Li, where the open-circuit cell potential never recovered to higher than 1.60 volts versus LiSn. This result indicates that discharging the cell is responsible for the non-equilibrium cell potentials.

Repeated attempts to measure the Li solubility in sulfur produced scattered and non-reproducible data. The uncertainity of the solubility of Li (as the sulfide) in these other cells was always within $^{+0.03}_{-0.01}$ mol% Li from the values reported in Table 4-1. However, the potentials before reaching this point varied by up to 300 mV from the value expected for a particular mole percent lithium. Appendix A lists the data from these cells. The low potentials, long relaxation periods, and the scattered data all point to some problem with these cells.

There are two probable sources of error in measuring the solubility of Li_2S in sulfur. One could be contamination from adsorbed oxygen on the surface of the solid sulfur, current collectors, or glass walls. The other source could be a corrosion reaction occurring between the glass and lithium polysulfides. In either case, the lithium might be scavenged out of the sulfur and this would result in two effects. First, the reaction between lithium and oxygen would give a higher potential (neglecting effects caused by activity differences) than would that between lithium and sulfur. The stoichiometric equations and the E^o's for the two reactions are

$$2Li + S \rightleftarrows Li_2S, \qquad E^o = 2.178 \text{ volts} \tag{4-19}$$

$$4Li + O_2 \rightleftarrows 2Li_2O, \qquad E^o = 2.654 \text{ volts.} \tag{4-20}$$

The oxygen could react with any existing lithium sulfide to form lithium oxide and sulfur,

$$2Li_2S + O_2 \rightleftarrows 2Li_2O + 2S. \tag{4-21}$$

Once all of the oxygen had reacted, the cell potential would drop to the potential for the lithium-sulfur reaction, corrected for the appropriate activities. However, by this time the second effect could be manifest, i.e., the unknown amount of scavenged lithium could falsify the count of Li_2S dissolving in the sulfur. A plot of cell potential versus mole percent lithium, in the range of pure sulfur to 0.1 mol% Li, could have errors in both the cell potential and the percent lithium. The possibility of the errors due to a reaction between the glass and lithium polysulfides was suggested by the static corrosion experiments presented earlier. The low potential and long relaxation periods could be attributed to the building of a reaction layer. It was decided that a more conclusive answer to whether a reaction between the glass and the lithium polysulfides was occurring could be found by discharging the cells further. Therefore, some cell performance experiments were devised.

4.4.2. Current-Voltage

The experiments for measuring the current-voltage performance of the Li-Sn/S cells were performed with cells whose sulfur electrodes were primarily in the two-immiscible-liquids region. The data from these experiments were recorded in two parts. The first part was a set of experiments to measure the pseudo-steady-state polarization, and the second part was an attempt to cycle the cells through charge-discharge cycles. In each of these experiments, the cell potentials were measured and found to be stable when current densities were in the range of 5-15 mA/cm^2. The maximum current densities obtainable were as high as 70 mA/cm^2, but the cell potentials were unstable when the current densities were this high.

Figure 4-8 is a plot of the pseudo-steady-state polarization η_{total} versus current density i of cell #18. The curves represent sets of data recorded with the cell at different states-of-charge and different rest conditions. The data for the curve labeled A were obtained when the cell was discharged for the first time, *i.e.* between 0.12 and 1.6 mol% Li. The data for curve B were taken

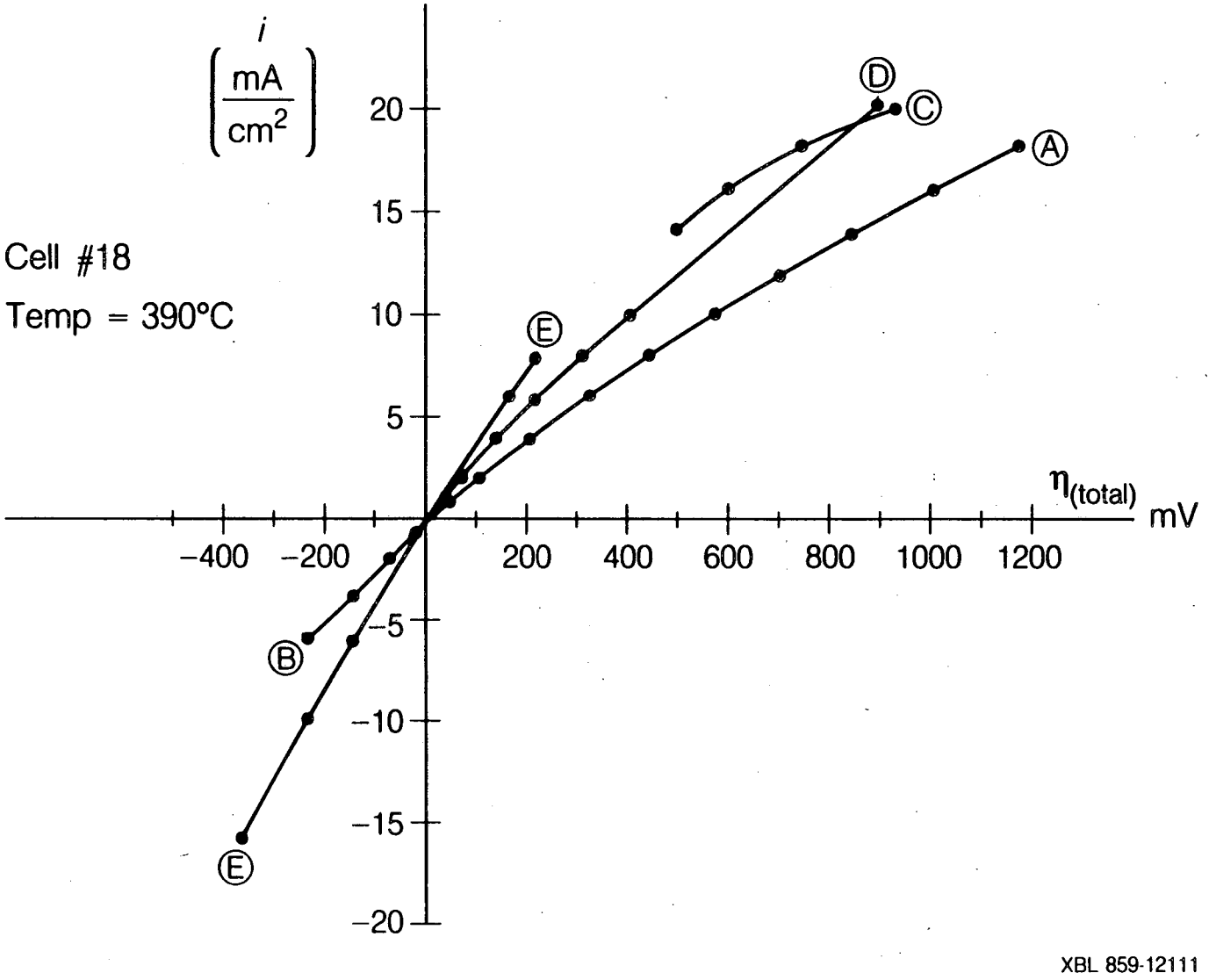

Figure 4-8. Pseudo-steady-state overpotential versus current density for cell #18.

when the cell was being recharged from curve A back to 0.9 mol% Li. Higher currents than shown on the graph were passed, but these caused the cell potential to climb very rapidly; this phenomenon was attributed to the formation of a sulfur passivation layer on the glass walls. Curve C represents data obtained by discharging the cell immediately following curve B, or between 0.9 and 3.9 mol% Li. The set of points for curve D were taken immediately after discharging the cell at a rate of 28 mA (approximately 5.5 mA/cm^2) for 8 hours. This resulted in 17 mol% Li in the sulfur electrode. The cell ohmic resistance was measured with an AC bridge and found to be 6.5 Ω. Finally, the set of points labeled E was taken by alternating every few minutes between charging and discharging at approximately 18 mol% Li in the sulfur electrode. At the conclusion of obtaining curve E, the cell ohmic resistance was measured with the AC bridge and found to be $\sim$4 Ω. This is equivalent to a glass conductivity of approximately 0.0025 $(\Omega \cdot cm)^{-1}$. These experiments were repeated with 4 other cells, and the results were found to be reproducible. Appendix B contains a table listing the results from these other cells.

There are two significant findings from these tests. First, a comparison of curves A and D shows that the pseudo-steady-state polarization was higher when the cell was nearly fully charged than when it was partially discharged. This is attributed to the low conductivity of nearly-pure sulfur. Second, for a given state-of-charge, the pseudo-steady-state polarization was higher following a long discharge period than it was following either a significant relaxation period or period of charging. Comparisons of curves A to C or D to E exhibit this trend. This phenomenon might be attributed to formation of a reaction layer, which either blocks some of the active transfer area or reduces the glass conductivity. The relaxation period and the charging could have helped to rid the glass of some of the reaction layer and, therefore, decrease the polarization caused by the blocking film.

The contribution of ohmic resistance to the total pseudo-steady-state polarization can be eliminated from the total polarization by subtracting the product of the total current and cell resistance from the total pseudo-steady-state polarization. This corrected polarization would, therefore, be the IR-free overpotential $\eta_{IR-free}$. Figure 4-9 is a plot of the IR-free overpotential versus current density for curves A and D shown in Figure 4-7. The shapes of these curves

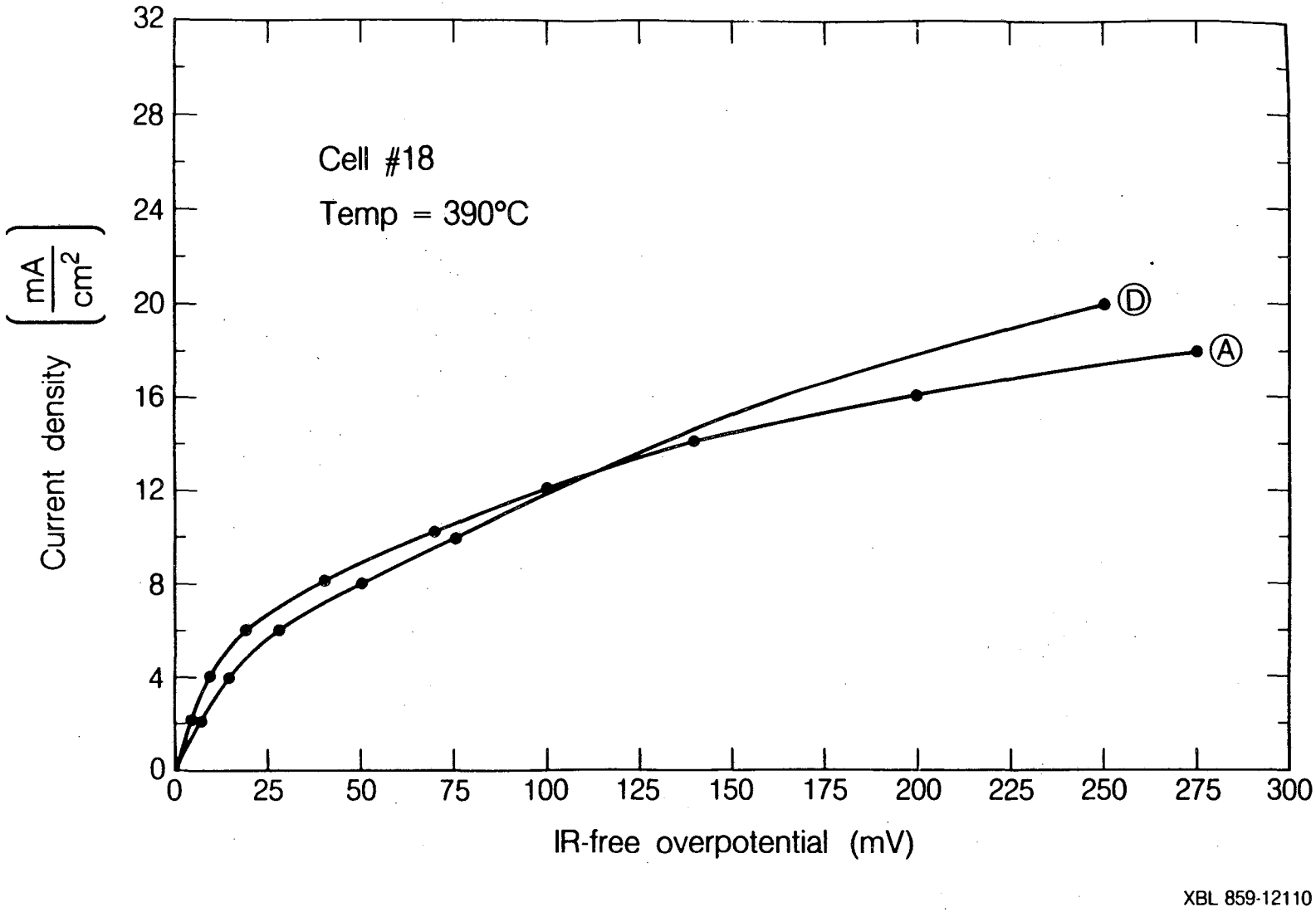

Figure 4-9. IR-free overpotential versus current density for cell #18.

qualitatively resemble the shape expected for a cell which has a mass-transfer-limiting current density i_L=23 mA/cm^2. However, the curves do not quantitatively follow the expected shape. Therefore, the limiting current can not solely be attributed to mass-transfer phenomena, but rather, a combination of mass transfer and other effects.

After recording data for curve E (Fig. 4-7), the cell was left on open-circuit for approximately 5 hours. At this point the cell shorted and the electrolyte broke. The pieces of glass, which had been below the level of liquid sulfur, and could be recovered after the failure, were observed to be coated with a yellow-white film. This yellow-white reaction layer was observed on the glass from every cell where post-analysis was possible. Figure 4-10 is the X-ray pattern from the reaction layer on cell #38; it had been discharged to approximately 22 mol% Li. This pattern is very similar to the patterns obtained in the static immersion tests, see Figure 3-4. Table 4-2 is a summary of the possible compounds present in the reaction layer for cell #38.

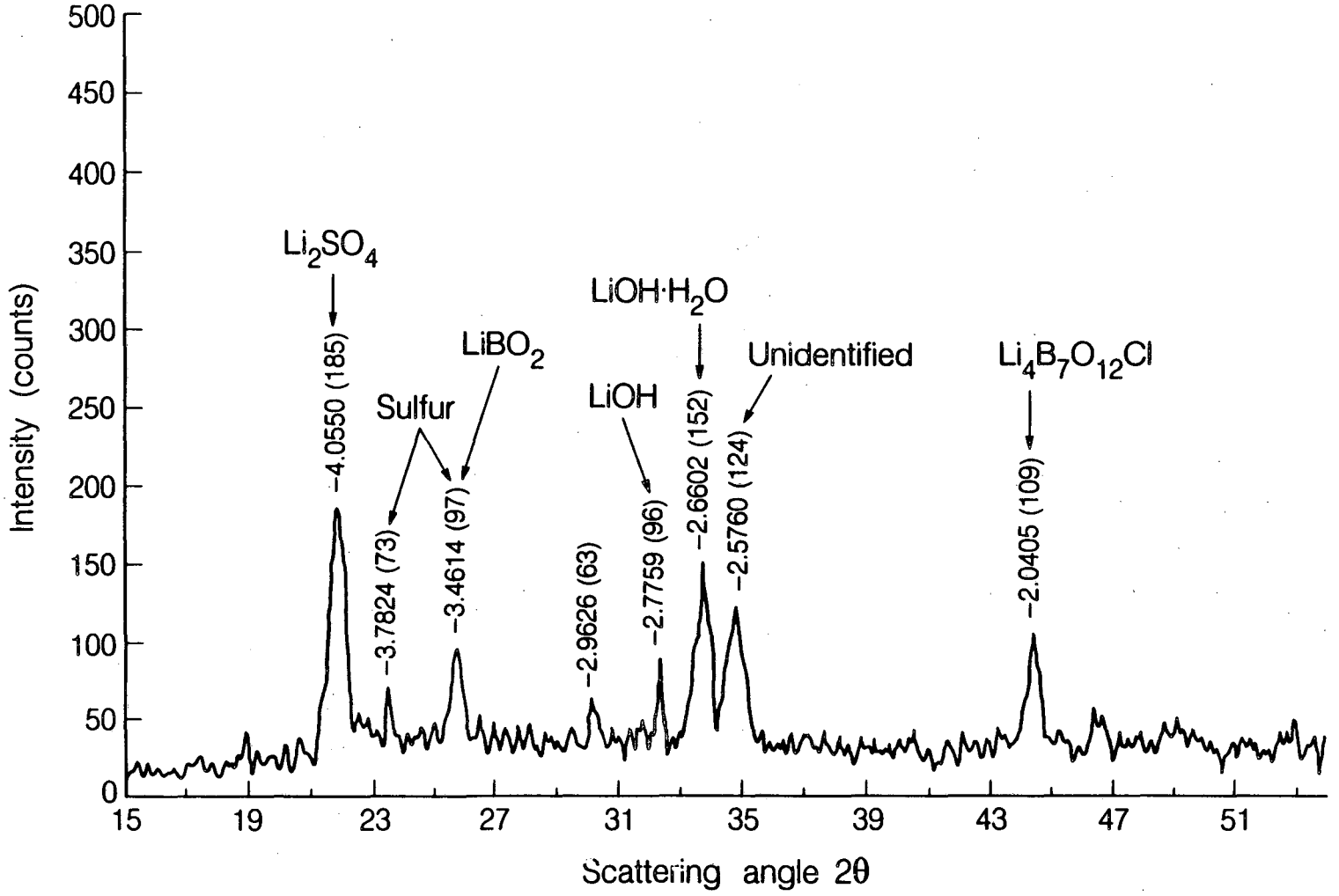

Figure 4-10. X-ray diffraction pattern for corrosion products of cell #38 in S-22 mol% Li_2S at 400 °C.

Table 4-2 Summary of Possible Compounds in the Reaction Layer from Cell #38 based on X-ray Diffraction Patterns.

Compound	d values	2θ values	Confidence	Comments
$Li_4B_7O_{12}Cl$	2.05_x 2.70_3 3.48_2	44.1 33.2 25.6	High	9.1 mol% $(LiCl)_2$ 27.3 mol% Li_2O 63.6 mol% B_2O_3
LiOH	2.75_x 4.35_4 2.51_2	32.5 20.4 35.8	Medium/High	Hydrated Li_2O
$LiOH{\cdot}H_2O$	2.67_x 2.70_5 2.44_5	33.5 33.2 36.8	Medium/High	Hydrated Li_2O
Li_2S	3.30_x 2.02_4 1.72_3	27.0 44.8 53.2	Medium/Low	Hygroscopic
Li_2SO_4	4.04_x 4.00_x 3.92_5	22.0 22.2 23.7	High	Caused by Contaminations
HBO_2	4.20_x 3.07_x 6.75_3	21.1 29.1 13.1	Low	Hydrated B_2O_3
$LiBO_2$	3.53_x 2.19_x 1.80_8	25.2 41.2 50.7	Medium	50% Li_2O 50% B_2O_3
Li_3BO_3	3.02_x 2.63_6 2.67_5	29.5 34.1 33.5	Medium	75% Li_2O 25% B_2O_3
Sulfur -#	3.89_x 2.73_7 3.12_3	22.8 32.8 28.6	Medium/High	Hexagonal
Sulfur -#	3.29_x 6.65_3 3.74_2	27.1 13.3 23.8	Low	Monoclinic
Sulfur -#	3.85_x 3.21_6 3.44_4	22.8 27.8 25.8	Medium/High	α-phase

References 25, 26, 27.

There was strong evidence that the reaction layer contained crystalline lithium chloroborate along with possibly some other lithium borates. As was the case with the X-ray patterns in static corrosion tests, there was a large and very prominent unidentified peak at approximately 35 degrees. This conceivably could have been caused by some type of lithium borosulfate, as postulated in section 3.4. There was also strong evidence of sulfur and possibly some Li_2S. This was expected because the tubes were not cleaned by soaking in carbon disulfide nor methanol, as were the discs in the static tests.

The second group of cell performance experiments involved attempting to pass cells through charge-discharge cycles. The cycles were started with the cells in both the fully-charged state and in a partially-discharged state. Figure 4-11 shows some results from attempted cycling of cells # 22, 23, and 24, which were all started in the fully-charged state. Unfortunately, the cells all shorted before a complete charge-discharge cycle was achieved. In fact, every cell which was loaded with pure sulfur shorted before completing a full charge/discharge cycle. Some of the shorts were catastrophic and others were gradual. In either case, the shorts were the result of discharging the cells either too fast or too far. A cell which was discharged incrementally, with periods of rest separating the discharge periods, could be discharged farther than if it were discharged continuously. This trend was especially evident in cell #20.

The cause of the shorts appeared to be structural failures of the glass. The cells which shorted catastrophically were those where the glass cracked below the molten sulfur level, while the cells which failed slowly were cells where the glass cracked above the molten sulfur. The former type of shorts caused violent reactions to occur as the molten sulfur and Li-Sn came into contact. The latter types of shorts were the result of the glass cracking above the molten sulfur and allowing the sulfur to evaporate. The decline in the potential of the latter cells was always preceded by a negative spike in the potential. These spikes were used to identify when the shorts had occurred. Table 4-3 is a summary of the cell data acquired from attempting to cycle the cells.

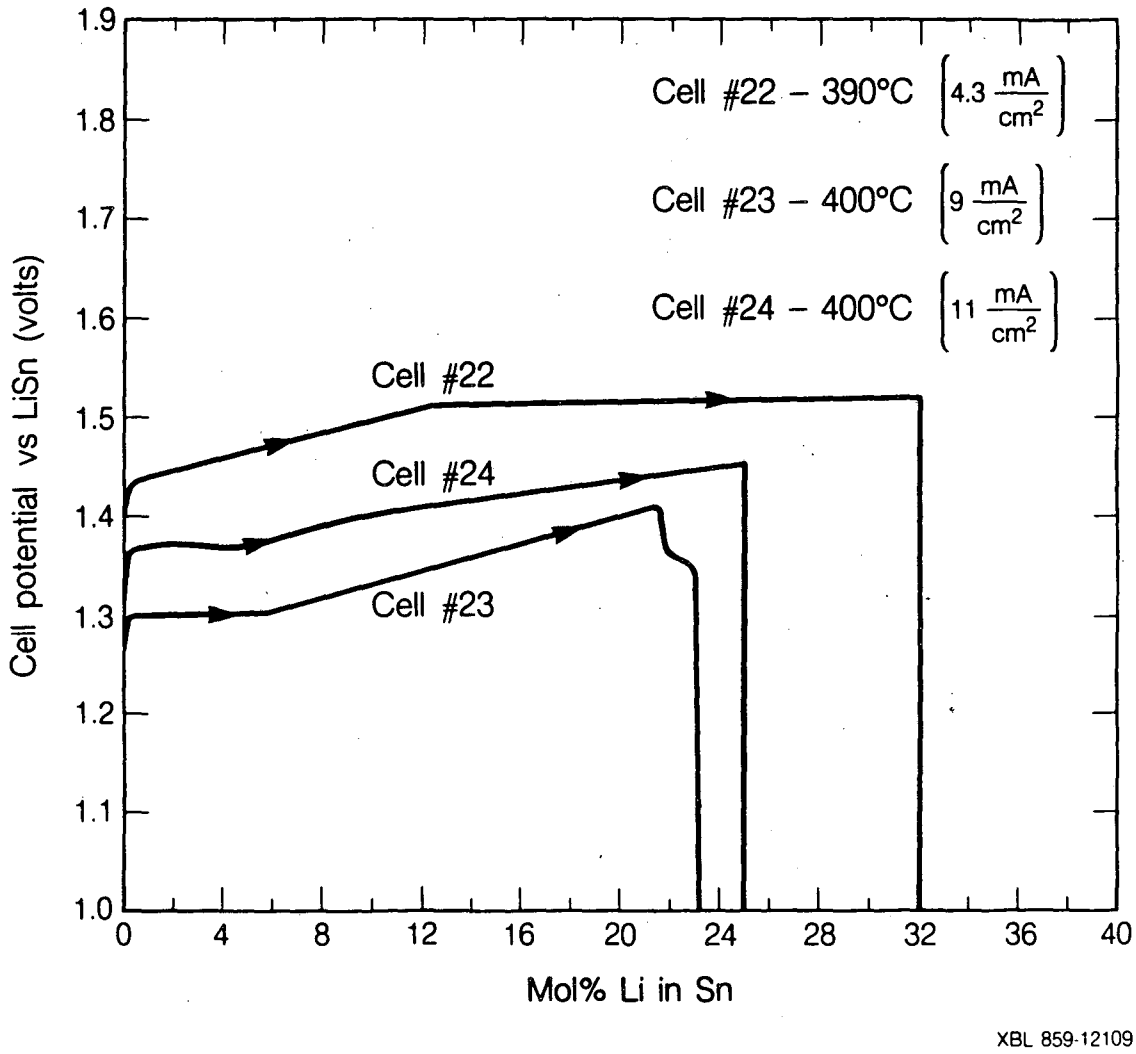

Figure 4-11. Galvanostatic discharge of three fully-charged cells.

Table 4-3 Summary of Cell Performance Data.

Cell	Temp. (°C)	Sulfur (gm)	Area (cm^2)	Average mA	Max. mA	Total Hours	Max. mol% Li	Adjusted # mol% Li
18	390	1.607	5	30	150	67	17	17
19	380	0.531	4	30	200	35	36	*
20	380	0.225	2	50	50	146	40	*
21	400	0.375	2	10	100	144	2	3
22	390	0.473	3	13	13	15	32	33
23	400	0.853	4	36	36	7	23	24
24	400	1.221	3	33	33	12	25	25
26	400	0.798	4	10	10	136	4	4
35	380	0.525	3	30	60	330	12	13
38	400	0.233	2	5	5	22	20	22
39	400	0.410	2	5	5	20	15	16

Corrected for non-reacting sulfur condensed on cell walls.
* No sulfur was observed.

The column labeled "Adjusted mol% Li" was an adjustment in the mole percent lithium due to an estimated amount of sulfur not participating in the bulk solution. A certain amount of sulfur was observed to condense on the walls of the tubes or around the alumina and, therefore, did not participate in the reaction of the sulfur electrode. The adjusted weight of sulfur was calculated by subtracting the estimated amount of sulfur on the walls from the beginning weight of sulfur. The amount of sulfur observed on the walls of the tubes was estimated to be approximately 0.025 gms, based on a density of 1.6 g/cm^3.

Figure 4-12 shows two plots for cell #25; the first is a current versus mol% Li plot showing a potentiostatic charge, and the second is a voltage versus mol% Li plot showing a galvanostatic discharge. Cell #25 which was loaded in the partially discharged state, 23.8 mol% Li; the open-circuit cell potential was initially 1.65 volts versus LiSn at 400 °C. However, the potential began to decline after approximately one hour at 400 °C. At this point the cell was charged potentiostatically until the sulfur electrode was approximately 6 mol% Li, where the cell resistance was approximately 800 Ω. This high resistance, attributed to the formation of a passivating layer of low-conductivity sulfur, made it impossible to charge the cell at an appreciable rate. At this

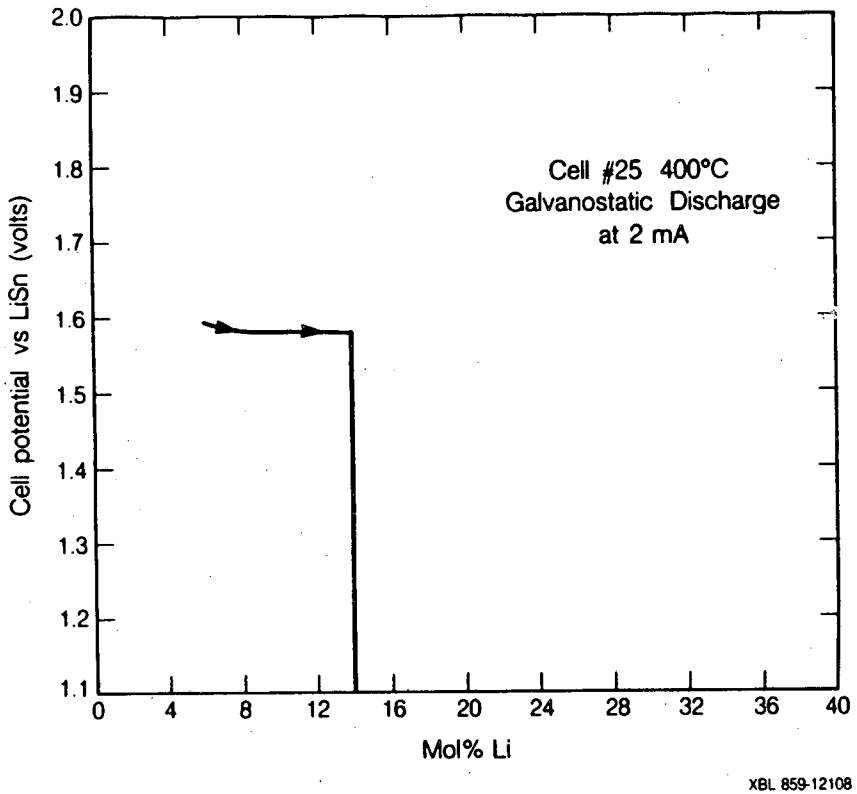

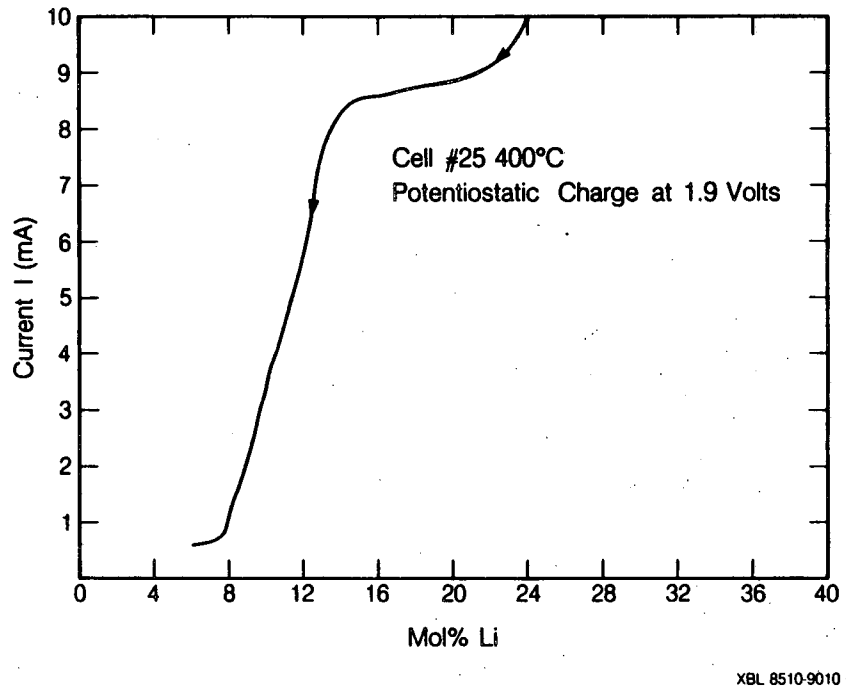

Figure 4-12. Potentiostatic charge and galvanostatic discharge versus mol% lithium for cell #25 at 400 °C.

point, the cell was discharged at a rate of 2 mA to 14 mol% Li, where it shorted. Before shorting, the open-circuit cell potential was measured and found to be stable at 1.606 volts versus LiSn at 400 °C.

4.4.3. Glass Conductivity

The data used for calculating the conductivity of the glass were obtained via current interruption with a Li-Sn/Sn cell as described earlier. The cell resistance for cell #34 was measured at four different temperatures: 400 °C, 375 °C, 355 °C, and 330 °C. The wall thickness of the tube was measured with a micrometer and found to be approximately 0.04 cm. The portion of the surface area of the tube which was in contact with the electrodes was measured before and after the experiment and found to be 2.0 cm^2. The ohmic resistance was measured and found to be the same for both anodic and cathodic current-interrupt. Table 4-4 is a summary of the cell resistances and glass conductivities calculated for cell # 34 using Equation (4-18).

Table 4-4 Summary of the Li Conductivity values for Lithium Chloroborate Glass in Cell # 34.

Temperature (°C)	Reciprocal Temperature K^{-1}	Cell Resistance (Ω)	Glass Conductivity σ ($\Omega^{-1}\cdot cm^{-1}$)
400	0.00145	7	0.0029
375	0.00154	10	0.0020
355	0.00159	15	0.0013
330	0.00166	22	0.0009

These data points are shown in Figure 4-13 on a plot of the natural logarithm of conductivity times temperature $\ln\sigma T$ versus $1000/T$. The slope of the line drawn through the points multiplied by the Boltzmann constant k yields the energy of activation. Its value was found to be 0.66 eV. Figure 4-14 shows the same data plotted as log of conductivity versus $1000/T$ with some data reported by Tuller *et al.*[1] The composition of the above glass reported in Tuller's format is $\frac{33}{22}$, corresponding to a composition of 67.0 mol% B_2O_3, 25.7 mol% Li_2O, and 7.3 mol% $(LiCl)_2$.

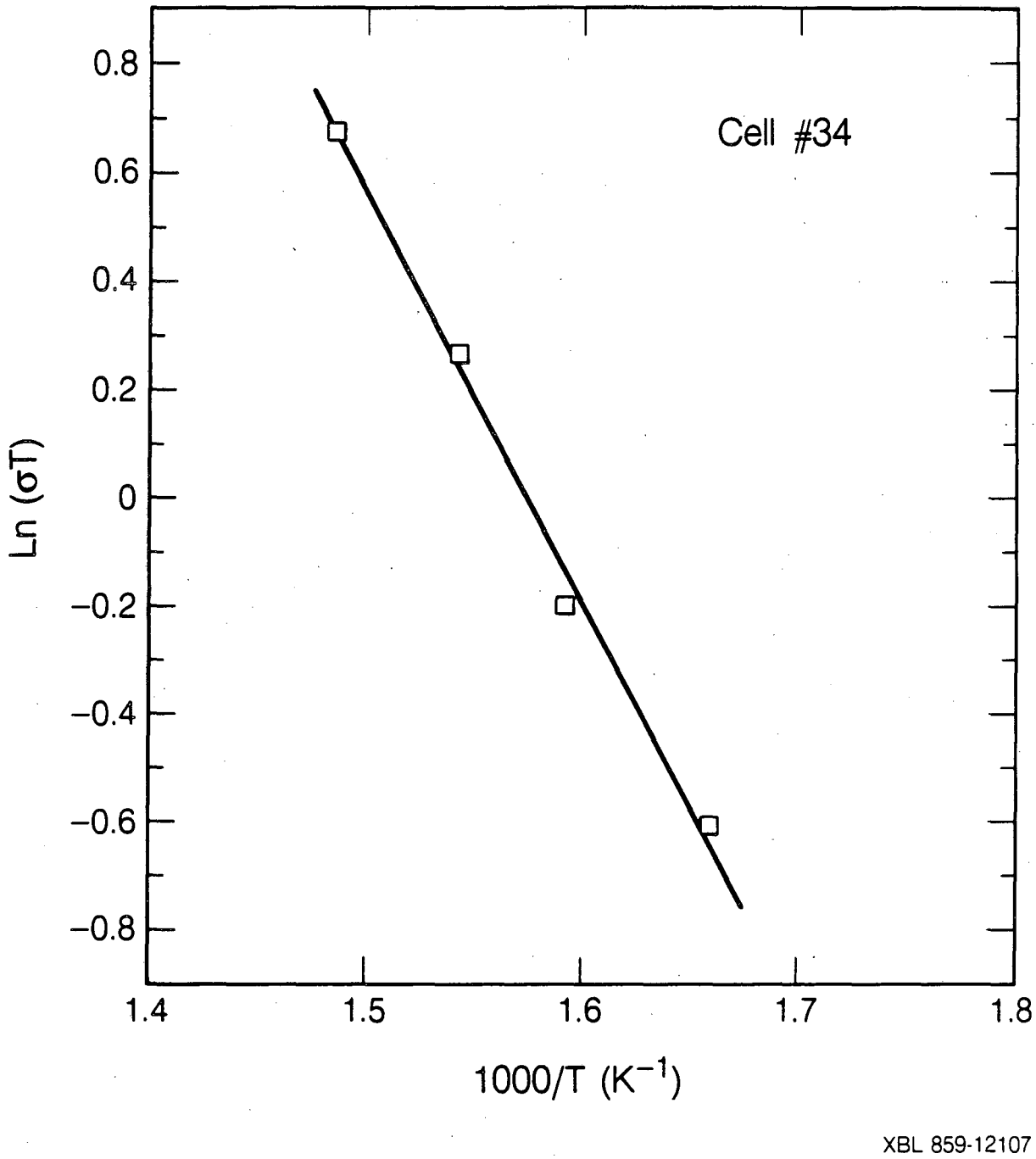

Figure 4-13. The product of conductivity times temperature versus reciprocal temperature.

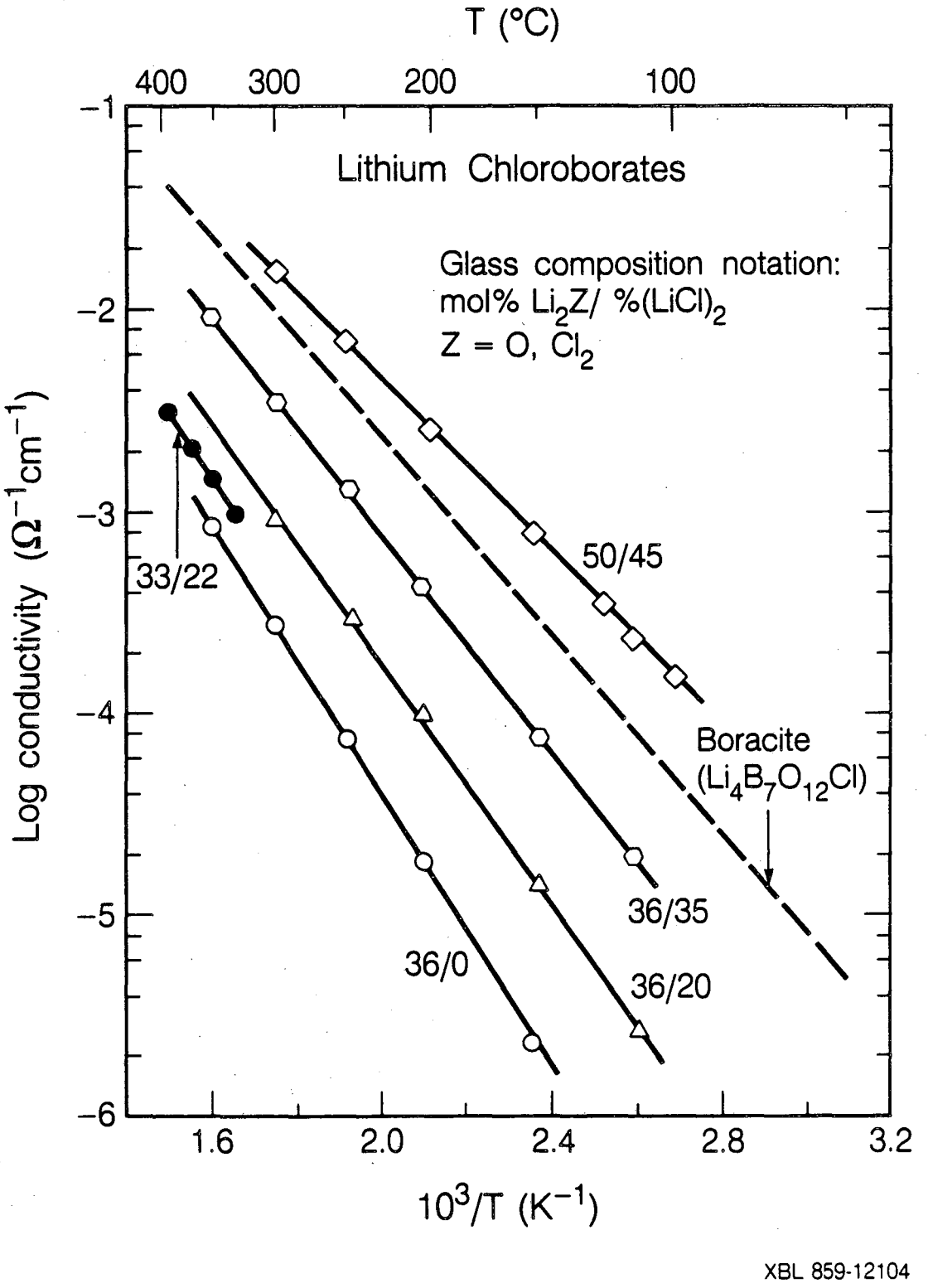

Figure 4-14. Log of conductivity versus reciprocal T for series of lithium chloroborate glasses (1).

The data for the above glass, made at LBL, matched well the trends in the conductivities of the similar glasses made at MIT.

Cell #34 from Table 4-4 was examined post-mortem, and it was found that a black reaction layer had formed on the walls of the tube. Other cells also contained this same reaction layer. The clearest evidence of this came in cell #28, which was loaded with pure lithium. This cell shorted in less than 3 hours of operation, and the glass was heavily coated with a black film. This indicates that Li is the attacking species to form the black reaction layer. Similar observations and conclusions were made by Tuller *et al.* who reported the composition of this layer to be $3Li_2O \cdot B_2O_3$.[49] This layer was reported to be ionic in nature, and it did not interfere with the intrinsic glass conductivity. It was also reported that a mismatch between the volume of the reaction layer and the glass substrate caused structural failures. However, no failures attributed to this black reaction layer were observed with the Li-Sn/Sn cells.

The conductivity of the glass could not be measured with the Li-Sn/Sn cells until the Sn electrode had been discharged to approximately 28 mol% Li at 350 °C. This corresponds to a composition near the phase boundary on the Sn-rich side of the Li-Sn phase diagram. This problem was attributed to poor wetting of the glass by nearly pure tin. For example, at 400 °C the cell resistance at 30 mol% Li was measured to be 7 Ω, while at 20 mol% it was 11 Ω and at 0.1 mol% Li it was 25 Ω. However, once the tube was wetted, the lithium mole fraction could be lowered to 20 mol% Li without causing dewetting.

Figure 4-15 is a plot of open-circuit cell potential versus the mole fraction of lithium in the Sn electrode for the Li-Sn/Sn cells. The solubility of Li in Sn occurred at approximately 30 mol% Li; this agrees well with the value reported by Wen *et al.*[44] This also corresponds with the findings of Tuller *et al.* that the transference number of Li^+ in the glass is 1. The Nernst equation for these concentration cells, written in terms of mole fractions and activity coefficients, is

$$E = \frac{-RT}{F} \ln \frac{\gamma_A x_A}{\gamma_B x_B} , \tag{4-22}$$

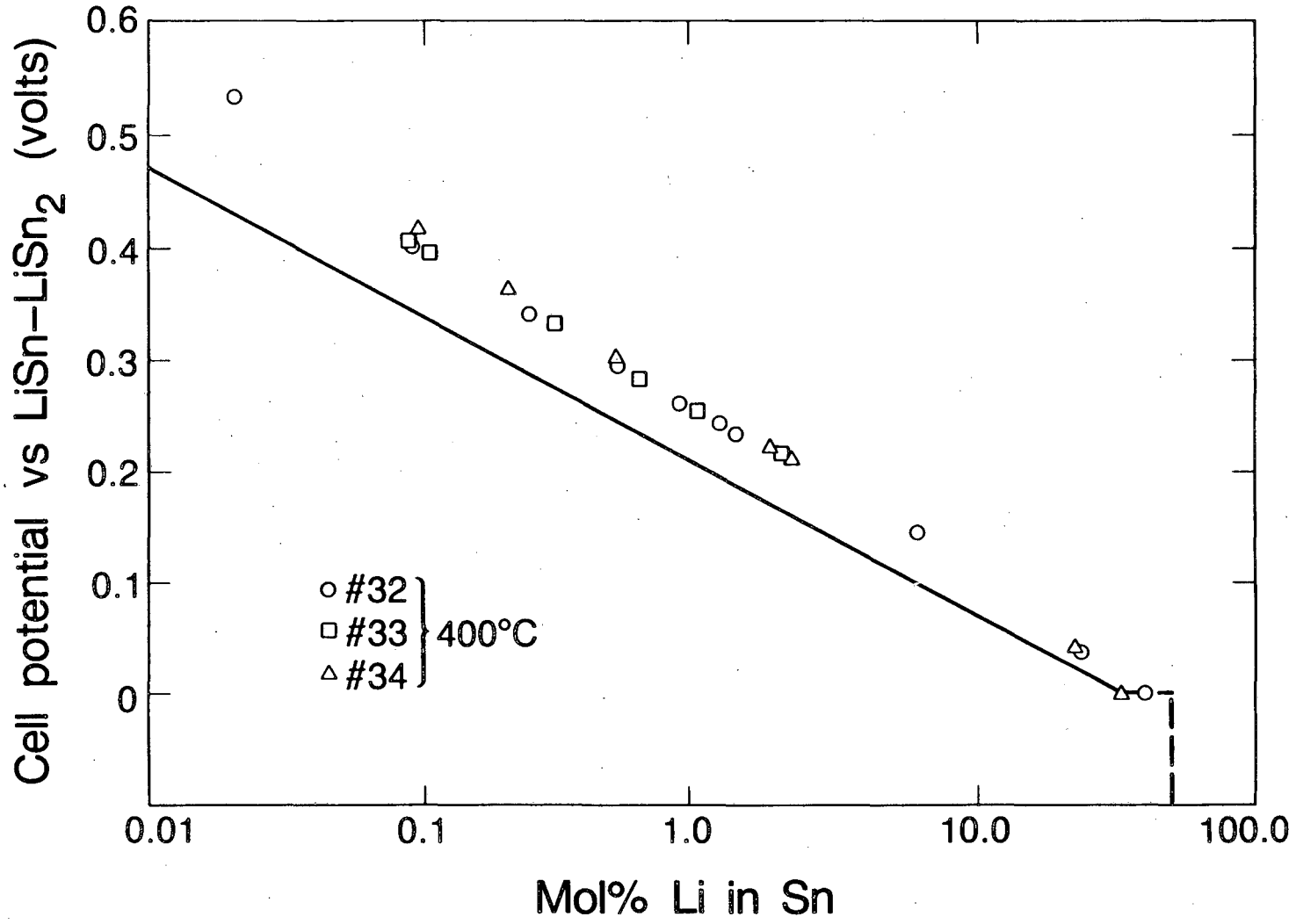

XBL 858-11268

Figure 4-15. Plot of open-circuit cell potential versus mol% lithium for three Li-Sn/Sn cells.

where the subscript A represents Li in the Sn electrode and B represents Li, at the liquidus phase boundary, in the constant activity Li-Sn electrode. A cell potential of zero volts, as indicated in Figure 4-15, would occur when the activity of lithium in the Sn electrode was equal to the activity of lithium in the Li-Sn electrode. The solid line drawn in Figure 4-15 is for the hypothetical case of equal lithium activity coefficients in the two electrodes; it has a slope of $\frac{-RT}{F}$. The fact that a line drawn through the data had approximately the same slope as the solid line was attributed to the fact that the Li in the Sn electrode had a constant activity coefficient. This can be explained by taking the derivative of Equation (4-22) with respect to $\ln x_A$ at constant temperature and constant $\gamma_B x_B$,

$$\frac{dE}{d\ln x_A} = \frac{-RT}{F}\left[\frac{d\ln\gamma_A}{d\ln x_A} + 1\right]. \tag{4-23}$$

For the slope, $\frac{dE}{d\ln x_A}$, to be equal to $\frac{-RT}{F}$ the derivative $\frac{d\ln\gamma_A}{d\ln x_A}$ must be equal to zero; that is, $\ln\gamma_A$ must be a constant. The fact that the data fell above the solid line signifies that the activity coefficient of lithium in the Sn electrode was lower than the activity coefficient of lithium in the Li-Sn electrode.

Figure 4-15 provides enough information so that, combined with the value reported in the literature for the activity of lithium in the two-phase region, the lithium activity or activity coefficient could be calculated for a Sn-rich Li-Sn liquid of any mole fraction. The Nernst equation can be rewritten

$$E = \frac{-RT}{F}\ln\frac{\gamma_A x_A}{a_B}. \tag{4-24}$$

The activity of lithium in the Li-Sn alloy at 400 °C has a value of 4.50×10^{-5} versus pure lithium. Therefore, after substituting the cell potential, as read from Figure 4-15, for a given mole fraction, the activity coefficient of lithium can be calculated. For example, at 400 °C the activity coefficient of lithium at 1.0 mol% Li is 5.4×10^{-5}. This compares to the values 6.44×10^{-5} at

415 °C and 3.23×10^{-5} at 372 °C reported by Wen *et al.*[44] They also reported that the activity coefficient of lithium in the liquid phase with the composition of less than 10 mol% Li was independent of temperature. Figure 4-16 is a plot of lithium activity coefficient versus mole percent lithium as calculated from the data shown in Figure 4-15. The deviation in the low concentration region is attributed to lithium being scavenged by the glass as explained above. Once the activity coefficient of lithium is known, its activity can be calculated by multiplying the activity coefficient by the mole fraction. For example, the activity of lithium at 1.0 mol% Li would be 5.4×10^{-7}.

4.5. Discussion

The attractiveness of using lithium chloroborate glass as the electrolyte in a Li-Sn/S cell was supported by the fact that the glass was able to support current densities of 5 to 15 mA/cm^2 for 15-20 hours, or as high as 70 mA/cm^2 for 3 to 5 minutes. There appeared to be a limiting current at approximately 23 mA/cm^2. Current densities in excess of this value caused the cell potential to decrease in a variable manner. As the cells were being discharged, there apparently was a reaction taking place between the glass and the lithium polysulfides which would eventually cause the cells to fail. The early formation of the reaction layer caused an increase in the overall cell resistance and a decrease in the open-circuit cell potential but did not destroy the cells. However, as the layer grew, it would eventually cause the cells to short. These shorts have been attributed to fractures in the glass. The fractures are the result of two effects: volume mismatches between the glass and reaction layer, and the reaction layer growing and blocking most of the cell's active area, which causes the remaining active area to support a high current density. Local current densities in excess of some critical value have been found to be responsible for failure of other solid electrolytes, e.g., the ceramic β'' - alumina used in sodium/sulfur cells.[50] This same phenomenon could be responsible for cracking the lithium chloroborate glass.

The composition of the yellow-white film could not be identified with more confidence in these experiments than it was in the static corrosion tests. However, as was the case in the static corrosion tests, it was clear that there were present some crystalline lithium chloroborate

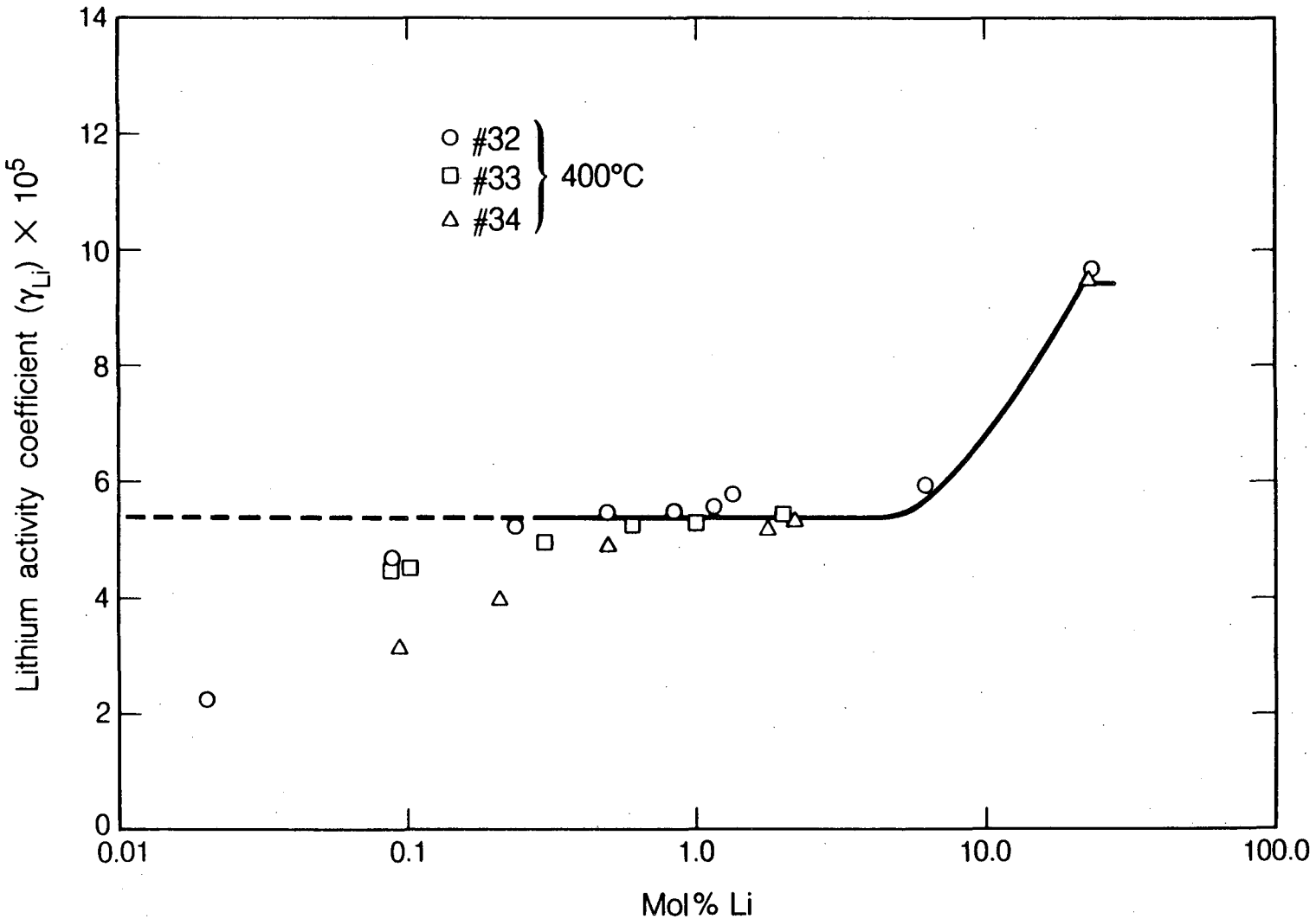

XBL 859-12106

Figure 4-16. Lithium activity coefficients versus lithium mol% in three Li-Sn/Sn cells.

compounds and possibly some unknown lithium borosulfides. Table 3-6 lists potential reactions between the lithium chloroborate glass and lithium polysulfides.

It is significant to note that as the reaction layer grew on the glass it would lower the cell potential by approximately 0.05 volts. This low potential was not merely a result of the state-of-charge, because a cell which was loaded partially-discharged gave the expected open-circuit cell voltage. However, after this same cell was recharged and *then* partially discharged, the open-circuit cell potential was low by 0.05 volts. This indicates that the act of discharging the cell had a significant effect on lowering the cell potential and presumably in causing the formation of the film.

It is not believed that discharging the cell is the cause of the corrosion, but rather that discharging the cell speeds up the reaction that naturally would occur between the glass and the polysulfides. This is consistent with the idea that polysulfides are the attacking species. The reaction between the glass and the polysulfides would be accelerated during discharge, because the concentration and composition of polysulfides near the walls would be greater than when the cells were being charged or on open-circuit. The conclusion that lithium polysulfides are the attacking species is strongly supported by the static corrosion tests. This conclusion is similar to some results reported for the sodium/sulfur system. For example, DeJonghe[51] has reported that "chemical attack seems to occur rather rapidly when x in Na_2S_x reaches into the two-phase region in equilibrium with Na_2S_2. Thus, it is the discharged sulfur electrode composition that is the most corrosive one."

CHAPTER 5

CONCLUSIONS

5.1. Summary

Novel Li/S cells have been built which employed lithium chloroborate glass tubes as their electrolytes. Current-voltage experiments were performed with the cells to determine the degree of polarization caused by the application of various currents. The glass was able to support current densities up to 15 mA/cm^2 for 15-20 hours or as high as 70 mA/cm^2 for 3-5 minutes. These performances were reproducible and showed similar polarization characteristics for anodic and cathodic currents. Limiting currents were observed for all cells at approximately 23 mA/cm^2, significantly higher than the 7 mA/cm^2 reported by Tuller *et al.*[52] The limiting currents were apparently caused by the formation of a reaction layer on the sulfur side of the electrolyte.

The cells could be loaded in the fully-charged state and then discharged to approximately 33 mol% Li or they could be loaded in a partially-discharged state and charged to approximately 6 mol% Li. However, complete cycles were not obtainable because the accumulation of the reaction layer would slowly block transport in the cells and ultimately cause the cells to short.

These cells were also used to measure the the solubility of lithium (as a polysulfide) in sulfur. It was found to be $0.04\ ^{+0.03}_{-0.01}$ mol% Li at 400 °C. This is in qualitative agreement with the value reported by Sharma.[2]

The high ionic conductivity and workability of lithium chloroborate glasses make them attractive candidates for use as electrolytes in Li/S cells. The conductivity is high enough that during discharge in a Li/S cell the drop in potential due to the ohmic resistance would be only a small fraction of the open-circuit cell potential. For example, assuming a glass conductivity of $2 \times 10^{-2}\ (\Omega^{-1}\cdot cm^{-1})$, a current density of 20 $\frac{mA}{cm^2}$, and a realistic wall thickness of 0.5 mm, the total overpotential would be less than 0.1 volt. This would leave the Li/S cell with a closed-

circuit potential (under a load of 20 mA/cm^2) of greater than 2 volts. However, there are problems with the lithium chloroborate glasses (e.g. life time) which must be overcome before they will be ready for use as practical electrolytes.

5.2. Recommendations

Lithium chloroborate glasses have some promising attributes combined with a few problems which presently prohibit them from being used as electrolytes in Li/S cells. However, with compositional modifications the glasses may possibly be made more resistive to polysulfide attack. With continued research it should be possible to improve the resistance to lithium attack as well. Tuller *et al.* have reported finding a glass composition which behaved as a perfect Li ion electrolyte over a very wide range of Li activity (up to 0.08 at 380 °C) and temperature (320 °C - 400 °C).[53] They also believe that with minor modifications, this glass composition could be stable in pure lithium. The composition was reported to be 2 mol% Al_2O_3, 49 mol% Li_2O, and 49 mol% B_2O_3. However, this glass has not been tested for stability in sulfur or lithium polysulfides.

The unknown compounds in the reaction layers should be identified. This could best be achieved through preparation of lithium borosulfide compounds followed by comparisons of the X-ray diffraction patterns with those seen in the reaction layers. This work would help to understand the nature of the lithium polysulfide attack and possibly help in the search for a more stable glass composition.

List of Symbols

a_{Li}	activity of Lithium
d	jump distance
D	diffusion coefficient, cm^2/s
e	electronic charge, 1.6021×10^{-19} C
e^-	symbol for the electron
E^o	standard potential difference, volts
E_a	activation energy, cal/mole-K
F	Faraday's constant, 96487 C/equiv.
F	degrees of freedom in the system
G_f	free energy of formation per mole, J/mol
h	cell height, cm
i_L	limiting current density, A/cm^2
k	Boltzmann constant, 1.38×10^{-23} J/K
k	constant in Equation (4-13), volts
k'	constant in Equation (4-17), volts
m	number of components in system
M_i	molecular weight of species i, g/mol
n	stoichiometric number of electrons transferred
n	concentration of charge carriers
r_i	inner radius, cm
R	universal gas constant, 1.984 cal/mol-K
R	resistance, ohms
T	absolute temperature, K

u	mobility, $cm^2 \cdot mole/J \cdot sec$
x_{Li}	mole fraction of lithium
Z	charge number

Greek Symbols:

α	geometrical factor
β	fraction of mobile ions, n/n_o
ΔG	change in free energy for overall reaction, J/mol
γ_{Li}	activity coefficient of lithium
$\eta_{IR\text{-}free}$	IR-free overpotential, volts
ν_i	number of moles of reactant i
ν_o	characteristic vibrational frequency
π	number of phases in system
ρ	density, g/cm^3
σ	conductivity, $\Omega^{-1} \cdot cm^{-1}$
σ_o	constant in Equation (2-6), $K/(\Omega \cdot cm)$

Subscripts:

A	Li in Sn electrode
B	Li in the Li-Sn electrode
i	species number i
i, o	inner, outer

Superscript:

o	standard state

References

1. D. P. Button, R. P. Tandon, H. L. Tuller, and D. R. Uhlmann, *Solid State Ionics,* **5**, 655-658 (1981).

2. R. A. Sharma, *Journal of the Electrochemical Society,* **119**, 1439 (1972).

3. E. J. Cairns, "Requirements of Battery Systems", *Materials for Advanced Batteries,* D. W. Murphy, J. Broadhead, and B. C. H. Steele, eds., 3-26, Plenum Publishing Corporation, New York (1980).

4. E. J. Cairns, "Batteries of the Future for Vehicle Applications", *Electrochemistry in Industry; New Directions,* Landau, Yeager, and Kortan, eds., 131-151, Plenum Publishing Corporation, New York (1982).

5. E. J. Cairns, "Secondary Batteries-New Batteries: High Temperature", *Comprehensive Treatise of Electrochemistry,* **3**, J. O. Bockris, B. E. Conway, E. Yeager, and R. E. White, eds., 341-370, Plenum Publishing Corporation, New York (1981).

6. E. J. Cairns and R. K. Steunenberg, "High Temperature Batteries", *Progress in High Temperature Physics and Chemistry,* **5**, 63 Pergamon Press, New York (1973).

7. E. J. Cairns, "Batteries", *Molten Salt Technology,* D. G. Lovering, ed., 287-321, Plenum Publishing Corporation, New York (1982).

8. J. L. Sudworth and A. R. Tilley, "The Sodium-Sulfur Battery with β-Alumina Electrolyte", *The Sulfur Electrode,* Tischer, R. P., ed., 235-322, Academic Press, New York (1983).

9. C. A. Levine, "Sodium-Sulfur Cells with Glass Electrolyte", *The Sulfur Electrode,* Tischer, R. P., ed., 327-328, Academic Press, New York (1983).

10. C. A. Levine, *Proceedings of the 25th Power Sources Symposium,* New Jersey, 75-77 (1972).

11. C. A. Levine, *Proceedings of the 10th IECEC,* 621-623, New York (1975).

12. D. P. Button, L. S. Mason, H. L. Tuller, and D. R. Uhlmann, *Solid State Ionics,* **9 & 10**, 585-592 (1983).

13. F. Haber and A. Mozer, *Zeitschrift fur Elektrochemie,* **11**, 593 (1905).

14. P. McGeehin and A. Hooper, *Journal of Materials Science,* **12**, 1-27 (1977).

15. D. H. Whitmore, *Journal of Crystal Growth,* **39**, 160-179 (1977).

16. K. Otto, *Physics and Chemistry of Glasses,* **7**, 29-37 (1966).

17. M. H. Velez, H. L. Tuller, and D. R. Uhlmann, *Journal of Non-Crystalline Solids,* **49**, 351-362 (1982).

18. H. L. Tuller, D. P. Button and D. R. Uhlmann, *Journal of Non-Crystalline Solids,* **40**, 93-118 (1980).

19. D. P. Button, R. P. Tandon, H. L. Tuller, and D. R. Uhlmann, *Journal of Non-Crystalline Solids,* **42**, 297-306 (1980).

20. D. P. Button, R. Tandon, C. King, M. H.Velez, H. L. Tuller, and D. R. Uhlmann, *Journal of Non-Crystalline Solids,* **49**, 129-142 (1982).

21. J. Biscoe and B. E. Warren, *Journal of the American Ceramic Society,* **21**, 287-293 (1938).

22. K. H. Mader and T. J. Lorentz, *Borate Glasses - Structure, Properties, Applications,* eds. L. D. Pye, V. D. Frechette, and N. J. Kreidl, 11, Plenum Press, New York (1978)

23. T. Takahashi and O. Yamamoto, *Chem. Letters,* **2**, 135-136 (1979).

24. J. M. Reau, A. Levasseur, C. Fouassier, B. Cales, and P. Hagenmuller, Brevet D. R. M. E. France **#77/11376** (1977).

25. Powder Diffraction File, *Inorganic Phases,* Joint Committee on Powder Diffraction Standards, (1983)

26. Donohue *et al., Journal of the American Chemical Society,* **83**, 3748 (1961).

27. D. Smith and Fausey, *Annual Report to the Joint Committee on Powder Diffraction Standards,* (1973).

28. L. Gmelin, *Gmelin Handbuch der Anorganischen Chemie,* **19**, 12-15 (1981)

29. J. C. Rosso and M. M. Dubusc, *Chimie et Industrie-Genie Chimique,* **102**, 409-415 (1969).

30. V. H. Noth and G. Mikulaschek, *Zeitschrift fur Anorganische und Allgemeine Chemie,* **311**, 241-248 (1961).

31. D. R. Uhlmann, H. L. Tuller, D. P. Button, and M. Velez, *Proceedings of 2nd Otto Schott Symposium,* 1982 in Wiss. Ztschr, Friedrich-Schiller-Univ. Jena, Math.-Naturwiss. R. **32**, 285-302 (1983).

32. *Handbook of Chemistry and Physics,* 58th ed., The Chemical Rubber Co., Cleveland, Ohio (1977-78).

33. I. Barin, O. Knacke, *Thermochemical Properties of Inorganic Subtances,* Springer Verlag, Berlin, New York (1973).

34. I. Barin, O. Knacke, and O Kubaschewski, *Thermochemical Properties of Inorganic Subtances,* Supplement, Springer Verlag, Berlin, New York (1973).

35. B. Cleaver, "Properties of Polysulfide Melts", *The Sulfur Electrode,* Tischer, R. P., ed., 35-77, Academic Press, New York (1983).

36. Argonne National Laboratory, *Annual DOE Review of the Lithium/Metal Sulfide Battery Program* (June 1979).

37. E. J. Cairns and H. Shimotake, *Science,* **164**, 1347 (1969).

38. E. J. Cairns, R. K. Steunenberg, and H. Shimotake, *Encyclopedia of Chemical Technology,* Supplement, 2nd ed, 120, John Wiley and Sons, Inc., New York (1971).

39. M. L. Kyle, H. Shimotake, R. K. Steunenberg, F. J. Martino, R. Rubischko, and E. J. Cairns, *Proceedings of Intersociety Energy Conversion Engineering Conference,* SAE 80 (1971).

40. G. J. Janz and D. J. Rogers, "Physical Properties Data: Sulfur and Polysulfides", *The Sulfur Electrode*, R. P. Tischer, ed., 339-363, Academic Press, New York (1983).

41. S. M. Upton, "Properties of Sodium and Lithium Polysulfides", Ph.D. Thesis, University of South Hampton (1980).

42. P. T. Cunningham, S. A. Johnson, and E. J. Cairns, *Journal of the Electrochemical Society*, **119**, 1448 (1972).

43. K. D. South, J. L. Sudworth, and J. G. Gibson, *Journal of the Electrochemical Society*, **119**, 554 (1972).

44. C. J. Wen and R. A. Huggins, *Journal of the Electrochemical Society*, **128**, 1181 (1981).

45. C. J. Wen, B. A. Boukamp, and R. A. Huggins, *Solid State Chem.*, **26**, 887 (1981).

46. J. M. Prausnitz, *Molecular Thermodynamics of Fluid-Phase Equilibria*, p. 17, Prentice-Hall, Inc., Englewood Cliff, NJ (1969).

47. J. C. Dobson, *Behavior of Metals in Sulfur/Polysulfide Melts*, M.S. Thesis, University of California at Berkeley, LBL-19518 (1985).

48. G. J. Rowlands, Ph.D. Thesis, University of South Hampton (1975).

49. H. L. Tuller and M. W. Barsoum, *Journal of Non-Crystalline Solids*, **73**, 331-350 (1985).

50. A. V. Virkar, "Degradation of Na-Beta$''$ -Alumina Electrolytes in Na-S Batteries", *Proceedings: DOE/EPRI Beta (Sodium-Sulfur) Battery Workshop V*, 5-63 - 5-82, EPRI EM-3631-SR, December (1984).

51. L. C. DeJonghe, "Solid Electrolyte Degradation: Problems and Solutions", *Proceedings: DOE/EPRI Beta (Sodium-Sulfur) Battery Workshop V*, 5-90, EPRI EM-3631-SR, December (1984).

52. M. W. Barsoum, H. L. Tuller, and D. R. Uhlmann, *Extended Abstracts*, **84-2**, Electrochemical Society, Abstract #157 (1984).

53. H. L. Tuller, Personal communication (1985).

Appendix A

Additional Lithium Solubility Data

Appendix A contains a group of tables which list the results of the lithium solubility measurements performed with cell numbers 18, 20, 21, and 26. The data for cell numbers 18 and 26 are also shown in Figure 4-6 whereas the data for cell numbers 20 and 21 appear only here.

Table A-1 contains the data for cell # 18. This cell was loaded with 1.607 grams of sulfur and was run at 390 °C. The surface area and wall thickness of this cell were 5 cm^2 and 0.05 cm, respectively. The data for this cell followed qualitatively the theoretical slope of $\frac{-RT}{2F}$ with a solubility of 0.03 $^{+0.03}_{-0.01}$ mol% lithium in sulfur.

Table A-1 Summary of Solubility Data for Cell # 18.

Cell	Coulomb count	Mol% lithium	Potential (volts)
18	0.108	0.0022	1.74
18	0.348	0.0072	1.72
18	1.13	0.0233	1.66
18	1.37	0.0283	1.63
18	1.39	0.0286	1.63
18	1.54	0.0319	1.61
18	1.85	0.0382	1.60

Table A-2 contains the results from the lithium solubility experiment with cell #20 at 380 °C. This cell was loaded with 0.225 grams of sulfur which was the smallest cell used; its surface area was approximately 2 cm^2.

Table A-2 Summary of Solubility Data for Cell # 20.

Cell	Coulomb count	Mol% lithium	Potential (volts)
20	0.006	0.0009	2.16
20	0.012	0.0018	2.15
20	0.026	0.0038	2.13
20	0.050	0.0074	2.14
20	0.099	0.0146	2.13
20	0.202	0.0298	1.66
20	0.568	0.0838	1.62

Table A-3 lists the results for cell # 21 at 400 °C. It was loaded with 0.375 grams of sulfur, had a surface area of 2.5 cm^2, and a wall thickness of 0.25 mm. A 0.08-mm thick piece of molybdenum ribbon spot-welded to a platinum wire served as the current collector.

Table A-3 Summary of Solubility Data for Cell # 21.

Cell	Coulomb count	Mol% lithium	Potential (volts)
21	0.012	0.0011	2.02
21	0.030	0.0027	1.95
21	0.050	0.0044	1.87
21	0.070	0.0062	1.82
21	0.162	0.0144	1.74
21	0.261	0.0231	1.74
21	0.345	0.0306	1.70
21	0.872	0.0772	1.68
21	1.172	0.1037	1.60

Table A-4 contains the results from the lithium solubility experiment for cell # 26. This cell was loaded with 0.798 grams of sulfur and run at 400 °C. The surface area and wall thickness were measured to be 4 cm^2 and approximately 0.3 mm, respectively. This data also followed qualitatively the theoretical slope of $\frac{-RT}{2F}$. The limit of solubility occurred at 0.04 $^{+0.03}_{-0.01}$ mol% lithium in the sulfur electrode. This data are also plotted in Figure 4-6.

Table A-4 Summary of Solubility Data for Cell # 26.

Cell	Coulomb count	Mol% lithium	Potential (volts)
26	0.036	0.0015	1.73
26	0.32	0.013	1.69
26	0.72	0.030	1.66
26	1.00	0.042	1.65
26	1.51	0.063	1.65

Appendix B

Additional Current-Voltage Performance Data.

Appendix B contains a tabulation of the results from current-voltage experiments performed with cell numbers 14, 18, 19, 20, and 21. The data for cell # 18 also appear in Figures 4-7 and 4-8 while the data for the other four cells appear only here.

Table B-1 is a summary of the polarization data obtained for cell #14 at 380 °C. The cell was loaded with 1.228 grams of sulfur with a 0.25 mm diameter tungsten wire as the current collector. The cell-wall thickness and surface area were found to be approximately 0.05 cm and 4 cm^2, respectively. These data were obtained when the cell had been discharged to only 1 mol% lithium in the sulfur electrode.

Table B-1 Summary of Data for cell # 14.

Cell	Total Current (mA)	Current Density (mA/cm^2)	Total Polarization $\eta_{(total)}$ (mV)
14-A	0.2	0.05	2
14-A	0.4	0.10	5
14-A	0.6	0.15	9
14-A	0.8	0.20	12
14-A	0.2	0.05	4
14-A	1	0.25	14
14-A	2	0.50	26
14-A	3	0.75	37
14-A	4	1.0	47
14-A	5	1.25	57
14-A	6	1.5	67

Table B-1 con't from previous page.

Cell	Total Current (mA)	Current Density (mA/cm^2)	Total Polarization $\eta_{(total)}$ (mV)
14-A	10	2.5	105
14-A	20	5.0	205
14-A	30	7.5	290
14-A	40	10	365
14-A	50	12	452
14-A	60	15	545
14-B	60	15	540
14-B	70	17	640
14-B	80	20	770
14-B	90	22	1000
14-C	-0.2	-0.05	-1
14-C	-0.3	-0.07	-2
14-C	-0.5	-0.12	-4
14-C	-1	-0.25	-7
14-C	-2	-0.50	-14
14-C	-3	-0.75	-21
14-C	-4	-1.0	-28
14-C	-10	-2.5	-70
14-C	-20	-5.0	-140
14-C	-30	-7.5	-210
14-C	-50	-12	-350

Table B-2 shows the current-voltage results for cell # 18. This cell was loaded with 1.607 gms of sulfur and was run at 390 °C. The wall thickness and surface area of this cell were measured to be 0.05 cm and 5 cm^2, respectively. The performance data for this cell also appear in Figures 4-7 and 4-8 with a description of the corresponding state-of-charge for each group of points (i.e. A, B, ...).

Table B-2 Summary of Data for Cell #18 also found in Figures 4-7 and 4-8.

Cell Id.	Total Current (mA)	Current Density (mA/cm^2)	Total Polarization $\eta_{(total)}$ (mV)	IR-free Overpotential $\eta_{IR-Free}$ (mV)
18-A	5	1	53	3
18-A	10	2	105	5
18-A	20	4	210	10
18-A	30	6	320	20
18-A	40	8	440	40
18-A	50	10	570	70
18-A	60	12	700	100
18-A	70	14	840	140
18-A	80	16	1000	200
18-A	90	18	1175	275
18-B	-5	-1	-52	
18-B	-10	-2	-70	
18-B	-20	-4	-145	
18-B	-30	-6	-235	
18-C	70	14	500	
18-C	80	16	600	
18-C	90	18	750	
18-C	100	20	930	

Table B-2 con't from previous page.

Cell	Total Current (mA)	Current Density (mA/cm^2)	Total Polarization $\eta_{(total)}$ (mV)	IR-free Overpotential $\eta_{(}$IR–Free) (mV)
18-D	10	2	75	10
18-D	20	4	145	15
18-D	30	6	225	30
18-D	40	8	310	50
18-D	50	10	400	75
18-D	100	20	900	250
18-E	40	8	220	
18-E	-30	-6	-150	
18-E	30	6	170	
18-E	-50	-10	-240	
18-E	-80	-16	-370	

Table B-3 is a tabulation of the results for cell #19. This cell was loaded with 0.531 grams of sulfur and was run at 380 °C. The cell data labeled 19-A were obtained when the cell was discharged to approximately 5 mol% lithium in the sulfur electrode while those labeled 19-B were obtained when the sulfur electrode contained approximately 33 mol% lithium. The surface area of this cell was approximately 4 cm^2. Due to the catastrophic manner in which the cell failed, the wall thickness could not be determined.

Table B-3 Summary of Data for cell # 19.

Cell	Total Current (mA)	Current Density (mA/cm^2)	Total Polarization $\eta_{(total)}$ (mV)
19-A	10	2.5	70
19-A	25	6.2	165
19-A	40	10	260
19-A	-25	-6.2	-122
19-A	25	6.2	145
19-A	30	7.5	170
19-B	10	2.5	40
19-B	20	5.0	80
19-B	50	12	180
19-B	100	25	400

Table B-4 contains the results for the current-voltage experiment performed with cell #20 at 380 °C. Cell # 20 was loaded with 0.225 grams of sulfur, which was the smallest capacity cell attempted. Its surface area was approximately 2 cm^2 with no recorded glass thickness. The current collector was a 0.25-mm diameter platinum wire.

Table B-4 Summary of Data for cell # 20.

Cell	Total Current (mA)	Current Density (mA/cm^2)	Total Polarization $\eta_{(total)}$ (mV)
20-A	5	2.5	50
20-A	50	25	700
20-A	-50	-25	-400
20-A	20	10	210
20-A	-20	-10	-267
20-A	-40	-20	-320
20-A	-30	-15	-240

Table B-5 is a summary of the results obtained for cell # 21. The cell was loaded with 0.375 grams of sulfur and was run at 400 °C. The surface area was measured to be 2.5 cm^2, and the wall thickness was estimated to be 0.25 mm thick. The life of this cell was not very long; it shorted at approximately 2 mol% lithium in the sulfur electrode.

Table B-5 Summary of Data for cell # 21.

Cell	Total Current (mA)	Current Density (mA/cm^2)	Total Polarization $\eta_{(total)}$ (mV)
21-A	0.1	0.04	10
21-A	1.0	0.4	25
21-A	10	4.0	85
21-A	-20	-8.0	-117
21-A	100	40.	-

This report was done with support from the Department of Energy. Any conclusions or opinions expressed in this report represent solely those of the author(s) and not necessarily those of The Regents of the University of California, the Lawrence Berkeley Laboratory or the Department of Energy.

Reference to a company or product name does not imply approval or recommendation of the product by the University of California or the U.S. Department of Energy to the exclusion of others that may be suitable.

LAWRENCE BERKELEY LABORATORY
TECHNICAL INFORMATION DEPARTMENT
UNIVERSITY OF CALIFORNIA
BERKELEY, CALIFORNIA 94720